AD NUMBER

AD-883 946

NEW LIMITATION CHANGE

TO **DISTRIBUTION STATEMENT - A**
Approved for public release;
distribution is unlimited

LIMITATION CODE: 1

FROM **No Prior DOD Distr Scty Cntrl St'mt Assigned**

AUTHORITY

Cmdr., Air Force Flight Dynamics Laboratory (AFFDL) Air Force Systems Command,WPAFB, Mar 8, 1972

19990226155

REPRODUCTION QUALITY NOTICE

This document is the best quality available. The copy furnished to DTIC contained pages that may have the following quality problems:

- Pages smaller or larger than normal.
- Pages with background color or light colored printing.
- Pages with small type or poor printing; and or
- Pages with continuous tone material or color photographs.

Due to various output media available these conditions may or may not cause poor legibility in the microfiche or hardcopy output you receive.

☐ If this block is checked, the copy furnished to DTIC contained pages with color printing, that when reproduced in Black and White, may change detail of the original copy.

AD883946

When Government drawings, specifications, or other data are used for any purpose other than in connection with a definitely related Government procurement operation, the United States Government thereby incurs no responsibility nor any obligation whatsoever; and the fact that the government may have formulated, furnished, or in any way supplied the said drawings, specifications, or other data, is not to be regarded by implication or otherwise as in any manner licensing the holder or any other person or corporation, or conveying any rights or permission to manufacture, use, or sell any patented invention that may in any way be related thereto.

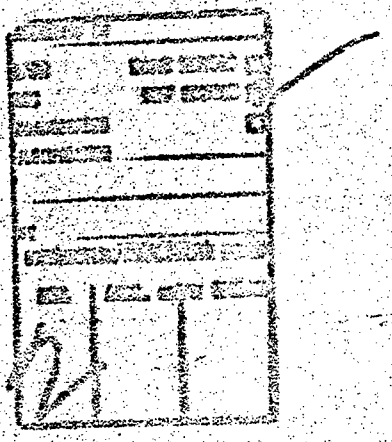

Copies of this report should not be returned unless return is required by security considerations, contractual obligations, or notice on a specific document.

Unclassified

DOCUMENT CONTROL DATA - R & D

(Security classification of title, body of abstract and indexing annotation must be entered when the overall report is classified)

1. ORIGINATING ACTIVITY (Corporate author)
Bolt Beranek and Newman Inc.
Cambridge, Massachusetts 02138

2a. REPORT SECURITY CLASSIFICATION
Unclassified

2b. GROUP

3. REPORT TITLE
The Use of Reflectors to Shape a Sound Field

4. DESCRIPTIVE NOTES (Type of report and inclusive dates)
Final - January 69 to March 70

5. AUTHOR(S) (First name, middle initial, last name)
Jerome E. Manning
James A. Moore

6. REPORT DATE
March 1971

7a. TOTAL NO. OF PAGES
107

7b. NO. OF REFS
17

8a. CONTRACT OR GRANT NO. F33615-69-C-1304

b. PROJECT NO. 4437

c. Task No. 463701

d.

9a. ORIGINATOR'S REPORT NUMBER(S)
BBN 1969

9b. OTHER REPORT NO(S) (Any other numbers that may be assigned this report)
AFFDL-TR-70-97

10. DISTRIBUTION STATEMENT
This document is subject to special export controls and each transmittal to foreign governments or foreign nationals may be made only with prior approval of AFFDL (FY) WPAFB, Ohio.

11. SUPPLEMENTARY NOTES

12. SPONSORING MILITARY ACTIVITY
Air Force Flight Dynamics Laboratory
Wright-Patterson AFB, Ohio 45433

13. ABSTRACT

The use of reflectors to control the distribution of the Sound Pressure Level (SPL) in sonic test chambers is investigated. The goal is to obtain more realistic SPL distributions on the test object. It is concluded that the use of reflectors will not increase the SPL on a test object unless the reflector and test object are in the near field of the sound generators. The results of the study are applied to the Air Force Flight Dynamics Laboratory's (AFFDL) Sonic Fatigue Facility at Wright-Patterson Air Force Base. Design charts are presented that relate predicted SPL distributions to reflector size and positioning.

"THE DISTRIBUTION OF THIS ABSTRACT IS UNLIMITED"

DD FORM 1 NOV 65 1473

Unclassified
Security Classification

Security Classification

14. KEY WORDS	LINK A		LINK B		LINK C	
	ROLE	WT	ROLE	WT	ROLE	WT
Acoustic Reflectors						
Acoustic Environment Simulation						
Sonic Fatigue Testing						
Sound Wave Propagation						

Security Classification

THE USE OF REFLECTORS TO SHAPE A SOUND FIELD

JEROME E. MANNING

JAMES A. MOORE

BOLT BERANEK AND NEWMAN INC.

FOREWORD

This report was prepared by Bolt Beranek and Newman Inc., Cambridge, Massachusetts for the Aero-Acoustics Branch, Vehicle Dynamics Division, Air Force Flight Dynamics Laboratory, Wright-Patterson Air Force Base, Ohio, under Contract F33615-69-C-1384. The research described herein was conducted under Project 4437, "High Intensity Sound Environment Simulation for Air Force Systems Testing"; Task 443701, "Sonic Facility Development for Air Force Systems Testing". Mr. Carl L. Rupert of the Vehicle Dynamics Division was the Project Engineer.

This report covers a work period from January 1969 through March 1970. The manuscript of this document was released by the authors in June 1970 for publication as an AFFDL Technical Report.

This report has been reviewed and approved.

WALTER J. MENTON
Asst. for Research & Technology
Vehicle Dynamics Division

ABSTRACT

The use of reflectors to control the distribution of the Sound Pressure Level (SPL) in sonic test chambers is investigated. The goal is to obtain more realistic SPL distributions on the test object. It is concluded that the use of reflectors will not increase the SPL on a test object unless the reflector and test object are in the near field of the sound generators. The results of the study are applied to the Air Force Flight Dynamics Laboratory's (AFFDL) Sonic Fatigue Facility at Wright-Patterson Air Force Base. Design charts are presented that relate predicted SPL distributions to reflector size and positioning.

TABLE OF CONTENTS

LIST OF FIGURES

LIST OF SYMBOLS

A	Area of a panel of reflector.
A_∞	The infinite plane of the reflector.
A_{plane}	Complex amplitude of an incident plane wave.
A_{pt}	Complex amplitude of a point source.
D	Step size in a numerical integration.
E_A	Modal energy in an acoustic-space.
E_p	Modal energy of a panel.
F	Focal length of a curved reflector.
G	Acoustic Green's function.
$H(\underline{x}_r, f)$	Complex frequency response.
I	Acoustic intensity.
L	Length of one side of a square reflector.
L_x, L_y	Dimensions of the reflector.
L_{in}	Panel side length in inches
$P(\underline{x})$	Complex pressure amplitude at point $\underline{x}$.
P_s	Complex pressure amplitude in the scattered sound field.
P_i	Complex pressure amplitude of the incident sound field.
$\lvert P_i \rvert$	Pressure amplitude of an incident plane wave.
$\lvert P_{r,max} \rvert$	Maximum pressure amplitude in the reflected field.

R	Surface of the reflector.
R_s	Distance from the center of the reflector to the source, see Fig. 7.
R_r	Distance from the center of the reflector to the receiver, see Fig. 7.
R_T	Room constant.
R_d	Distance from source to receiver.
S	A three-dimensional surface identified in Fig. 6.
$S_i(f)$	Spectrum of the source pressure.
$S_{p(\underline{x}_r)}(f)$	Spectrum of the pressure at point $\underline{x}_r$.
s	Distance from point $\underline{x}_s$ to point $\underline{x}$.
T	Time, see Eq. 122.
T_{rev}	Reverberation time.
Q	Source directivity factor.
V	Volume of an acoustic space.
Re	Real part of.
HK	Helmholtz-Kirchhoff.
FRS	First Rayleigh-Sommerfeld.
SRS	Second Rayleigh-Sommerfeld.
c_o	Speed of sound.
c_ℓ	Longitudinal wavespeed in the panel material.
d	Diameter of a curved reflector.
e	2.73.
f	Frequency in Hertz.
f_{cr}	Critical frequency of a panel.

f_c	Band center frequency in Hertz.
i	$\sqrt{-1}$.
k	Acoustic wavenumber at the frequency in question.
n_A	Modal density of an acoustic-space.
n_P	Modal density of a panel.
$p(\underline{x},t)$	Sound pressure at point $\underline{x}$ and time t.
$\langle p_s^2 \rangle_t$	Mean-square sound pressure in the scattered sound field.
r	Distance from point $\underline{x}_r$ to point $\underline{x}$.
t	Time.
t_{in}	Panel thickness in inches.
$\underline{x}$	A point in a three-dimensional space.
$\underline{x}_r$	Location of the receiver
$\underline{x}_s$	Location of the source.
x,y	Location of a point on the reflector in a Cartesian coordinate system.
x_s,y_s,z_s	Source location in a Cartesian coordinate system centered on the reflector, see Fig. 7.
x_r,y_r,z_r	Receiver location in a Cartesian coordinate system centered on the reflector, see Fig. 7.
Δf	Frequency bandwidth in Hertz.
Π_r	Reflected acoustic power.
Π_r	Incident acoustic power.
Π_{trans}	Acoustic power transmitted through the panel.
$\Pi_{reflected}$	Reflected acoustic power.
Π_{inc}	Incident acoustic power.
Π_{rad}	Radiated acoustic power.
$\bar{\alpha}$	Wall absorption coefficient

α	See Eq. 103.
β	See Eq. 104.
β_s	Angle between a line normal to the reflector and a line from $\underline{r}_s$ to $\underline{r}$.
β_r	Angle between a line normal to the reflector and a line from $\underline{r}_r$ to $\underline{r}$.
η_{rad}	Radiation loss factor.
η_{tot}	Total loss factor.
θ_s	Angle measured from a normal to the reflector and a line from the center of the reflector to the source.
θ_i	Angle of incidence.
θ_r	Angle measured from a normal to the reflector and a line from the center of the reflector to the receiver.
κ	Radius of gyration.
λ_f	Acoustic wavelength at the frequency in question.
λ_c	Acoustic wavelength at f_c.
π	3.14.
ρ_a	Acoustic medium density.
ρ_s	Surface density of a panel.
$\bar{\tau}$	Mass-law transmission coefficient.
ϕ_s	Angle in a spherical coordinate system identifying the source location, see Fig. 6.
ϕ_r	Angle in a spherical coordinate system identifying the receiver location.
ϕ_i	Angle defined in Fig. 9.
ω	Frequency in radians per second.
$\partial/\partial n$	Derivative normal to the surface.
$\lvert\ \rvert$	Magnitude-squared.
$*$	Complex conjugate.
$\langle\ \rangle$	Average.

SECTION I

INTRODUCTION

Many studies of the effects of an intense sonic environment on aircraft structures and components are being conducted in sonic fatigue facilities. These studies are often hindered by limitations in simulating actual sonic environments. This report considers the potential uses of acoustic reflectors in shaping a sound field in acoustic test chambers in order to simulate better the actual sonic environment encountered by operational aircraft.

Sonic fatigue facilities have sound sources capable of generating controlled sound output at pressure levels equal to those encountered in actual environments. The principal problem that remains in simulating the sonic environment is to obtain the correct distribution of sound pressure level (SPL) on the test object. For example, SPL's on the bottom surface of an aircraft horizontal stabilizer may be 10 dB higher than the levels on the top surface. A realistic test requires acoustic field shaping to obtain this distribution of SPL. The second basic problem that remains in simulating the actual sonic environment is to obtain the correct directional properties of the sound field. The directionality of the field determines the spatial correlation pattern on the surface of the test object, and thereby its response. At the present time, measurements of the spatial correlation pattern in an actual environment are not generally available. Therefore, field shaping to obtain the correct directionality of the acoustic field can only be accomplished in a qualitative way.

Field shaping is presently accomplished by programming the number and combination of noise generators used, by positioning mobile noise generators, by selective use of anechoic treatment, and by judicious location of the test object. However, the amount of field shaping that can be obtained using these methods is not always sufficient to simulate actual environments. More field shaping could be obtained by use of a larger number of sound sources. But this approach would be expensive and would require enlargement of the control system complex to the extent that sufficient space surrounding the structure would not be available.

The use of reflectors to shape the acoustic field seems promising. A simple 4 ft × 4 ft aluminum panel serves as a satisfactory reflector of sound waves with frequencies above 100 Hz. In using such a reflector, it is necessary only to position it correctly relative to the sound sources and the test object. No controls, supply lines, drive systems, or heavy supports are needed.

An acoustic reflector can be used in basically three ways. First, it can be used to reflect sound waves coming from the source onto the test object, as shown in Fig. 1. Second, it can be used to reflect sound waves away from the test object, thereby shielding it from an intense sonic environment. The use of a reflector for this purpose is shown in Fig. 2. A third way in which an acoustic reflector can be used is to place it close to the test object, thereby forming a resonant cavity. The sound pressure levels in the cavity will exceed those in the surrounding acoustic field at the resonant frequencies of the cavity. The use of a reflector to form a resonant cavity is shown in Fig. 3.

There are, of course, limitations in the use of acoustic reflectors to shape sound fields. It is easy to overestimate the effectiveness of a reflector on the basis of familiar effects obtained with optical reflectors. Acoustic reflectors, unlike optical reflectors, are comparable to or only slightly larger than an acoustic wavelength. Consequently, much if not all of their useful effects will be associated with highly complex wave phenomena rather than the relatively simple geometric effects commonly valid for optical systems.

A reflector used to reflect sound waves onto a test object can be flat or curved. With a curved reflector, some focusing of the acoustic energy occurs. However, the effect is not as strong as commonly encountered in optics since the acoustic wavelength is comparable to the size of the reflector. The amount of focusing that can be obtained with a curved reflector is given by the equation [1]

$$\frac{|P_{r,max}|}{|P_i|} \approx \frac{\pi d^2}{F\lambda_0} \qquad (1)$$

where $|P_{r,max}|$ is the maximum pressure amplitude of the reflected field, $|P_i|$ is the pressure amplitude of an incident plane wave, d is the diameter of the reflector, F is the focal length, and λ_0 is the acoustic wavelength.

In this report we have limited our consideration to the use of flat, rectangular panels as acoustic reflectors. The use of a flat reflector to reflect sound waves onto a test object in a *diffuse* field will produce no significant effect. At any point in a diffuse field, equal acoustic energy comes from all directions. Therefore, the reflector deflects as much energy away from the test object as towards it. The use of an acoustic reflector as a mirror is limited to the direct field where the acoustic

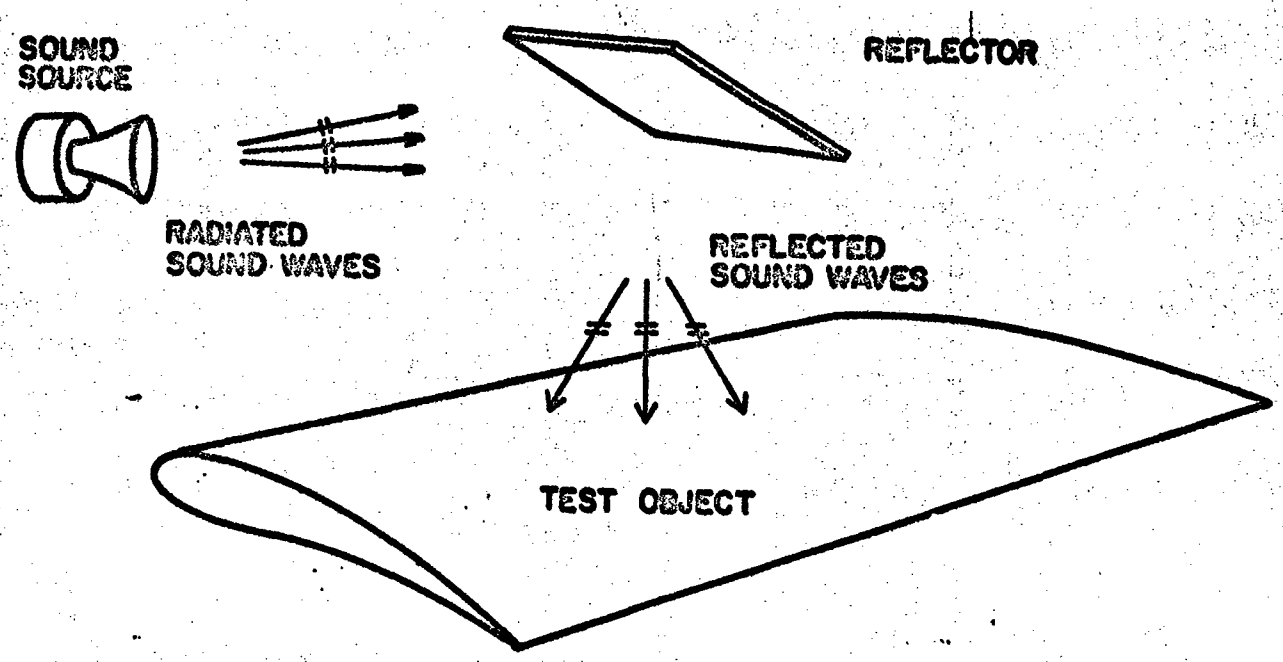

FIG. 1 REFLECTION OF SOUND WAVES ONTO A TEST OBJECT.

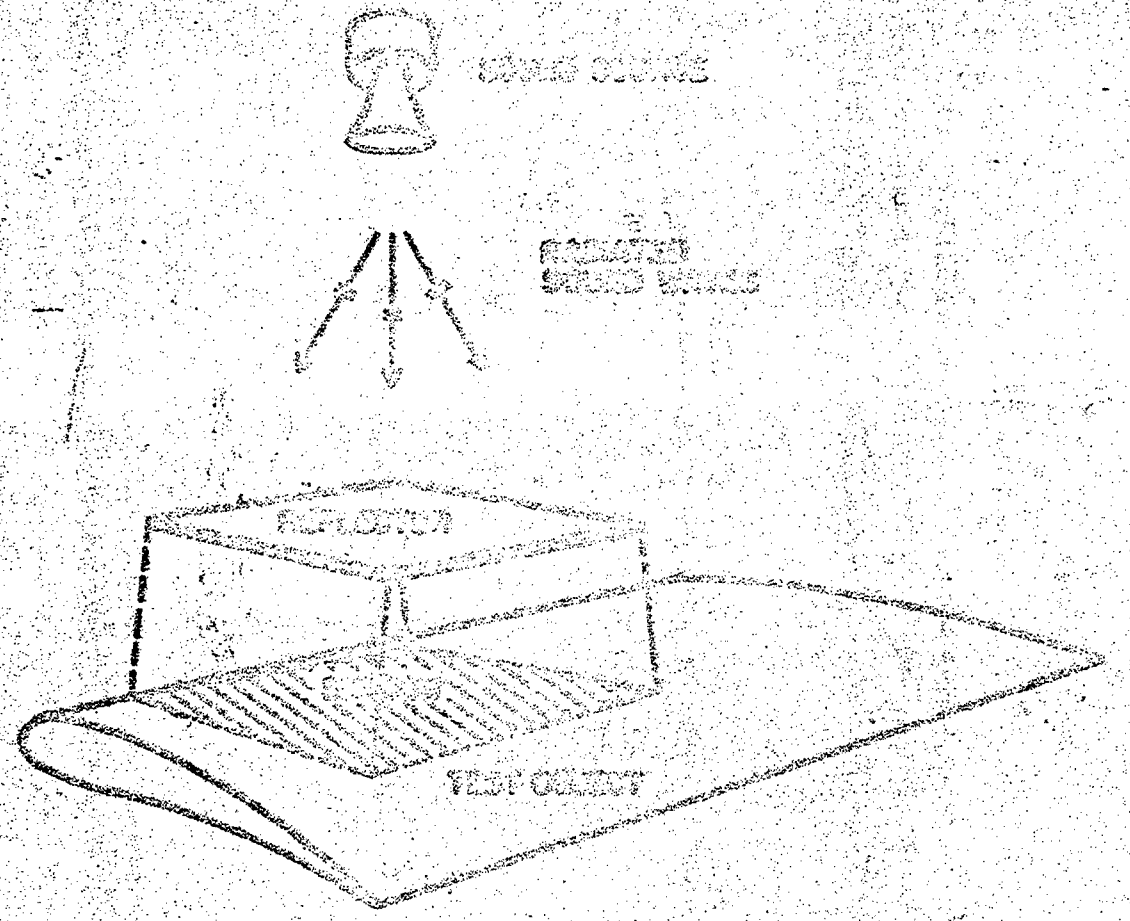

FIG. 2 REFLECTION OF SOUND WAVES AWAY FROM A TEST OBJECT.

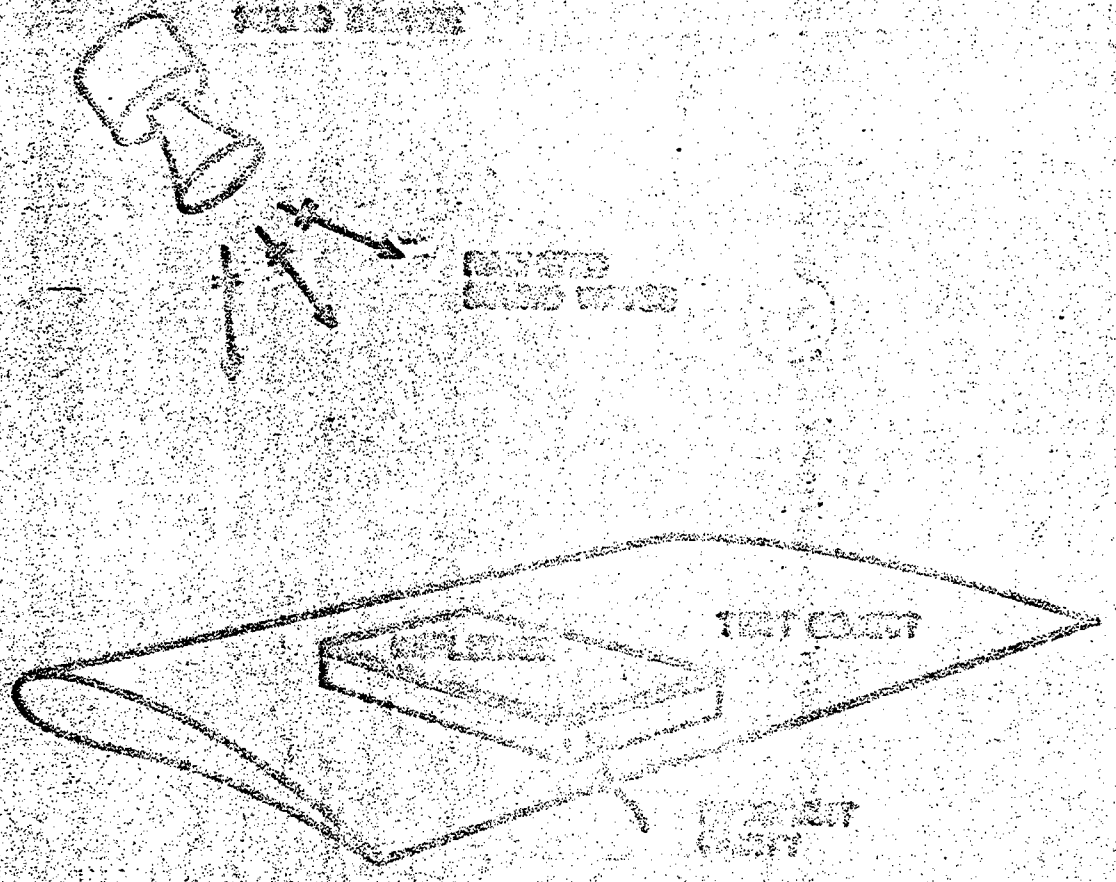

FIG. 3 USE OF A REFLECTOR TO FORM A CAVITY.

energy coming directly from the sound source is greater than the acoustic energy in the reverberant field. The extent and shape of the direct field depends upon the acoustic dissipation in the test chamber and the directivity of the source. When the noise fatigue facility is operated with all surfaces lagged, the acoustic dissipation in the chamber will be extremely low so that the direct field will dominate the reverberant field only in a small region near the source. The region is so small that acoustic reflectors used as mirrors are of no practical use. In the semi-anechoic mode of operation, the direct field is greater than the reverberant field in a fairly large region surrounding the sources. The use of reflectors as mirrors for this situation may be practical.

In the direct field, reflectors can be used in two ways. First, the directivity of the sound sources is such that most of the acoustic energy is radiated directly in front of the sources. This energy can be directed by an acoustic reflector so that it impinges on a test object, as shown in Fig. 4. Second, if the test object is placed directly in front of the sound sources a shadow may exist behind the test object. This shadow can be filled in by use of an acoustic reflector, as shown in Fig. 5. The emphasis of our study was on the use of reflectors for these two purposes.

Acoustic reflectors can also be used as shields. When used as shields, they reflect acoustic energy away from the test object, thereby reducing the sound pressure level in a region behind the reflector. An acoustic reflector used as a shield can be used both in the direct field by placing it between the test object and the source and in the reverberant field, since the test object blocks sound from one direction while the shield blocks sound from the other. However, when using an acoustic reflector as a shield, care must be taken to avoid forming an acoustic cavity in which resonant amplification of the sound pressure level can occur. In experiments conducted for this program, no shielding was found when the reflector was placed near the test object. When the reflector was placed very close to the test object, a resonant buildup occurred in the cavity. When the reflector was moved further away, diffraction of sound around the reflector occurred to such an extent that no shielding resulted. The resonant build-up of sound pressure level could be eliminated by the use of absorptive material on the back of the acoustic reflector. By eliminating the problem of resonant building, it seems highly probable that reflectors could be used as shields to shape the sonic environment both in the direct and in the reverberant fields.

The third use of acoustic reflectors is to place them sufficiently close to the test object as to form a resonant cavity.

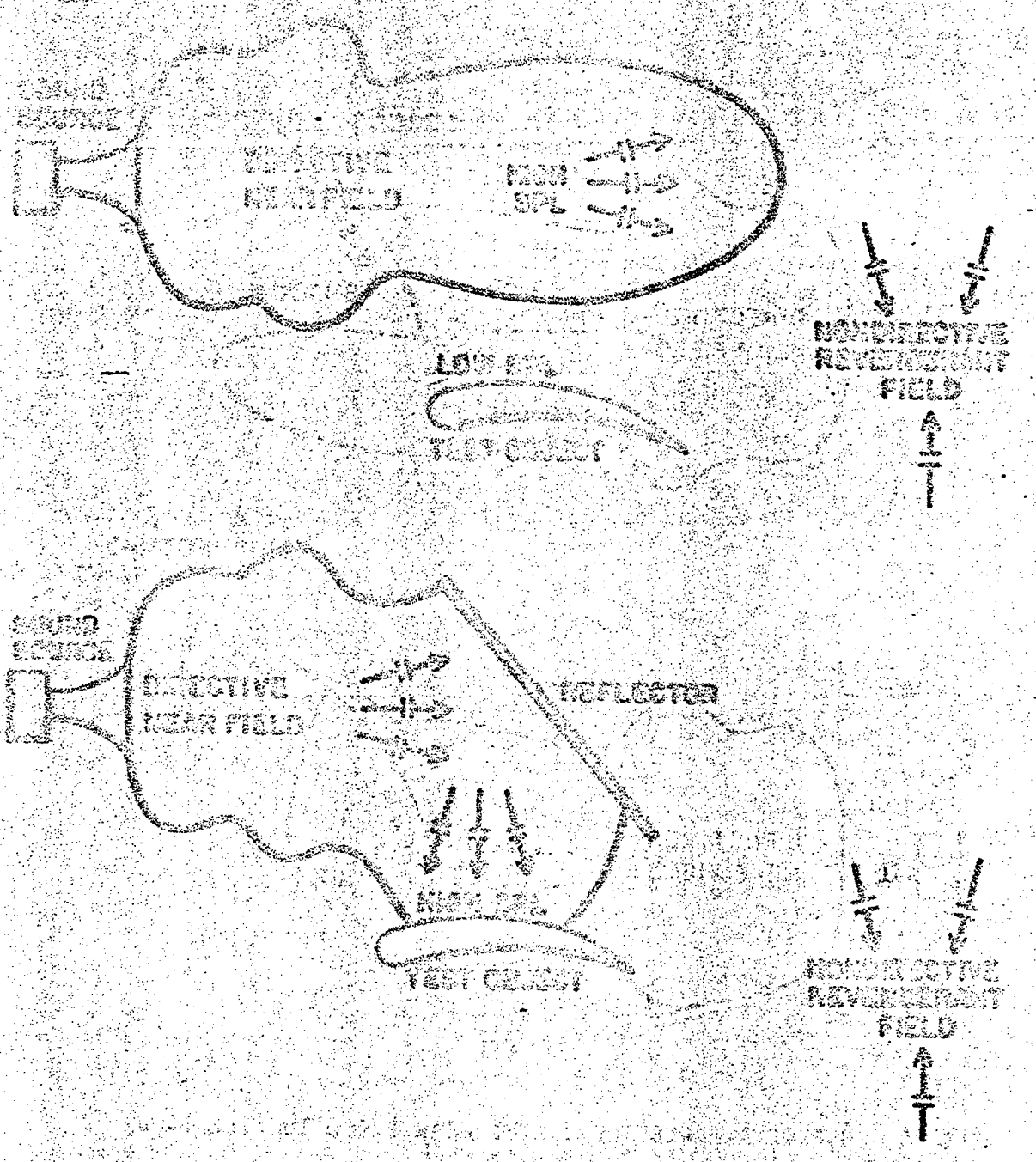

FIG. 4 USE OF A REFLECTOR TO DIVERT SOUND WAVES IN THE NEAR FIELD.

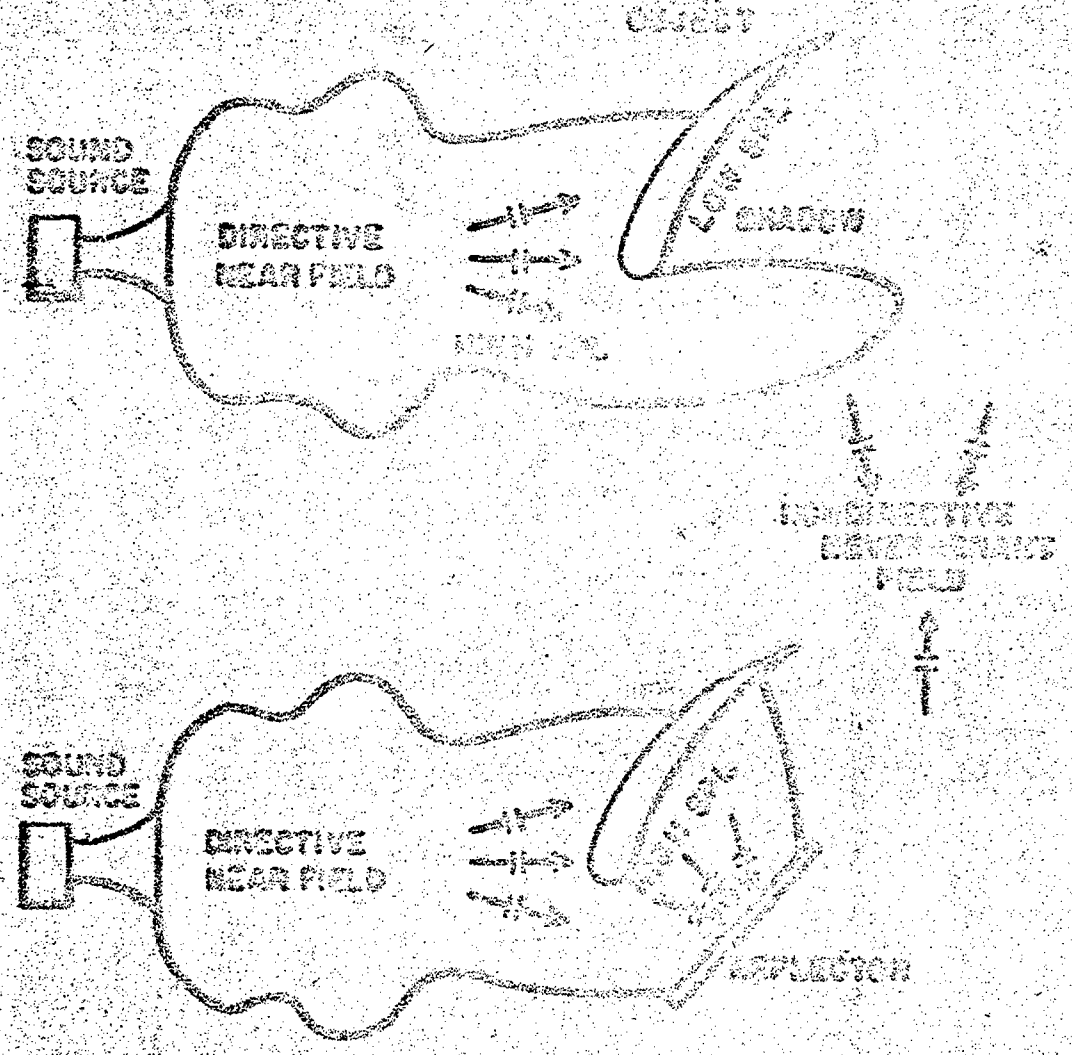

FIG. 5 USE OF A REFLECTOR IN THE NEAR FIELD TO FILL IN A SHADOW.

A resonant buildup of the sound pressure level occurs at the resonant frequencies of the cavity. The resonant frequencies depend on the physical shape of the acoustic reflector. The amount of resonant buildup depends upon how close the reflector is placed to the test object. No resonant buildup occurs unless the reflector is within one-half wavelength of the test object. By placing the reflector within a one-half wavelength of the test object, the radiation loads due to the vibration of the test object will be changed. This change may or may not be important to the vibration of the object. The inertial radiation loads are usually not important. However, the radiation loads for some structures such as honeycomb panels can be important in establishing the total damping of the panels.

Because of the complexity of the cavity behavior, we did not obtain theoretical solutions for the resonance buildup. Instead, we conducted a carefully set of experiments. These are described in Sec. III. Since the resonant buildup in the cavity is limited to specific resonant frequencies, no practical utilization of reflectors in this way is foreseen.

In Sec. II of the report, the theoretical formulation for reflection by a flat, rectangular reflector is presented. An exact solution for this problem is not presently within the state of the art. Therefore, we relied upon approximate techniques commonly used in wave optics. These techniques were originally introduced by Kirchhoff and have been supported by comparison of the theoretical predictions with experimental data. Three approximate formulations exist. We have obtained all three of these formulations for a point source and for a plane wave. The basic formulation gives the reflected pressure as a function of frequency, angle of incidence, reflector size, and angle of reflection. The different formulations give approximately the same results except for cases where the angle of incidence, or the angle of reflection, approaches 90° relative to a normal to the reflector. The experiments which we conducted did not offer conclusive evidence as to which formulation was more accurate. Data from the literature did not help in establishing the accuracy of any one formulation. However, since the reflectivity is quite low at angles near 90°, the question of which theory to use is not of great importance for our problem since we are interested in those angles near specular reflection at which most of the sound is reflected. To support the validity of the approximate techniques, we have compared the approximate solutions with the exact solution for a disk with sound incident from a direction normal to the plane of the disk.

The basic theory used to find the reflection by a rigid reflector was used to find the effect of reflector vibrations on

the reflected field. No effect was found unless the reflector was very thin. This conclusion was supported by our experimental data. The basic theory for reflection of a pure tone was also used to predict the reflection of bands of noise, the total acoustic power reflected, reflection of a sawtooth wave representative of high amplitude sound waves, and the interaction of the reflected sound waves with the incident sound waves.

The theory for shadow formation behind the reflector is not worked out in this report. However, the same approximate techniques would be valid. Vibrations of the reflector would have a significant effect on the sound pressure level in the shadow zone.

In Sec. III of this report, an experimental program is outlined. The purpose of this program is to obtain data to support the theoretical formulations and to explore the structure-reflector interaction. The theoretical formulation for reflection of a pure tone is compared with data from Ref. 3 and from data taken in our own experiments. In all cases, the agreement between theory and experiment is sufficient to support the use of the theory. Experiments were conducted with very thin reflectors to determine the effect of reflector vibrations on the reflected field. No effect was found. A second set of experiments was conducted to study the interaction of the test object and the reflector. A test structure was fabricated and a small reflector was placed over the structure. Sound pressure levels with and without the reflector were measured. Also, vibration levels were taken. Resonant buildup of the sound pressure level was found at specific resonant frequencies. However, the vibration did not change appreciably. This is due, in part, to the fact that the proximity of the reflector affects the vibrational behavior of the panel.

Sec. IV of this report describes practical utilization of reflectors as mirrors. Design charts are presented in Figs. 44 through 48, and it is hoped that these will facilitate the use of acoustic reflectors.

Section II

Theoretical Formulations

2.1 General Solution for Scattering

Reflection of sound waves by an object, such as a flat reflector, is part of a more general physical phenomenon called scattering. Many areas of physics – optics, acoustics, electromagnetics, etc. – have generated scattering problems so that this subject has been studied extensively for more than 100 years. The pioneering work of Helmholtz, Kirchhoff, and Sommerfeld is still widely used.

In conducting our study of reflection we will initially limit our consideration to single frequency pure tones. The solutions which we obtain for reflection of a pure tone will be used in Sec. 2.6 to find the reflection of noise in a band of frequencies. We will use complex notation in studying the reflection of pure tones. The sound pressure at any point can then be written as

$$p(\underline{x},t) = \mathrm{Re}\left\{P(\underline{x})e^{-i\omega t}\right\} \tag{2}$$

where $p(\underline{x},t)$ is the sound pressure at point $\underline{x}$ at time t, Re signifies "real part of", $P(\underline{x})$ is a complex amplitude, and ω is the radian frequency. Note that we use $e^{-i\omega t}$ time dependence rather than $e^{+i\omega t}$, since, most published literature on scattering uses this time dependence.

The complex amplitude of the sound pressure around a scattering object can be written as

$$P(\underline{x}) = P_i(\underline{x}) + P_s(\underline{x}) \tag{3}$$

where $P(\underline{x})$ is the complex pressure amplitude at point $\underline{x}$, $P_i(\underline{x})$ is the complex pressure amplitude of the incident sound waves – the complex pressure amplitude that would exist if the scatterer were removed – and $P_s(\underline{x})$ is the complex pressure amplitude of the scattered sound field.

Three exact formulations for the complex pressure amplitude in the scattered sound field follow:

Helmholtz-Kirchhoff Formulation

The complex pressure amplitude in the scattered field in an arbitrary closed region bounded by the surface S at a field point $\underline{x}_p$ is given by the Helmholtz-Kirchhoff formula, [4-6]

$$P_s(\underline{x}_p) = \frac{1}{4\pi} \iint_S dS \left\{ G\left(\frac{\underline{x}_p}{\underline{x}}\right) \frac{\partial P_s}{\partial n}(\underline{x}) - P_s(\underline{x}) \frac{\partial G}{\partial n}\left(\frac{\underline{x}_p}{\underline{x}}\right) \right\} \tag{4}$$

where $\underline{x}_p$ is a point inside the surface S, $\underline{x}$ is a point on the surface S, $G(\underline{x}_p/\underline{x})$ is the Green's function for infinite space -- the complex pressure amplitude at $\underline{x}_p$ due to a point volume velocity source at $\underline{x}$ in an infinite unbounded space -- and $\partial/\partial n$ is a derivative with respect to a normal to the surface S taken from inside to outside the surface. The Green's function $G(\underline{x}_p/\underline{x})$ is

$$G(\underline{x}_p/\underline{x}) = \frac{e^{ikr}}{r} \tag{5}$$

where k is the acoustic wavenumber and r is the distance from point $\underline{x}_p$ to point $\underline{x}$. The derivative of the Green's function in Eq. 4 is

$$\frac{\partial G}{\partial n}\left(\frac{\underline{x}_p}{\underline{x}}\right) = \frac{e^{ikr}}{r}\left(ik - \frac{1}{r}\right)\cos\beta_r \tag{6}$$

where β_r is the angle between the line from point $\underline{x}_p$ to point $\underline{x}$ and a line normal to the surface, $0 < \beta < 90°$.

In the case of a plane scatterer, the surface S is taken to be an infinite hemisphere, as shown in Fig. 6. Then, since the complex pressure amplitude in the scattered field must satisfy the Sommerfeld radiation condition,

$$\lim_{R \to \infty} R\left[\frac{\partial P_s}{\partial n}(\underline{x}_p) - ikP_s(\underline{x}_p)\right] = 0 \tag{7}$$

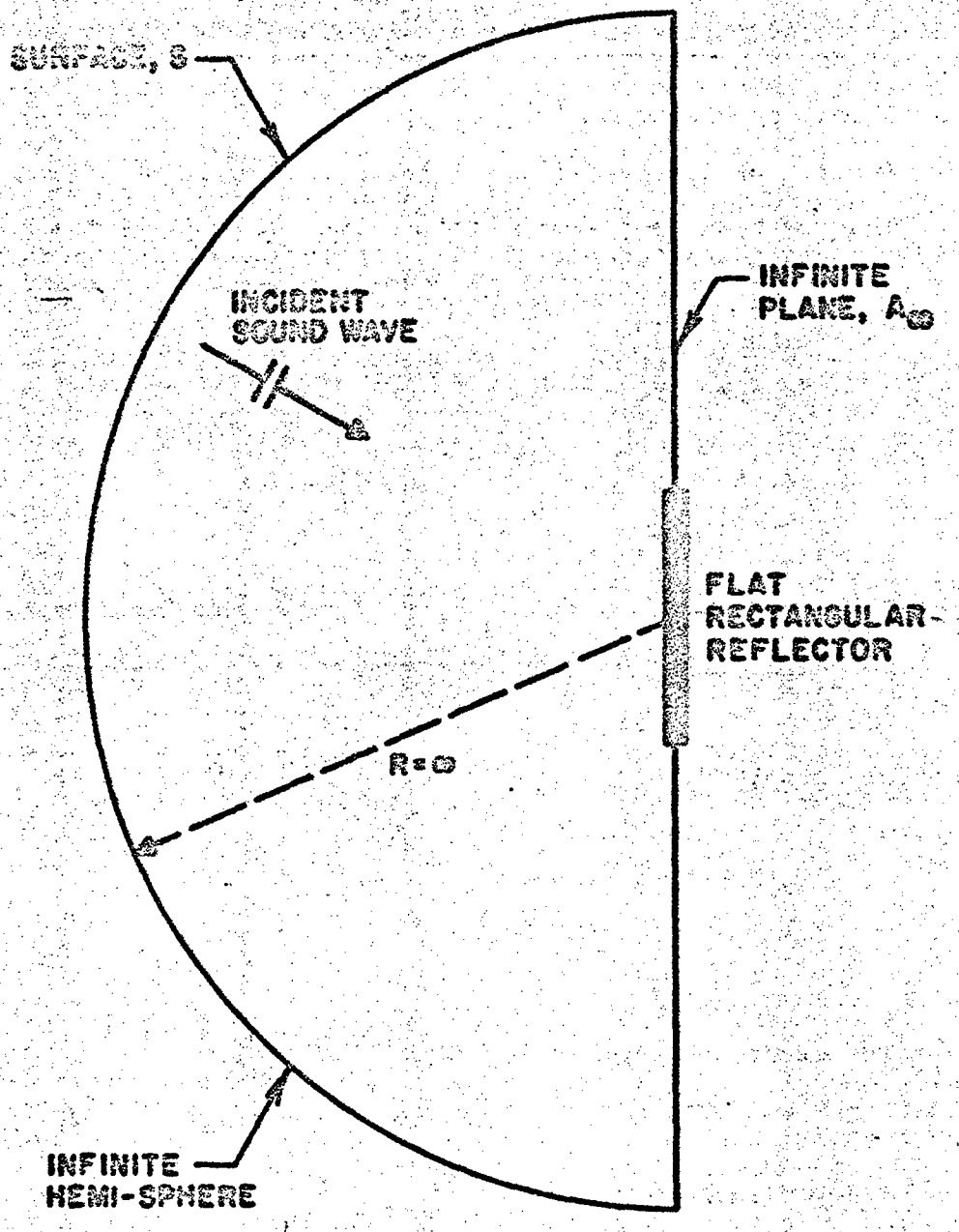

FIG. 6 THE SURFACE S FOR THE INTEGRAL FORMULATION.

where R is the distance from the center of the scatterer to point $\underline{x}_r$, the integral over the surface, S, can be replaced by an integral over the infinite plane including the scatterer, A_∞. Solution of Eq. 4 now requires the complex pressure amplitude and its derivative on the surface A_∞. Techniques to determine these quantities are discussed in Sec. 2.2.

First Rayleigh-Sommerfeld Formulation

The first Rayleigh-Sommerfeld formulation [7,8] can be used only for plane scatterers. Using this formulation, the complex pressure amplitude in the scattered field can be expressed as

$$P_s(\underline{x}_r) = \frac{1}{2\pi} \iint_{A_\infty} d\underline{x}\, G\left(\frac{\underline{x}_r}{\underline{x}}\right) \frac{\partial P_s}{\partial n}(\underline{x}) \qquad (8)$$

where $G(\underline{x}_r/\underline{x})$ is given by Eq. 5. The exact solution of Eq. 8 will agree identically with that of Eq. 4. However, as we will see, the approximate solutions to Eqs. 4 and 8 will differ somewhat.

Second Rayleigh-Sommerfeld Formulation

The second Rayleigh-Sommerfeld formulation [7,8] is also limited to plane scatterers. Using this formulation the complex pressure amplitude of the scattered field is given by

$$P_s(\underline{x}_r) = \frac{1}{2\pi} \iint_{A_\infty} d\underline{x}\, P_s(\underline{x}) \frac{\partial G}{\partial n}\left(\frac{\underline{x}_r}{\underline{x}}\right) \qquad (9)$$

where $\partial G/\partial n$ is given by Eq. 6.

The exact solution to Eq. 9 will agree identically with the solutions of Eq. 4 or 8. However, approximate solutions for this equation will differ from both the approximate solution of Eq. 4 and that of Eq. 8.

Exact solutions of Eqs. 4, 8 or 9 have been found for only one case — a circular disk with a normally incident plane wave. Numerical techniques to obtain solutions for more general cases have been developed [9,10]. However, these techniques are quite complex and do not necessarily converge to the proper solution.

An approximate solution technique which is commonly used is described in the next Section.

2.2 Approximate Solutions for the Scattering by a Plane Reflector

Approximate solutions for the complex pressure amplitude in the scattered field around a plane reflector can be obtained by making the Kirchhoff approximations [11]. These are

$$\frac{\partial P_s}{\partial n}(\underline{x}) = 0 , \qquad \underline{x} \text{ off the reflector} \tag{10}$$

and

$$P_s(\underline{x}) = P_i(\underline{x}) , \qquad \underline{x} \text{ on the illuminated side of the reflector.} \tag{11}$$

Also, if we take the reflector to be rigid, the particle velocity normal to the reflector will be zero so that

$$\frac{\partial P_s}{\partial n}(\underline{x}) = -\frac{\partial P_i}{\partial n}(\underline{x}) , \qquad \underline{x} \text{ on the reflector} , \tag{12}$$

and finally symmetry for the plane reflector requires that

$$P_s(\underline{x}) = 0 , \qquad \underline{x} \text{ off the reflector} . \tag{13}$$

We can use these four equations for the complex pressure amplitude and its derivative in Eqs. 4, 8 and 9 to obtain approximate solutions.

The Helmholtz-Kirchhoff (HK) formulation, Eq. 4, gives

$$P_s^{HK}(\underline{x}_r) = -\frac{1}{4\pi} \iint_R d\underline{x} \left\{ G\left(\frac{\underline{x}_r}{\underline{x}}\right) \frac{\partial P_i}{\partial n}(\underline{x}) + P_i(\underline{x}) \frac{\partial G}{\partial n}\left(\frac{\underline{x}_r}{\underline{x}}\right) \right\} \tag{14}$$

where $P_s^{HH}(\underline{x}_p)$ is the approximate solution that the complex pressure amplitude of the scattered field, R is the surface of the plane reflector, $P_1(\underline{x})$ is the complex pressure amplitude of the fundamental sound field at point $\underline{x}$ in the plane of the boundary, and the Green's function, G, and its derivative are given by Eqs. 5 and 6 respectively.

The First Rayleigh-Sommerfeld (FRS) formulation, Eq. 8, gives

$$P_s^{FRS}(\underline{x}_p) = -\frac{1}{2\pi} \iint_R dR\, G\left(\frac{\underline{x}_p}{\underline{x}}\right) \frac{\partial P_1}{\partial n}(\underline{x}) \qquad (15)$$

where $P_s^{FRS}(\underline{x}_p)$ is the approximate solution obtained using this formulation and Eqs. 10 and 12.

The Second Rayleigh-Sommerfeld (SRS) formulation, Eq. 9, gives

$$P_s^{SRS}(\underline{x}_p) = -\frac{1}{2\pi} \iint_R dR\, P_1(\underline{x}) \frac{\partial G}{\partial n}\left(\frac{\underline{x}_p}{\underline{x}}\right) \qquad (16)$$

where $P_s^{SRS}(\underline{x}_p)$ is the approximate solution obtained using this formulation and Eqs. 11 and 13.

The average of the approximate solutions from the FRS and SRS formulations is equal to the approximate solution from the HK formulation,

$$P_s^{HH}(\underline{x}_p) = \frac{1}{2}\left\{P_s^{FRS}(\underline{x}_p) + P_s^{SRS}(\underline{x}_p)\right\}. \qquad (17)$$

Therefore, in the future we need calculate only the solutions from the FRS and SRS formulations.

2.2.1 Reflection of the sound waves from a point volume velocity source

The approximate solutions obtained in the last section can be used to predict the reflection by a plane rectangular panel of the sound waves coming from a point source. For this section, we will assume that the panel is rigid. In a future section, we will show that this assumption is not a practical limitation.

The complex pressure amplitude of the sound waves incident on the panel from a point source at point $\underline{x}_s$ is given by

$$P_i(\underline{x}) = A_{pt} \frac{e^{iks}}{s} \tag{18}$$

where $P_i(\underline{x})$ is the complex pressure amplitude of the incident sound waves, A_{pt} is the complex amplitude of the source, and s is the distance from the point $\underline{x}_s$ to point $\underline{x}$. The derivative of the incident complex pressure amplitude is

$$\frac{\partial P_i}{\partial n}(\underline{x}) = A_{pt} \frac{e^{ikx}}{s} \left[ik - \frac{1}{s}\right] \cos\beta_s \tag{19}$$

where β_s is the angle between a line connecting point $\underline{x}$ and point $\underline{x}_s$ and a normal to the panel, $0 < \beta_s < 90°$. The geometry for this problem is shown in Fig. 7.

The FRS approximate solution for the problem being considered is

$$P_s^{FRS}(\underline{x}_p) = -\frac{A_{pt}}{2\pi} \iint_R d\underline{x} \frac{e^{ik(s+r)}}{sr} \left[ik - \frac{1}{s}\right] \cos\beta_s \tag{20}$$

where $P_s^{FRS}(\underline{x}_p)$ is the complex amplitude of the scattered field.

The SRS approximate solution for the scattered pressure amplitude for this problem is

$$P_s^{SRS}(\underline{x}_p) = -\frac{A_{pt}}{2\pi} \iint_R d\underline{x} \frac{e^{ik(s+r)}}{rs} \left[ik - \frac{1}{r}\right] \cos\beta_r \tag{21}$$

where β_r is the angle between a line from the point $\underline{x}_p$ to point $\underline{x}$ and a line normal to the panel.

Evaluation of Eq. 20 or 21 requires that we select a coordinate system in which to carry out the surface integral. It is most convenient to use a Cartesian coordinate system since we are

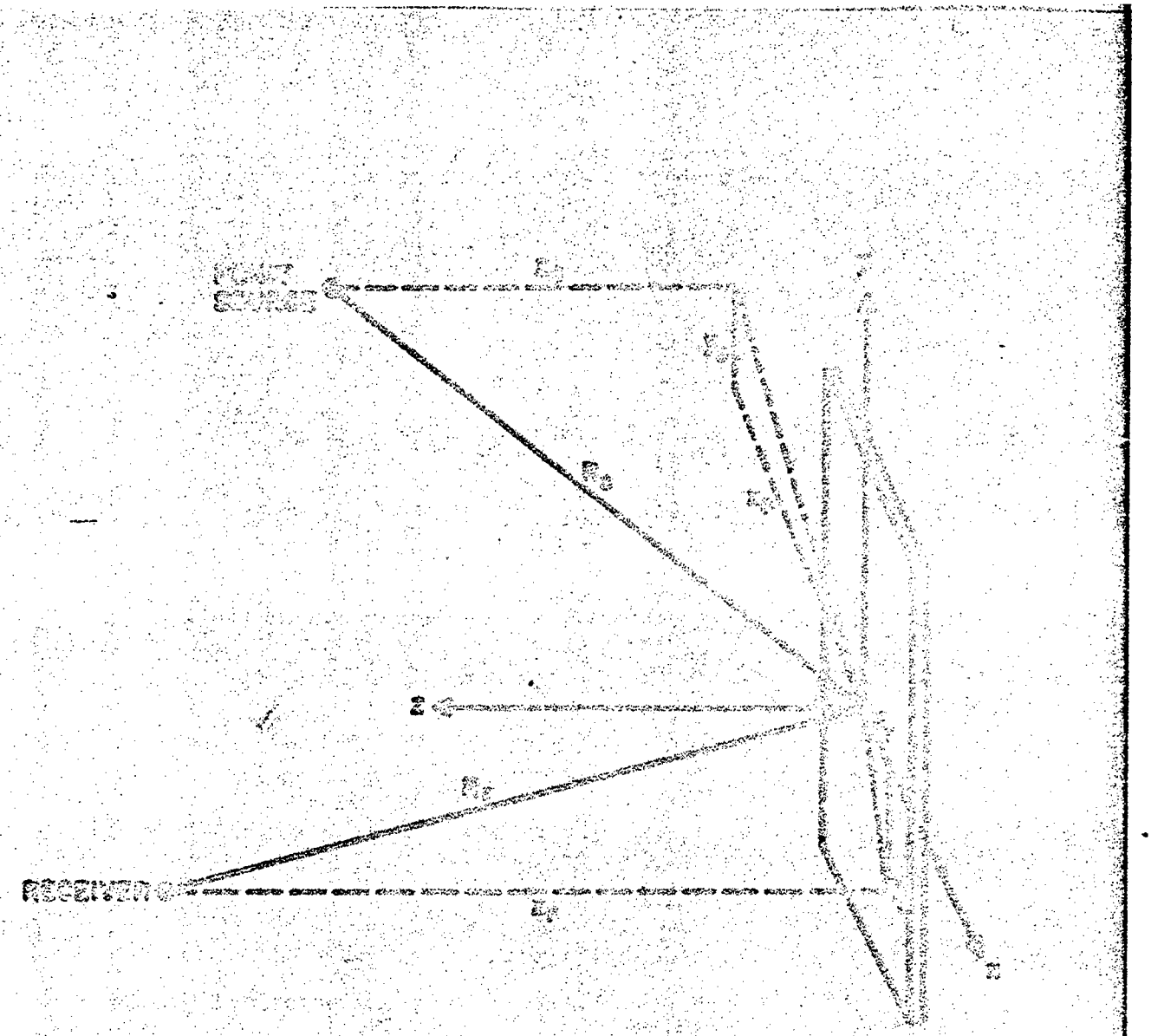

FIG. 7 POINT SOURCE GEOMETRY.

studying rectangular panels. We will use Cartesian coordinates x, y, and z with the origin at the center of the panel as shown in Fig. 7. The location of the source will be given by the coordinates x_s, y_s, and z_s. The location of the receiver point will be given by the coordinates x_r, y_r, and z_r. A location on the panel surface will be specified by coordinates x and y. In terms of these coordinates, the distance, s, is given by

$$s = \left[(x_s-x)^2 + (y_s-y)^2 + (z_s)^2\right]^{1/2} \tag{22}$$

The distance r is given by

$$r = \left[(x_r-x)^2 + (y_r-y)^2 + (z_r)^2\right]^{1/2} \tag{23}$$

The terms $\cos\beta_s$ in Eq. 20 and $\cos\beta_r$ are given by

$$\cos\beta_s = \frac{z_s}{s} \tag{24}$$

and

$$\cos\beta_r = \frac{z_r}{r} . \tag{25}$$

For some applications it will be convenient to represent the source and receiver point in a spherical coordinate system with its origin at the center of the panel, as shown in Fig. 8. The Cartesian coordinates x_s, y_s and z_s are given in terms of the spherical coordinates by

$$x_s = R_s \sin\theta_s \cos\phi_s$$

$$y_s = R_s \sin\theta_s \sin\phi_s$$

$$z_s = R_s \cos\theta_s \tag{26}$$

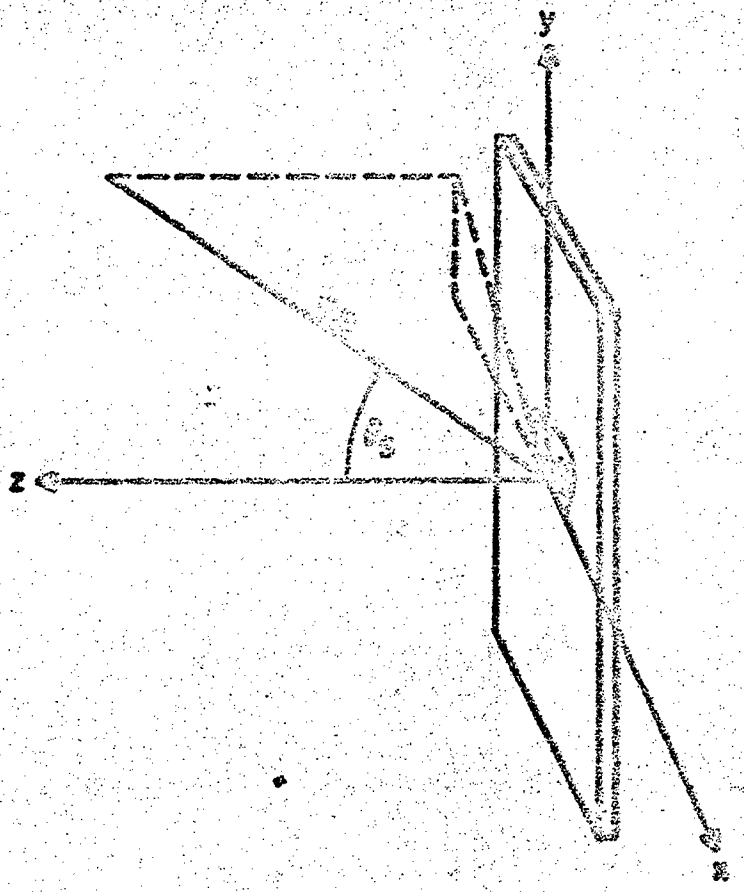

FIG. 8 CARTESIAN AND SPHERICAL COORDINATE SYSTEMS.

where R_s is the distance from the center of the panel to the source and the angles θ_s and ϕ_s are defined in Fig. 8. A similar set of equations can be written for the coordinates x_r, y_r and z_r,

$$x_r = R_r \sin\theta_r \cos\phi_r$$

$$y_r = R_r \sin\theta_r \sin\phi_r$$

$$z_r = R_r \cos\theta_r \tag{27}$$

The distances s and r can be written after some algebraic manipulation in terms of these spherical coordinates as

$$s = R_s\left[1 - \frac{2(x \sin\theta_s \cos\phi_s + y \sin\theta_s \sin\phi_s)}{R_s} + \frac{x^2+y^2}{R_s^2}\right]^{1/2} \tag{28}$$

and

$$r = R_r\left[1 - \frac{2(x \sin\theta_r \cos\phi_r + y \sin\theta_r \sin\phi_r)}{R_r} + \frac{x^2+y^2}{R_r^2}\right]^{1/2} \tag{29}$$

Selection of the Cartesian coordinates for the source and receiver points or the spherical coordinates for these points depends simply on relative convenience. As we will see, the use of spherical coordinates allows us to use the point source solutions for the case of an incident plane wave.

2.2.2 Reflection of a plane sound wave

The complex pressure amplitude of an incident plane wave is given by

$$P_i(\underline{x}) = A_{plane}\, e^{-ik(x \sin\theta_i \cos\phi_i + y \sin\theta_i \sin\phi_i + z \cos\theta_i)} \tag{30}$$

where A_{plane} is the complex amplitude of the plane wave, θ_i and ϕ_i are angles defining the direction of propagation of the wave as

shown in Fig. 9, and x, y and n define a Cartesian coordinate system with an origin at the center of the panel. The normal derivative of the incident complex pressure amplitude evaluated in the plane of the panel, z = 0, is given by

$$\frac{\partial P_i}{\partial n}(\underline{x}) = iA_{plane} k \cos\theta \, e^{-ik(x \sin\theta_i \cos\phi_i + y \sin\theta_i \sin\phi_i)} \tag{31}$$

where point $\underline{x}$ is on the panel.

By using Eq. 31 in Eq. 15 we obtain for the FRS approximate solution

$$p_s^{FRS}(\underline{x}_p) = -\frac{iA_{plane}}{2\pi} k \cos\theta_i \iint_R dxdy \, \frac{e^{ikr}}{r} \, e^{-ik(x \sin\theta_i \cos\phi_i + y \sin\theta_i \sin\phi_i)} \tag{32}$$

where r is given by Eq. 23 or 29. The SRS approximate solution is found by using Eq. 30 in Eq. 16,

$$p_s^{SRS}(\underline{x}_p) = -\frac{A_{plane}}{2\pi} \iint_R dxdy \, \frac{e^{ikr}}{r} \left[ik - \frac{1}{r}\right] \cos\theta_r \, e^{-ik(x \sin\theta_i \cos\phi_i + y \sin\theta_i \sin\phi_i)} . \tag{33}$$

Equations 32 and 33 for plane wave incidence can also be obtained from our solutions for a point source by letting the distance from the center of the panel to the point source go to infinity while the point source strength goes to infinity such that

$$A_{pt} \frac{e^{ikR_s}}{R_s} = A_{plane} \quad \text{as} \quad R_s \to \infty \tag{34}$$

where A_{plane} is a constant.

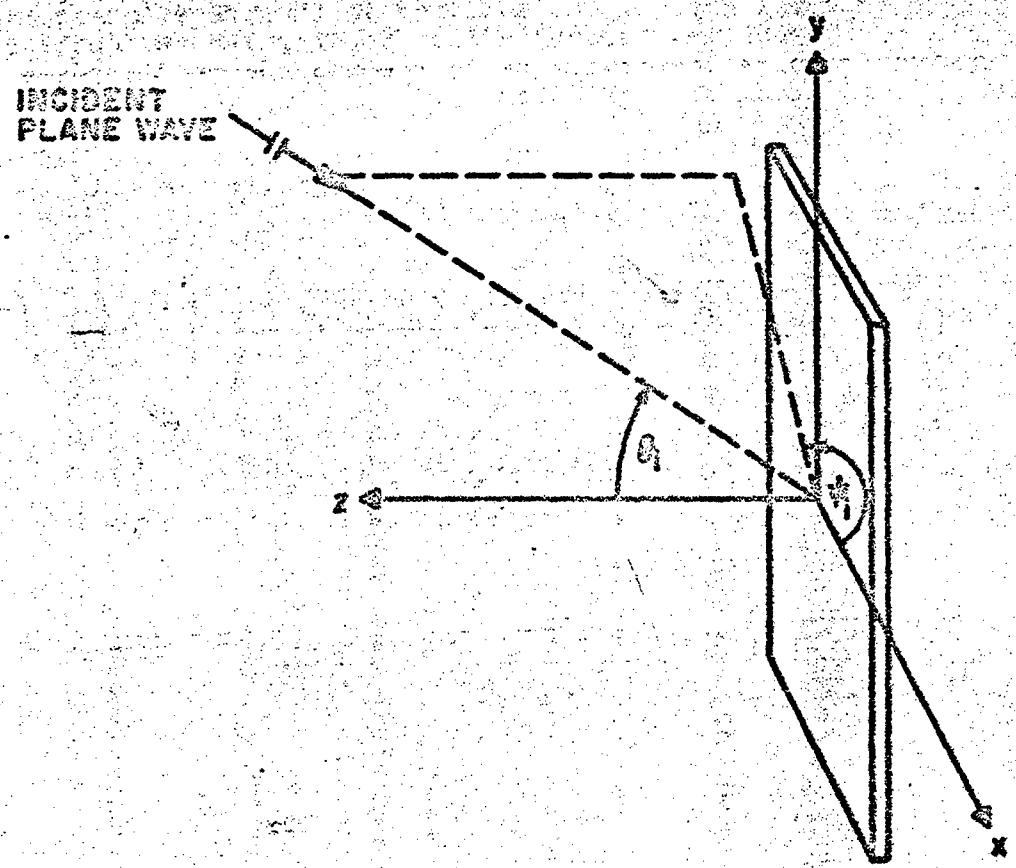

FIG. 9 PLANE WAVE GEOMETRY.

2.3 Scattering Solutions for the Far Field

The integral expressions obtained in the preceding sections for the scattered field around a flat rectangular reflector can be evaluated analytically if the source and the receiver are sufficiently far from the reflector.

To evaluate the surface integrals required for the PMS and SBS approximate solutions, we will make approximations in the distances s and r. The distance s is given by Eq. 35,

$$s = R_s\left[1 - \frac{2(x\sin\theta_s\cos\phi_s + y\sin\theta_s\sin\phi_s)}{R_s} + \frac{x^2+y^2}{R_s^2}\right]^{1/2} \qquad (35)$$

where x and y are points on the panel and R_s, θ_s and ϕ_s are spherical coordinates identified in Fig. 8. When R_s is large in comparison to the panel dimensions we can expand s in a power series in x/R_s and y/R_s ,

$$s = R_s\left[1 - \frac{x\sin\theta_s\cos\phi_s + y\sin\theta_s\sin\phi_s}{R_s} + \frac{x^2+y^2}{2R_s^2}\right.$$

$$\left. - \frac{1}{2}\left(\frac{x\sin\theta_s\cos\phi_s + y\sin\theta_s\sin\phi_s}{R_s}\right)^3 + - - -\right] . \qquad (36)$$

Similarly, we can expand R in a power series in x/R_r and y/R_r

$$r = R_r\left[1 - \frac{x\sin\theta_r\cos\phi_r + y\sin\theta_r\sin\phi_r}{R_r} + \frac{x^2+y^2}{2R_r^2}\right.$$

$$\left. - \frac{1}{2}\left(\frac{x\sin\theta_r\cos\phi_r + y\sin\theta_r\cos\phi_r}{R_r}\right)^2 + - - -\right] . \qquad (37)$$

To evaluate the integrals for the FRS and SRS approximate solutions we will assume that R_s and R_r are sufficiently large that we can drop the higher order terms in the series expansion. We can then make the following approximations,

$$\frac{1}{s} \approx \frac{1}{R_s}, \qquad \text{if } R_s >> L \ , \tag{38}$$

$$\frac{1}{r} \approx \frac{1}{R_r}, \qquad \text{if } R_r >> L \ , \tag{39}$$

$$ik >> \frac{1}{s} \ , \qquad \text{if } k >> \frac{1}{R_s} , \tag{40}$$

$$ik >> \frac{1}{r} \ , \qquad \text{if } k >> \frac{1}{R_r} , \tag{41}$$

$$\cos\beta_s \approx \cos\theta_s , \qquad \text{if } R_s >> L \ , \tag{42}$$

$$\cos\beta_r \approx \cos\theta_r , \qquad \text{if } R_s >> L \ , \tag{43}$$

where L is the minimum dimension of the panel. The conditions for these approximations require that the distances from the source to the panel and the receiver to the panel be much larger than both the panel size and an acoustic wavelength. With these approximations the FRS approximate solution from Eq. 20 becomes

$$p_s^{FRS}(\underline{x}_r) = -\frac{A_{pt}}{2\pi} ik \cos\theta_s \frac{e^{ik(R_s+R_r)}}{R_s R_r} \int_{-L_x/2}^{L_x/2} dx \int_{-L_y/2}^{L_y/2} dy \, e^{ikf(x,y)} \tag{44}$$

where L_x and L_y are the dimensions of the panel and

$$f(x,y) = -(x \sin\theta_r \cos\psi_r + y \sin\theta_r \sin\psi_r)$$

$$-(x \sin\theta_s \cos\psi_s + y \sin\theta_s \sin\psi_s)$$

$$+ \frac{x^2+y^2}{2R_s} + \frac{x^2+y^2}{2R_r} - \frac{(x \sin\theta_r \cos\psi_r + y \sin\theta_r \sin\psi_r)^2}{2R_r}$$

$$- \frac{(x \sin\theta_s \cos\psi_s + y \sin\theta_s \sin\psi_s)^2}{2R_s} + \text{---} \; . \qquad (45)$$

If we keep only the first two terms of Eq. 45 in evaluating the surface integrals, we obtain the Frauenhofer or far-field solution. If we keep the first six terms of Eq. 45, we obtain the Fresnel solution. Fortunately, the simpler of these two solutions — the Frauenhofer solution — is of great practical use for scattering problems. The condition required to ignore all but the first two terms in Eq. 45 is that

$$k\left[\frac{x^2+y^2}{2R_s} + \frac{x^2+y^2}{2R_r} - \frac{(x \sin\theta_r \cos\psi_r + y \sin\theta_r \sin\psi_r)^2}{2R_r}\right.$$

$$\left. - \frac{(x \sin\theta_s \cos\psi_s + y \sin\theta_s \sin\psi_s)^2}{2R_s}\right] << \pi/2 \; . \qquad (46)$$

This condition will be met if

$$R_s >> \frac{k}{4\pi} (L_x^2 + L_y^2)$$

and

$$R_r >> \frac{k}{4\pi} (L_x^2 + L_y^2) \; . \qquad (47)$$

Note that as the acoustic wavenumber gets large at high frequencies, the region of validity of the far-field solution is limited to distances far from the panel. The familiar geometric effects in optics are not contained in the far-field solution.

A far field evaluation of the FRS formulation can be found by evaluating the surface integral in Eq. 44,

$$P_s^{FRS}(\underline{x}_r) = -\frac{2A_{pt}ik}{\pi}\frac{e^{ik(R_s+R_r)}}{R_sR_r}G(\underline{x}_r,\underline{x}_s)\cos\theta_s \qquad (48)$$

where $\underline{x}_r$ is in the far field and

$$-G(\underline{x}_r,\underline{x}_s) = \frac{\sin\frac{kL_x}{2}(\sin\theta_r\cos\psi_r + \sin\theta_s\cos\psi_s)}{k(\sin\theta_r\cos\psi_r + \sin\theta_s\cos\psi_s)}$$

$$\frac{\sin\frac{kL_y}{2}(\sin\theta_r\sin\psi_r + \sin\theta_s\sin\psi_s)}{k(\sin\theta_r\sin\psi_r + \sin\theta_s\sin\psi_s)} \qquad (49)$$

The procedure followed in the preceding paragraphs can also be followed to obtain a far field evaluation for the SRS formulation. The result is

$$P_s^{SRS}(\underline{x}_r) = -\frac{2A_{pt}ik}{\pi}\frac{e^{ik(R_s+R_r)}}{R_sR_r}G(\underline{x}_r,\underline{x}_s)\cos\theta_r \qquad (50)$$

where $\underline{x}_r$ is in the far field and G is given by Eq. 49.

Far field solutions for scattering of an incident plane wave can be obtained from Eqs. 48 and 50 by setting

$$A_{pt}\frac{e^{ikR_s}}{R_s} = A_{plane} \qquad (51)$$

where A_{plane} is the complex amplitude of the incident plane wave. The angles θ_s and ψ_s in Eqs. 48, 49, and 50 define the direction of propagation of the plane wave.

In many cases we will not be interested in the phase characteristics in the scattered pressure field, but will need only the

mean-square pressure. The mean-square pressure can be found from the complex pressure amplitude by using the relation

$$\langle p_s^2 \rangle_t = \frac{1}{2} |p_s|^2 \tag{52}$$

where $\langle p_s^2 \rangle_t$ is the mean-square pressure and $|\ |$ signifies "the magnitude of". The mean-square pressure from the FRS approximate formulation, Eq. 48, is

$$\langle p_s^2 \rangle_t^{FRS} = \frac{2|A_{pt}|^2 k^2}{\pi^2 R_s^2 R_r^2} G^2(\underline{x}_r, \underline{x}_s) \cos^2\theta_s \ . \tag{53}$$

The mean-square pressure from the SRS approximate formulation, Eq. 50, is

$$\langle p_s^2 \rangle_t^{SRS} = \frac{2|A_{pt}|^2 k^2}{\pi^2 R_s^2 R_r^2} G^2(\underline{x}_r, \underline{x}_s) \cos^2\theta_r \ . \tag{54}$$

In a previous section we showed that the complex pressure amplitude from the approximate HK formulation is the average of the complex pressure amplitudes from the approximate FRS and SRS formulations. The far field evaluations of the FRS and SRS formulations, Eqs. 48 and 50, differ only by the angle of the cosine factor. Therefore, in the far field the root-mean-square (rms) pressure from the HK formulation is the average of the rms pressures from the other two formulations,

$$P_{s,rms}^{HK} = \frac{1}{2}\left[P_{s,rms}^{FRS} + P_{s,rms}^{SRS}\right] . \tag{55}$$

To illustrate the far-field solutions we have calculated the pressure field reflected by a 4 ft sq panel. The angle of incidence of the incident sound waves was taken to be zero-normal incidence. The normalized pressure amplitudes of the reflected field are plotted in Figs. 10, 11, and 12 as a function of receiver angle θ_r and the frequency of the incident sound waves. The angle ψ_r is taken to be zero. The pressure amplitudes are normalized since we have plotted 20 $LOG_{10}[8\pi \cos\theta_s/L^2]$, 20 $LOG_{10}[8\pi \cos\theta_r/L^2]$, and

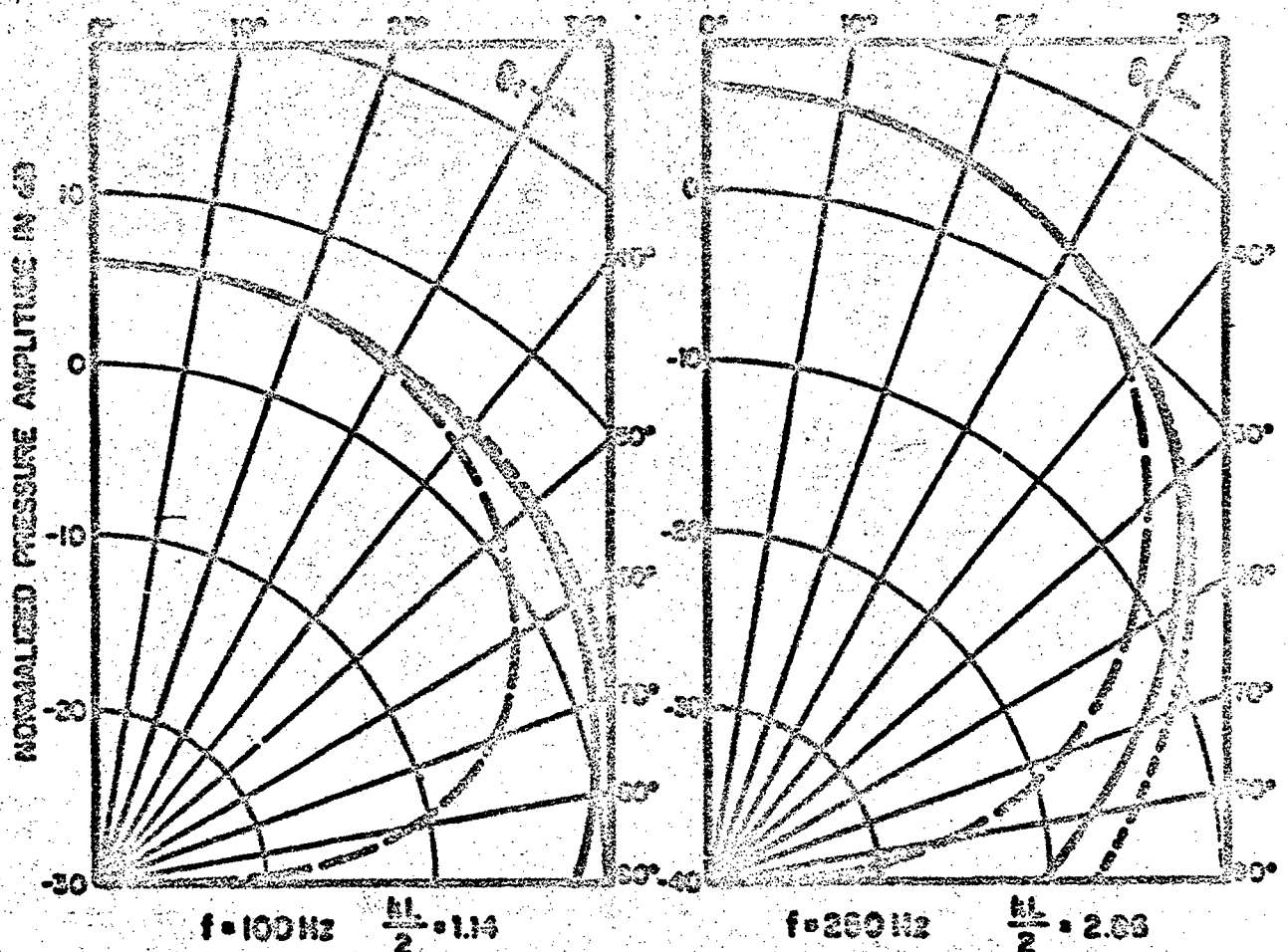

AMPLITUDES ARE NORMALIZED TO REMOVE DECREASE IN AMPLITUDE DUE TO SPHERICAL SPREADING OF THE REFLECTED FIELD

FIG. 10 REFLECTED FARFIELD PRESSURE AMPLITUDES OBTAINED FROM THE THREE APPROXIMATE FORMULATIONS.

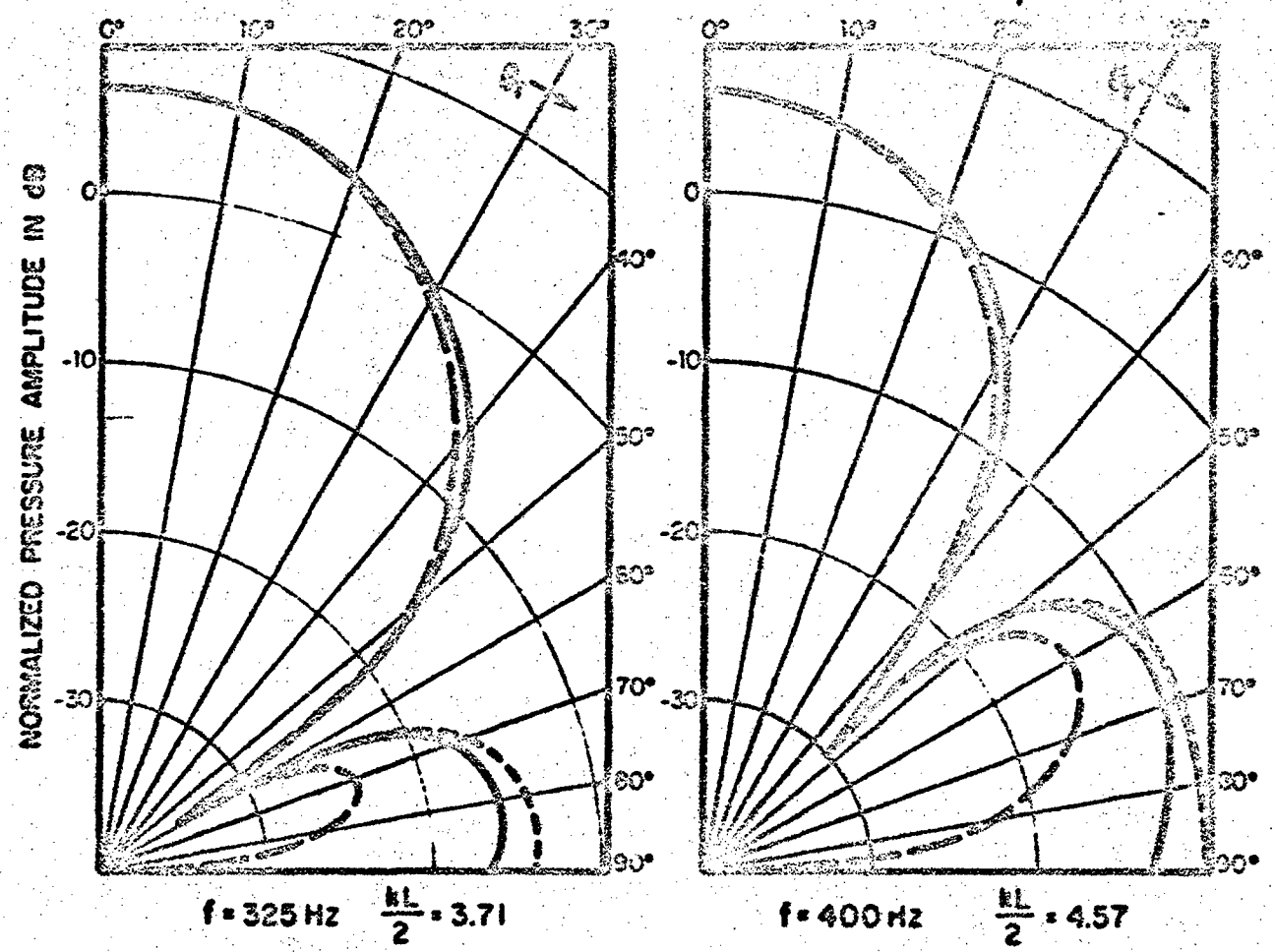

AMPLITUDES ARE NORMALIZED TO REMOVE DECREASE IN AMPLITUDE DUE TO SPHERICAL SPREADING OF THE REFLECTED FIELD

FIG. 11 REFLECTED FARFIELD PRESSURE AMPLITUDES OBTAINED FROM THE THREE APPROXIMATE FORMULATIONS.

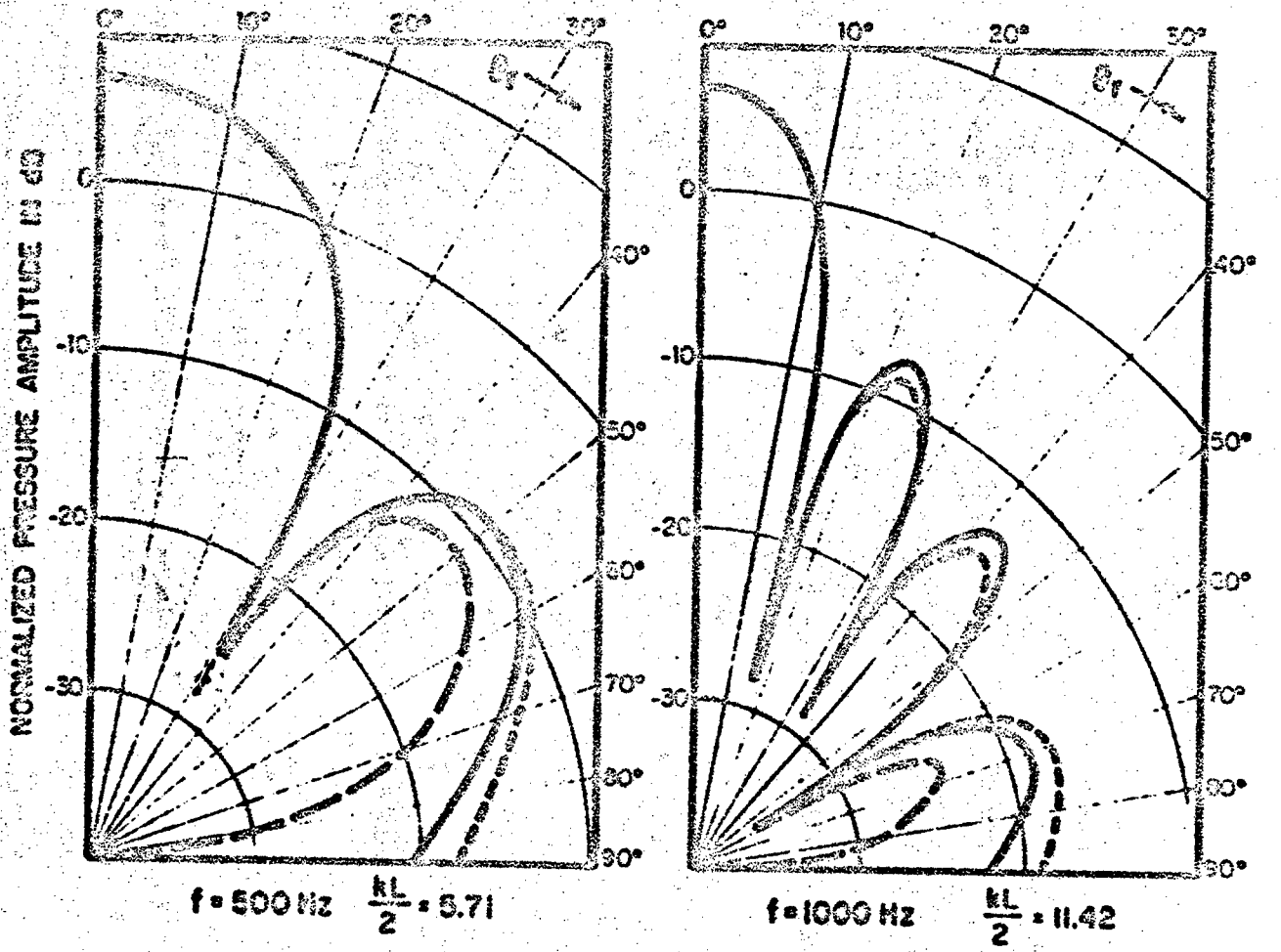

FAR FIELD SOLUTIONS

- HELMHOLTZ-KIRCHHOFF
- FIRST SOMMERFELD
- SECOND SOMMERFELD

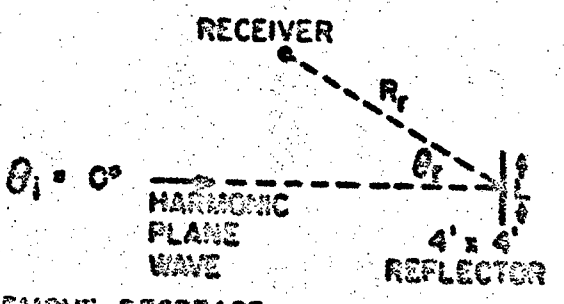

AMPLITUDES ARE NORMALIZED TO REMOVE DECREASE IN AMPLITUDE DUE TO SPHERICAL SPREADING OF THE REFLECTED FIELD

FIG. 12 REFLECTED FARFIELD PRESSURE AMPLITUDES OBTAINED FROM THE THREE APPROXIMATE FORMULATIONS.

$20 \log_{10}[4Q(\cos\theta_s + \cos\theta_r)/L^2]$, for the FRS, the SRS, and the KH approximate formulations.

The three different formulations for the reflected pressure amplitude give identical results for $\theta_r = 0$ and agree closely for angles up to 45°. Consideration of Eqs. 40 and 50 indicates a general result – the three different formulations for the reflected pressure amplitude in the far field give the same result for $\theta_r = \theta_s$, i.e., specular reflection. The reflected pressure amplitude will be greatest also at $\theta_r = \theta_s$. Thus, if we are only interested in locations where the reflected pressures are large, we can use any of the three formulations. The question as to which formulation gives more accurate results when $\theta_r \neq \theta_s$ has never been satisfactorily answered. We know that the reflected pressure at $\theta_r = 90°$ must be zero because of the symmetry of the flat panel scattering problem. This tends to favor use of the SRS approximate formulation. However, we also know that the reflected pressure for all θ_r will be zero if $\theta_s = 90°$. This favors the FRS formulation. A satisfactory solution is probably to use the SRS formulation when θ_r is large.

At low frequencies the reflected pressure amplitude does not vary significantly as a function of θ_r. However, at higher frequencies the reflected pressure amplitude shows a number of minima or nulls at different values of θ_r. The number of nulls is equal to the integer part of the length of the panel divided by the acoustic wavelength,

$$N = \text{I.P.}\ \frac{L}{\lambda} \qquad (56)$$

where λ is the acoustic wavelength and N is the number of nulls. Strictly speaking, Eq. 56 is only valid when $\theta_s = 0$. It will give a reasonable approximation, however, for other values of θ_s. The location of each null is frequency dependent and tends to smaller angles as frequency increases. Therefore, if we average the reflected pressure over bands of frequencies, the nulls disappear. This result will be shown in a future section when we consider the reflection of random noise.

The pressure amplitudes plotted in Figs. 10, 11 and 12 are normalized so that the value at $\theta_r = 0$ is the same for every

frequency. The unnormalized pressure amplitude increases with k^2 or equivalently f^2 since

$$k = \frac{2\pi f}{c_s} \tag{57}$$

where k is the acoustic wavenumber, f is the frequency, and c_s is the speed of sound. To show more clearly the frequency dependence we consider the case of a plane wave normally incident on a 4 ft by 4 ft panel. For this case we normalize the pressure amplitude by the factor $R_r|A_{plane}|$ where $|A_{plane}|$ is the magnitude of the complex pressure amplitude of the plane wave, i.e., the pressure amplitude. The pressure amplitudes normalized in this way are plotted in Fig. 13 for various frequencies. At low frequencies the reflected pressure amplitude is small and not strongly dependent on the angle θ_r. At higher frequencies a large peak at $\theta_r = 0$ develops.

For other angles of incidence the peak in the reflected pressure amplitude will occur at the specular angle of reflection, $\theta_r = \theta_s$ and $\phi_r = \phi_s + 180°$. The amplitude of the reflected pressure at this peak is given by

$$|P_s(R_r, \theta_r = \theta_s, \phi_r = \phi_s + 180°)| = \frac{|A_{pt}|}{2\pi} k \frac{L_x L_y}{R_s R_r} \cos\theta_s \tag{58}$$

where $|P_s|$ is the amplitude of the reflected pressure at the specular angle and $|A_{pt}|$ is the amplitude of the point source. Equation 58 is valid for any of the three formulations. Note that the peak of the reflected pressure amplitude varies with $L_x L_y \cos\theta_s$, the projected area of the panel on a surface normal to the direction of propagation of the incident sound waves.

The calculations used to illustrate the far-field solutions have been somewhat impractical since θ_s has been taken to be zero. It is intended only that they illustrate the type of solutions which are obtained. More practical calculations of the reflected field pressures are presented in Part 4 of this report.

The importance of the far-field solutions will become evident in future sections. We will find that the far-field solution is a reasonable approximation to the exact evaluation of the

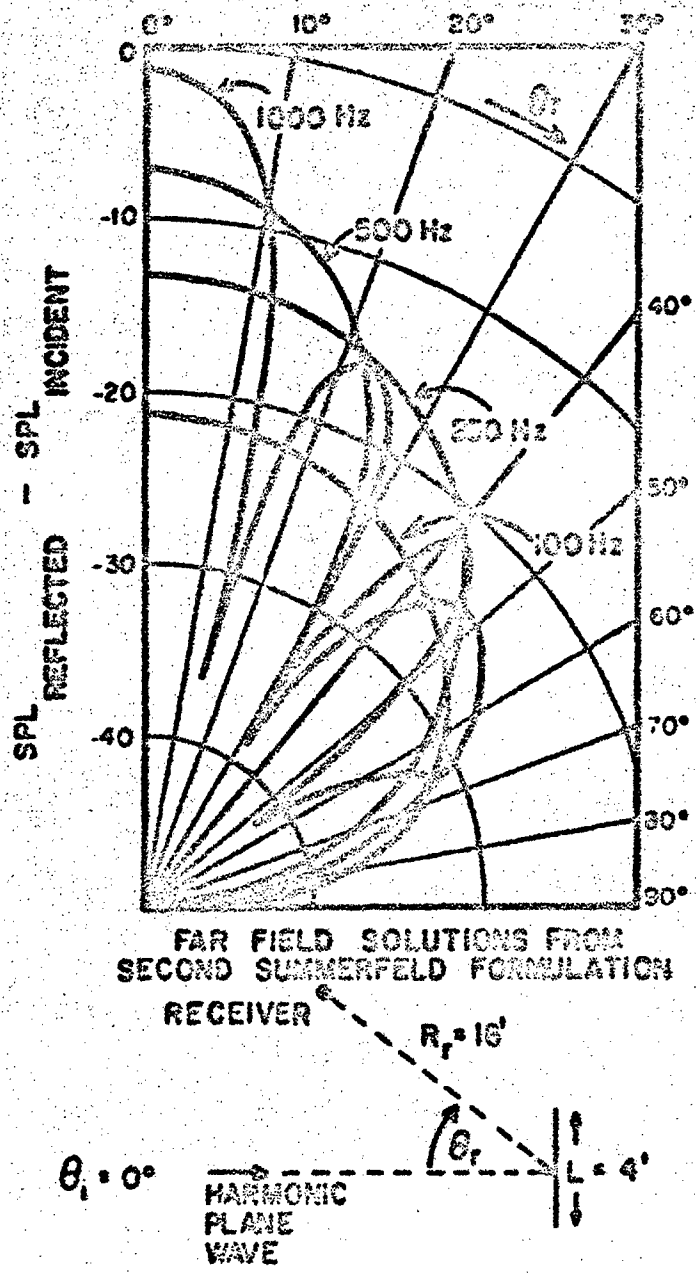

FIG. 13 REFLECTED FARFIELD PRESSURE AMPLITUDES OBTAINED FROM THE SECOND SOMMERFELD FORMULATION.

integral expressions for the FRS and SRS formulations even when the receiver point is fairly close to the panel. Then we will use the far field solutions to calculate the total acoustic power reflected and the directivity of that power.

2.4 Scattering Solutions for the Near Field

The integral expressions obtained in Secs. 2.1 and 2.2 for the scattered field around a flat rectangular reflector must be evaluated numerically when the receiver point is close to the reflector.

The scattered complex pressure amplitude around a flat reflector is given by the FRS formulation, the SRS formulation or the HK formulation. To illustrate the numerical evaluation of these expressions we will consider the SRS formulation for the reflection of an incident plane wave. The integral expression for this case is given by Eq. 33, repeated below

$$p_s^{SRS}(\underline{x}_r) = -\frac{A_{plane}}{2\pi} \iint_R dxdy \, \frac{e^{ikr}}{r} \left[ik - \frac{1}{r}\right] \cos\beta_r$$

$$e^{-ik(x \sin\theta \cos\psi + y \sin\theta \sin\psi)} \quad (33)$$

A numerical evaluation of the surface integral in Eq. 33 requires that we replace the integral by a summation of terms. Toward this end we let

$$x_i = iD \frac{L_x}{2} - \frac{D}{2} \quad (59)$$

where D is the step size, L_x is the length of one side of the reflector and $1 \leq i \leq L_x/D$. Similarly we let

$$y_j = jD - \frac{L_y}{2} - \frac{D}{2} \quad (60)$$

with $1 \leq j \leq L_y/D$. Then the Eq. 33 can be written as

$$P_s^{SRS}(\underline{x}_r) = -\frac{A_{plane}}{2\pi} D^2 \sum_{i=1}^{L_x/D} \sum_{j=1}^{L_y/D} \frac{e^{ikr_{ij}}}{r_{ij}} \left[ik - \frac{1}{r_{ij}}\right]$$

$$\cos\beta_{r_{ij}} e^{-ik(x_i \sin\theta \cos\psi + y_i \sin\theta \sin\psi)} \quad . \qquad (61)$$

where x_i and y_i are given by Eqs. 59 and 60, r_{ij} is found from Eq. 23,

$$r_{ij} = \left[(x_r - x_i)^2 + (y_r - y_j)^2 + (z_r)^2\right]^{1/2} \qquad (62)$$

and

$$\cos\beta_{r_{ij}} = \frac{z_r}{r_{ij}} \quad . \qquad (63)$$

The summation in Eq. 61 will be a good approximation to the surface integral if the step size D is made small enough so that the integrand does not vary significantly between steps. Unless $\underline{x}_r$ is very close to the reflector, the most rapidly varying term in the integrand of Eq. 33 is the complex exponential term. This term will not vary from step to step if we make the step size small in comparison to an acoustic wavelength,

$$D << \lambda_0 \quad , \qquad (64)$$

where λ_0 is the acoustic wavelength. By varying the step size we found that accurate numerical evaluation could be obtained by making the step size less than one-half the acoustic wavelength or one-half the panel dimension whichever is smaller. The step size must be such that L_x/D and L_y/D are integers.

The double summation in Eq. 61 can be carried out easily using a digital computer. At high frequencies where the acoustic wavelength is small compared to the panel dimensions, a large number of steps in the summation are required and the computation time becomes long.

It should be pointed out that the exact evaluations of the integral expression given by Eq. 33 are not exact solutions to the scattering problem since Eq. 33 is in itself an approximation to the exact solution.

Numerical evaluations of the SRS approximate formulation for plane wave incidence on a 4-ft square reflector are presented in Figs. 14, 15, and 16. The angle of incidence was taken to be zero. The pressure amplitudes plotted in these figures have been normalized to remove the decrease in amplitude due to spherical spreading. The normalization is accomplished by multiplying the actual pressure amplitude by the factor

$$\frac{\pi}{2} \frac{R_r}{|A_{plane}|k} \tag{65}$$

where $|A_{plane}|$ is the amplitude of the incident plane wave. The numerical evaluations can be compared with the far-field expressions when we use the above normalization. The numerical evaluations for $R_r = 50$ ft agree almost exactly with the far-field solution. However, for $R_r = 8$ ft the numerical evaluations are as much as 15 dB below the far-field solutions.

The accuracy of the far-field solutions as a function of distance R_r and frequency is shown in Fig. 17. This curve was established by comparing the numerical evaluations with the far-field solutions for θ_r and θ_i equal to zero. However, the plot is probably also valid for other values of the angle of incidence θ_i as long as $\theta_r = \theta_i$ and $\phi_r = \phi_i + 180°$, i.e., as long as we consider only specular reflection.

The numerical evaluations for the near-field pressure amplitude will be used in Sec. III of this report to obtain theoretical predictions which can be compared with data obtained in an experimental study.

2.5 The Effect of Panel Response on the Reflected Pressure Field

The results presented in previous sections were, strictly speaking, valid only for rigid panels. We will show in this section that the panel response has no significant effect on the reflected pressure field. The panel response will, however, be important in designing a reflector which will not fatigue under an intense sonic environment.

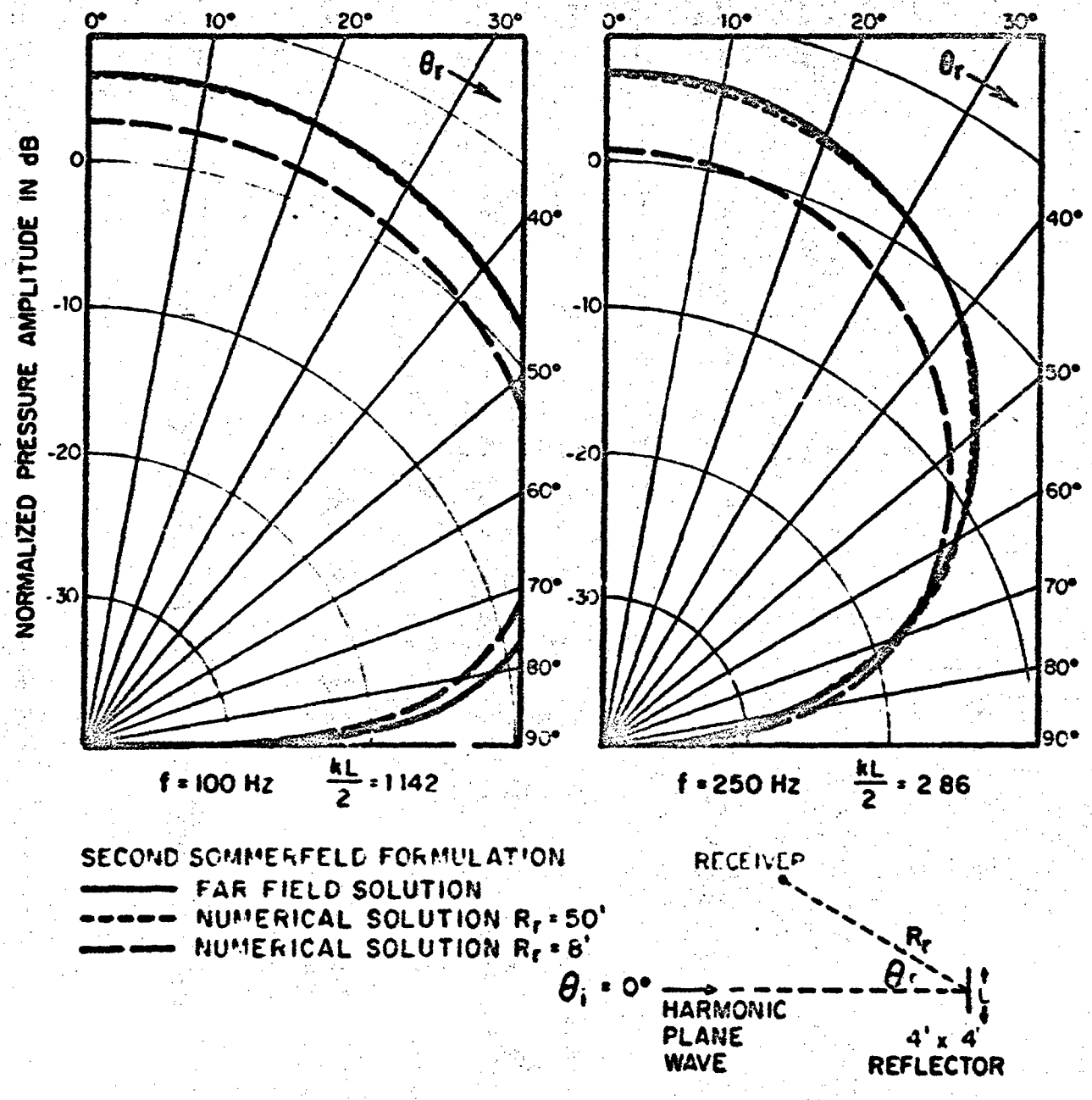

FIG. 14 COMPARISON OF THE REFLECTED PRESSURE AMPLITUDES IN THE FAR- AND NEAR-FIELDS.

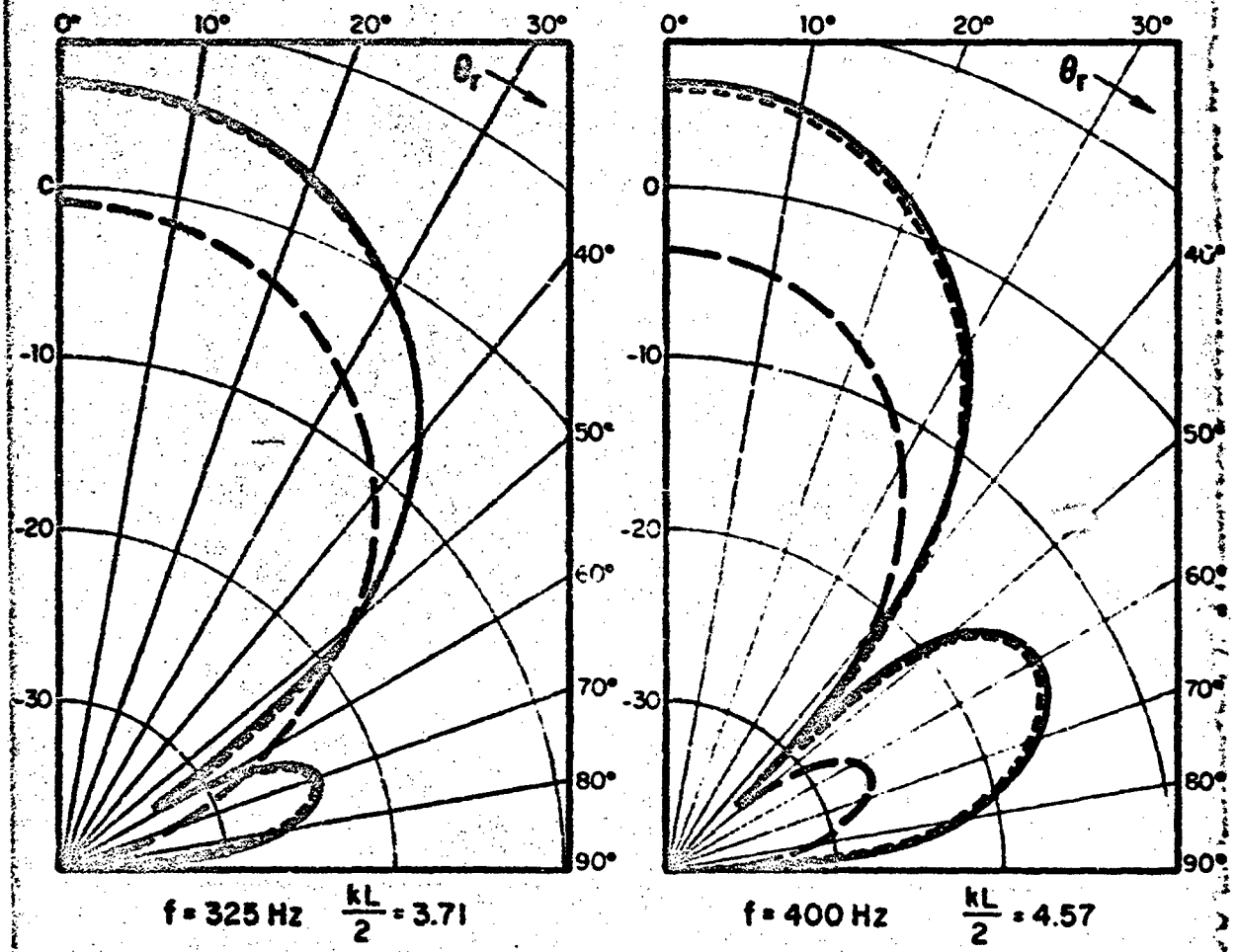

FIG. 15 COMPARISON OF THE REFLECTED PRESSURE AMPLITUDES IN THE FAR- AND NEAR-FIELDS.

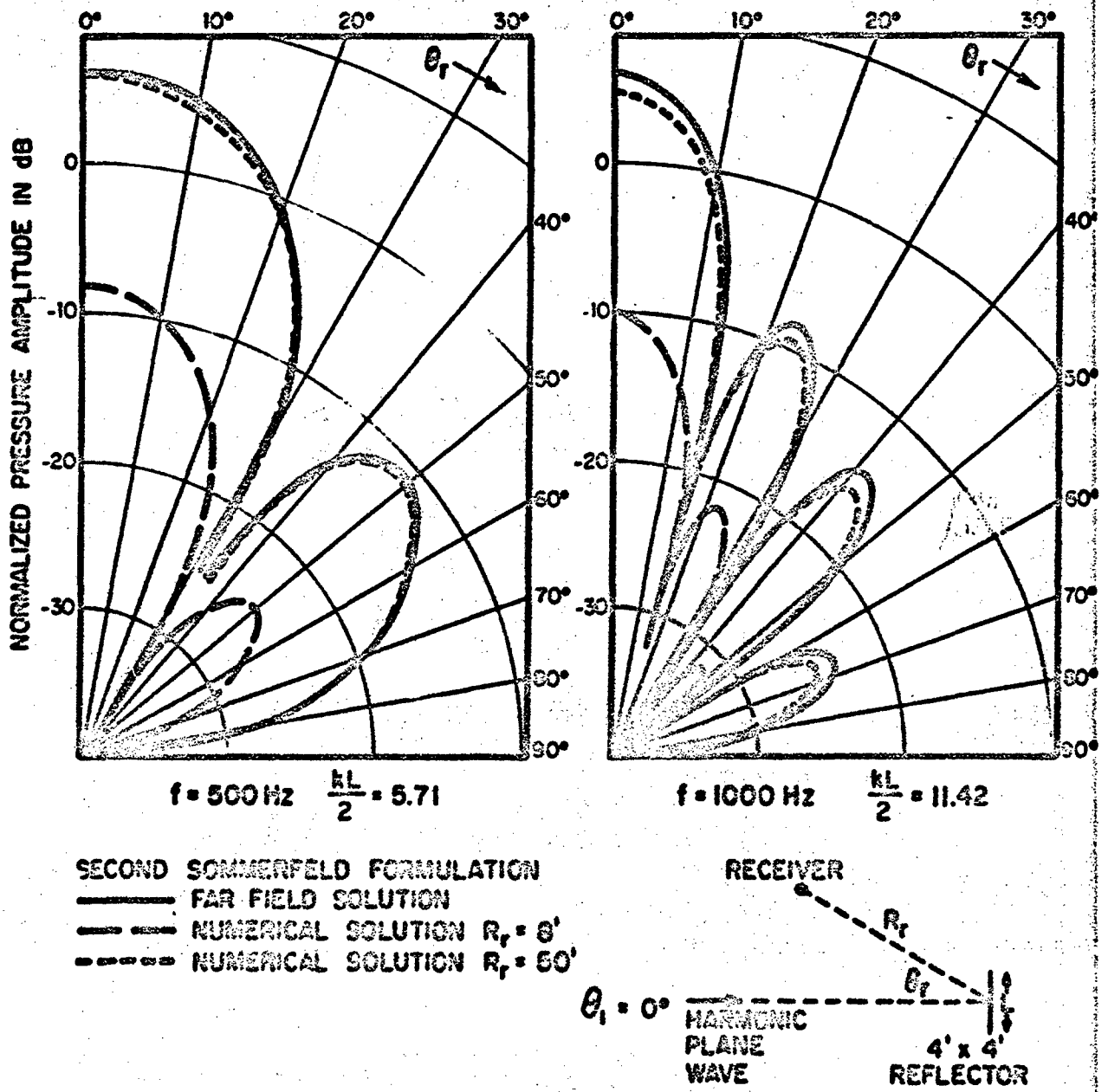

AMPLITUDES ARE NORMALIZED TO REMOVE DECREASE IN AMPLITUDE DUE TO SPHERICAL SPREADING OF THE REFLECTED FIELD

FIG. 16 COMPARISON OF THE REFLECTED PRESSURE AMPLITUDES IN THE FAR- AND NEAR-FIELDS.

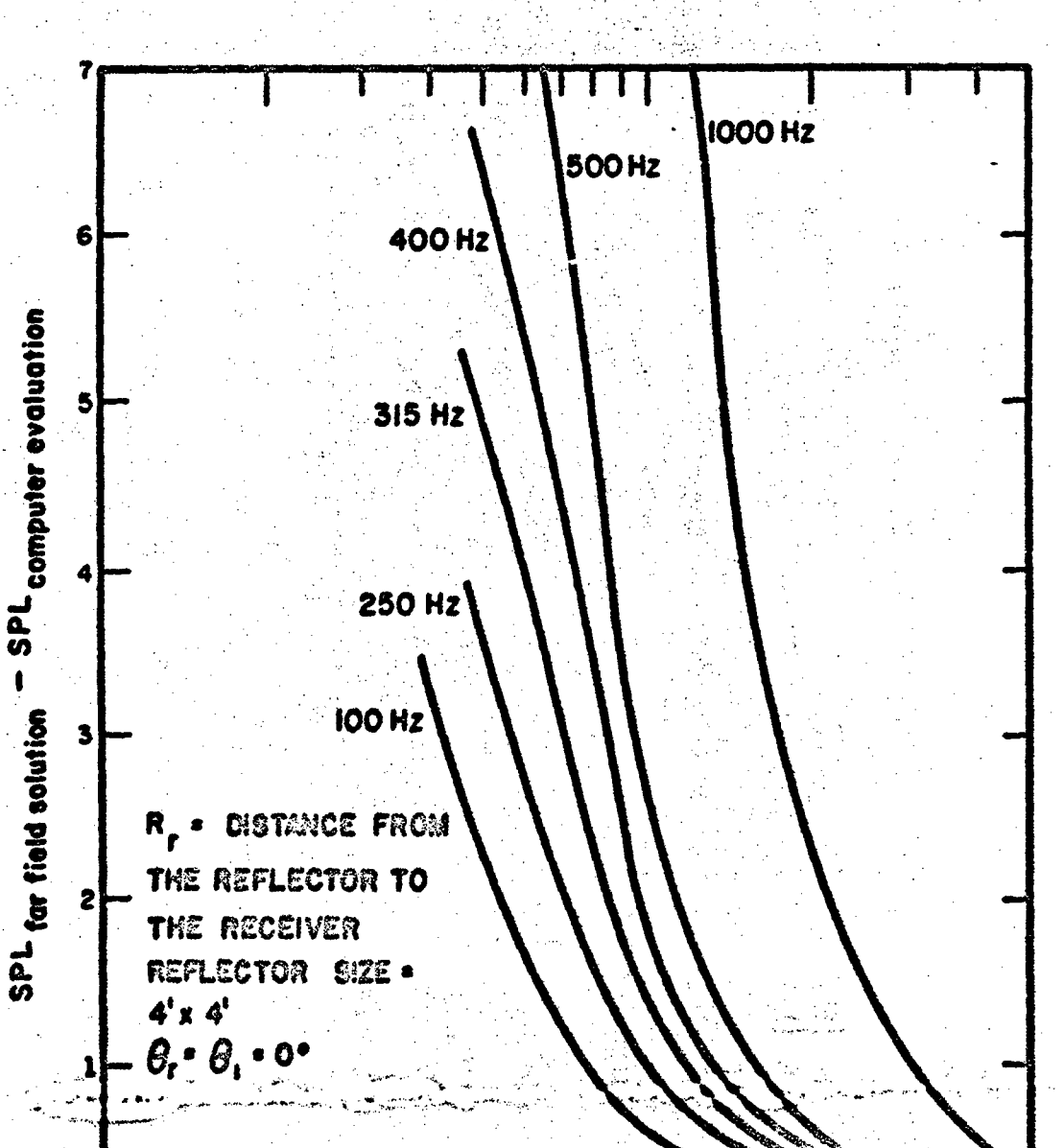

FIG. 17 COMPARISON OF THE FARFIELD EVALUATION WITH THE COMPUTER EVALUATION OF THE NEARFIELD FOR SPECULAR REFLECTION OF A NORMALLY INCIDENT PLANE WAVE.

To show the effect of panel response on the reflected field we will consider the excitation, response and radiation of a panel in an infinite rigid baffle which is excited by a diffuse field of noise. The solution of this problem is relevant to the unbaffled panel problem in that the response and radiation of a baffled panel will be above that of the unbaffled panel and, therefore, will be a conservatively high estimate of the effect of panel response on the reflected field. The response and radiation of a baffled panel has been carefully and completely studied [15]. We will use the results of this study.

To calculate the response and radiation in any given frequency band we must consider both the modes with resonance frequencies in the band (resonant modes) and the modes with resonance frequencies outside the band (nonresonant modes). The response of the resonant modes will dominate the response of the panel. However, the nonresonant modes usually dominate the acoustic transmission through the panel. We will consider first the response and radiation of resonant modes.

The acoustic power incident on both sides of a panel in a large reverberant chamber is given by

$$\Pi_{inc} = \frac{c_0 A}{2V} E_A \tag{66}$$

where Π_{inc} is the time-average power incident on the panel, E_A is the mean-square total acoustic energy in the chamber, V is the volume of the chamber, c_0 is the speed of sound in air and A is the area of the panel. The resonant response of the baffled panel is given by

$$\frac{E_p}{E_A} = \frac{n_p}{n_A} \frac{\eta_{rad}}{\eta_{tot}} \tag{67}$$

where E_p is the mean-square vibratory energy of the panel, n_p is the modal density of the panel, n_A is the modal density of the chamber, η_{rad} is the radiation loss factor, and η_{tot} is the total dissipation loss factor. The radiation loss factor of a clamped flat plate in a baffle is given by

$$\eta_{rad} = \frac{4}{\pi^3} \frac{\rho_0 c_0^2}{f \rho_s} \frac{P}{A} \frac{1}{f_{cr}} \sqrt{\frac{f}{f_{cr}}} \quad \text{for } f < \frac{f_{cr}}{2} \tag{68}$$

where ρ_0 is the density of air, ρ_s is the surface density of the panel, P is the perimeter of the panel, and f_{cr} is the critical frequency which is given by

$$f_{cr} = \frac{1}{2\pi} \frac{c_0^2}{\kappa c_\ell} \tag{69}$$

where κ is the radius of gyration of the panel, and c_ℓ is the longitudinal wavespeed in the panel material. The modal density of the panel is given by

$$n_P = \frac{A}{2\kappa c_\ell} \tag{70}$$

and the modal density of the chamber is given by

$$n_A = \frac{4\pi f^2 V}{c_0^3} \tag{71}$$

The total time-average acoustic power radiated by both sides of the vibrating panel is given by

$$\Pi_{rad} = 2\pi f \, \eta_{rad} \, \bar{F}^2 \tag{72}$$

Combining Eqs. 66 through 72 gives

$$\frac{\Pi_{rad}}{\Pi_{inc}} = \frac{8}{\pi^3} \left(\frac{\rho_0 c_0}{\rho_s}\right)^2 \left(\frac{P}{A}\right)^2 \left(\frac{c_\ell}{c_0}\right)^2 \left(\frac{\kappa}{f}\right)^2 \frac{1}{\eta_{tot}} \, . \tag{73}$$

For a square aluminum panel in air

$$\frac{\rho_0 c_0}{\rho_s} = \frac{84}{14} \frac{1}{t_{in}} , \tag{74}$$

where t_{in} is the panel thickness in inches,

$$\frac{P}{A} = \frac{4}{L} , \tag{75}$$

where L is a dimension of the panel in inches,

$$\frac{c_\ell}{c_0} = \frac{17,000}{1130} , \tag{76}$$

and

$$\kappa = \frac{t_{in}}{2\sqrt{3}} \tag{77}$$

Using these values in Eq. 73 gives

$$\frac{\Pi_{rad}}{\Pi_{inc}} = \frac{3 \times 10^3}{L_{in}^2 f^2 \eta_{tot}} \tag{78}$$

Note the important result that the ratio of the power radiated by resonant modes to the total incident power is independent of panel thickness.

The lowest frequency at which a panel effectively reflects an incident sound wave is given by

$$f = \frac{c_0}{\pi L} \tag{79}$$

At this frequency

$$\frac{\Pi_{rad}}{\Pi_{inc}} = \frac{1.7 \times 10^{-4}}{\eta_{tot}} . \tag{80}$$

Finally, a typical value for the total loss factor of a lightly damped structure is approximately

$$\eta_{tot} = 3 \times 10^{-3} \tag{81}$$

so that

$$\frac{\Pi_{rad}}{\Pi_{inc}} = 5.7 \times 10^{-2} \tag{82}$$

For a typically damped panel, then, the acoustic power radiated by the induced resonant vibration is at least 12-1/2 dB below the incident acoustic power.

Our consideration of the effects of vibration on the reflector performance must also include the nonresonant motion of the reflector. The acoustic power transmitted through a panel via nonresonant motion is given by

$$\Pi_{trans} = \bar{\tau} \Pi_{inc} , \tag{83}$$

where τ is the mass law transmission coefficient which is approximately given for diffuse field incidence by [13]

$$\tau = \left(\frac{2\rho_0 c_0}{\pi f \rho_s} \right)^2 . \tag{84}$$

The time-average power reflected is given by

$$\Pi_{reflected} = \Pi_{inc} - \Pi_{trans} - \Pi_{rad} \tag{85}$$

where Π_{trans} is the power transmitted through the reflector by nonresonant motion and Π_{rad} is the power radiated from the back

of the reflector by resonant vibration. We can ignore Π_{rad} relative to Π_{inc} so that

$$\frac{\Pi_{reflected}}{\Pi_{inc}} = 1 - \bar{\tau} . \tag{86}$$

For an aluminum reflector in air the mass law tranmission coefficient can be written as

$$\bar{\tau} = \left(\frac{3.8}{ft_{in}}\right)^2 \tag{87}$$

where t_{in} is the reflector thickness in inches. If we require that 90% of the incident energy be reflected for frequencies above 100 Hz, the reflector thickness must be greater than 0.12 in. For a 1/16-in. reflector, 63% of the incident energy at 100 Hz is reflected.

We conclude that the flexibility of a 4-ft square aluminum reflector 1/8-in. thick (a typical reflector) will not alter the reflected field by more than 1 dB so that the reflected field from a rigid reflector can be used for our calculations.

2.6 Reflected Acoustic Power

An evaluation of the performance of a reflector can be best made by looking at the reflected acoustic power. A reflector with satisfactory performance will reflect most of the power incident on its surface in a colimated beam which can be directed at the test object.

Our theoretical predictions for the reflected pressure field have been obtained for an acoustic medium which has no energy dissipation mechanisms. Thus, the acoustic intensity in the far field can be used to calculate the reflected power and the directionality of that power.

The time-average acoustic intensity of the reflected far field is directed away from the reflecting panel and has a magnitude equal to

$$I(R_r,\theta_r,\psi_r) = \frac{1}{2\rho_0 c_0} |P_s(R_r,\theta_r,\psi_r)|^2 \tag{88}$$

where I is the time-average acoustic intensity, R_r, θ_r, ψ_r are spherical coordinates defining a point in the far field, $\rho_0 c_0$ is the specific acoustic impedance, and P_s is the complex amplitude of the scattered field. The complex amplitude of the scattered field can be obtained from one of the three approximate formulations presented in Sec. 2.3.

The total acoustic power reflected by a panel can be found by integrating the far-field intensity given by Eq. 88 over a hemisphere of radius R_r which is centered on the panel,

$$\Pi_r = \int_0^{2\pi} d\psi_r \int_0^{\pi/2} d\theta_r \, R_r \sin\theta_r \, I(R_r, \theta_r, \psi_r) \tag{89}$$

where Π_r is the total time-average power reflected by the panel.

The acoustic power incident on the reflector takes a very simple form for a plane wave. The intensity of a plane wave is aligned with the direction of propagation and has a magnitude given by

$$I_i = \frac{1}{2\rho_0 c_0} |P_i|^2 \tag{90}$$

where I_i is the time-average intensity, $\rho_0 c_0$ is the acoustic impedance and P_i is the complex amplitude of the plane wave. It follows from Eq. 90 that the total power incident on the reflector is

$$\Pi_i = \frac{1}{2\rho_0 c_0} |P_i|^2 A \cos\theta_i \tag{91}$$

where Π_i is the time-average incident power, A is the area of the reflector, and θ_i is the angle of incidence of the plane wave measured from a normal to the reflector.

The ratio of reflected power to incident power as a function of $kL \cos\theta_i/2$, where k is the acoustic wavenumber and L the length of one side of the reflector, has been calculated numerically using a digital computer and is plotted in Figs. 18 through 21 for

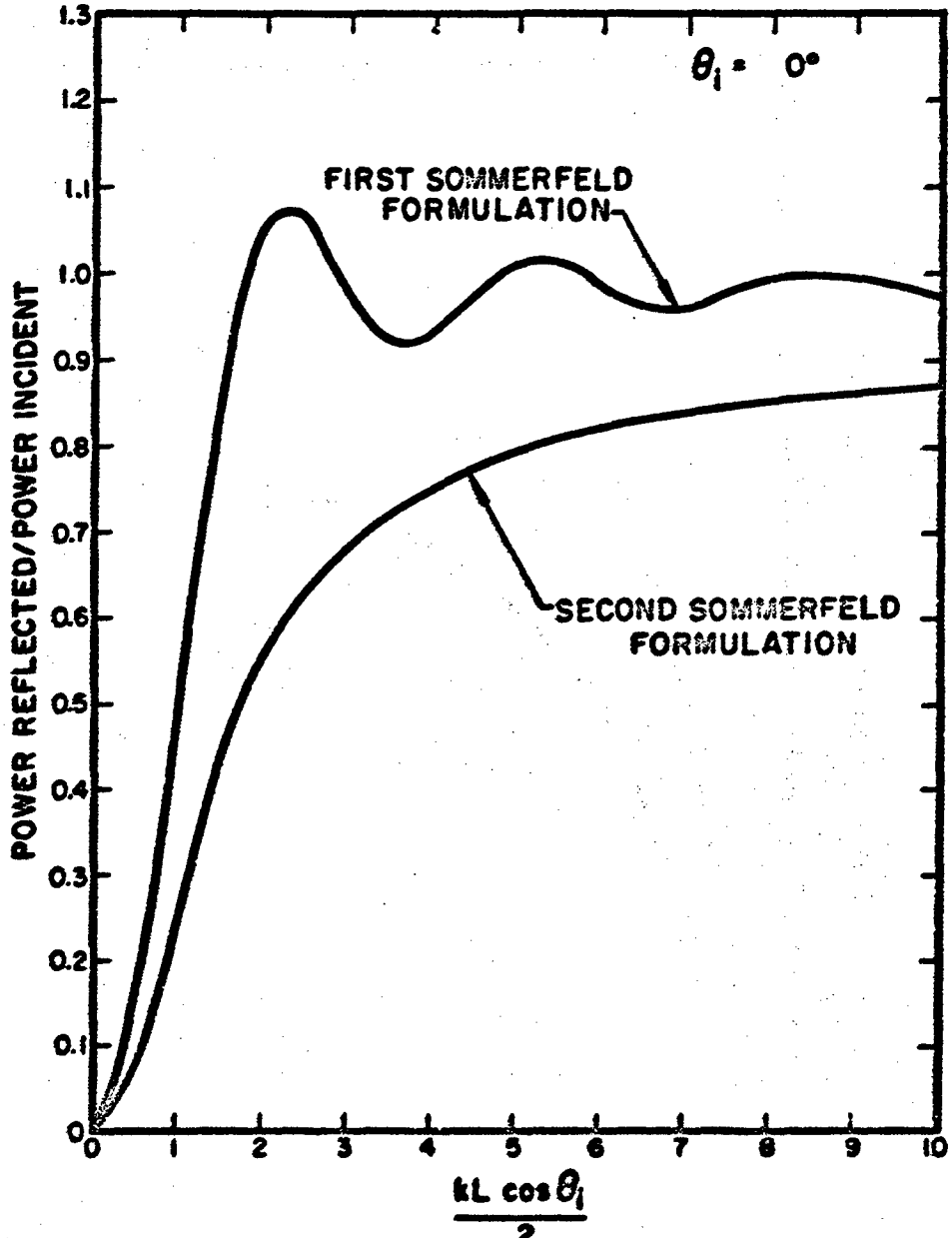

k ACOUSTIC WAVENUMBER

L LENGTH OF ONE SIDE OF THE REFLECTOR

θ_i ANGLE OF INCIDENCE FROM A NORMAL TO THE REFLECTOR

FIG. 18 REFLECTED ACOUSTIC POWER FOR A PLANE WAVE INCIDENT FROM 0°.

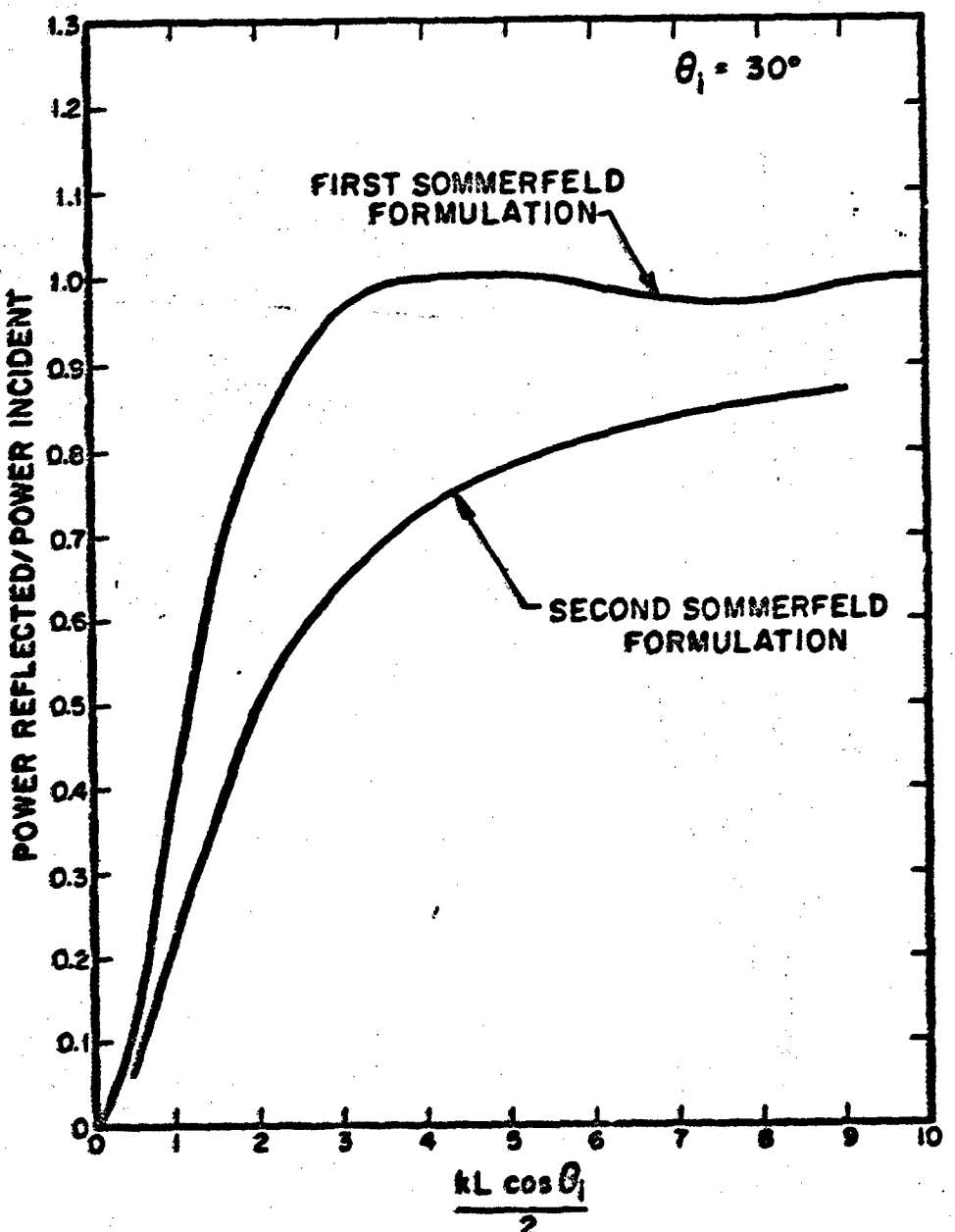

k ACOUSTIC WAVENUMBER

L LENGTH OF ONE SIDE OF THE REFLECTOR

θ_i ANGLE OF INCIDENCE FROM A NORMAL TO THE REFLECTOR

FIG. 19 REFLECTED ACOUSTIC POWER FOR AN INCIDENT PLANE WAVE.

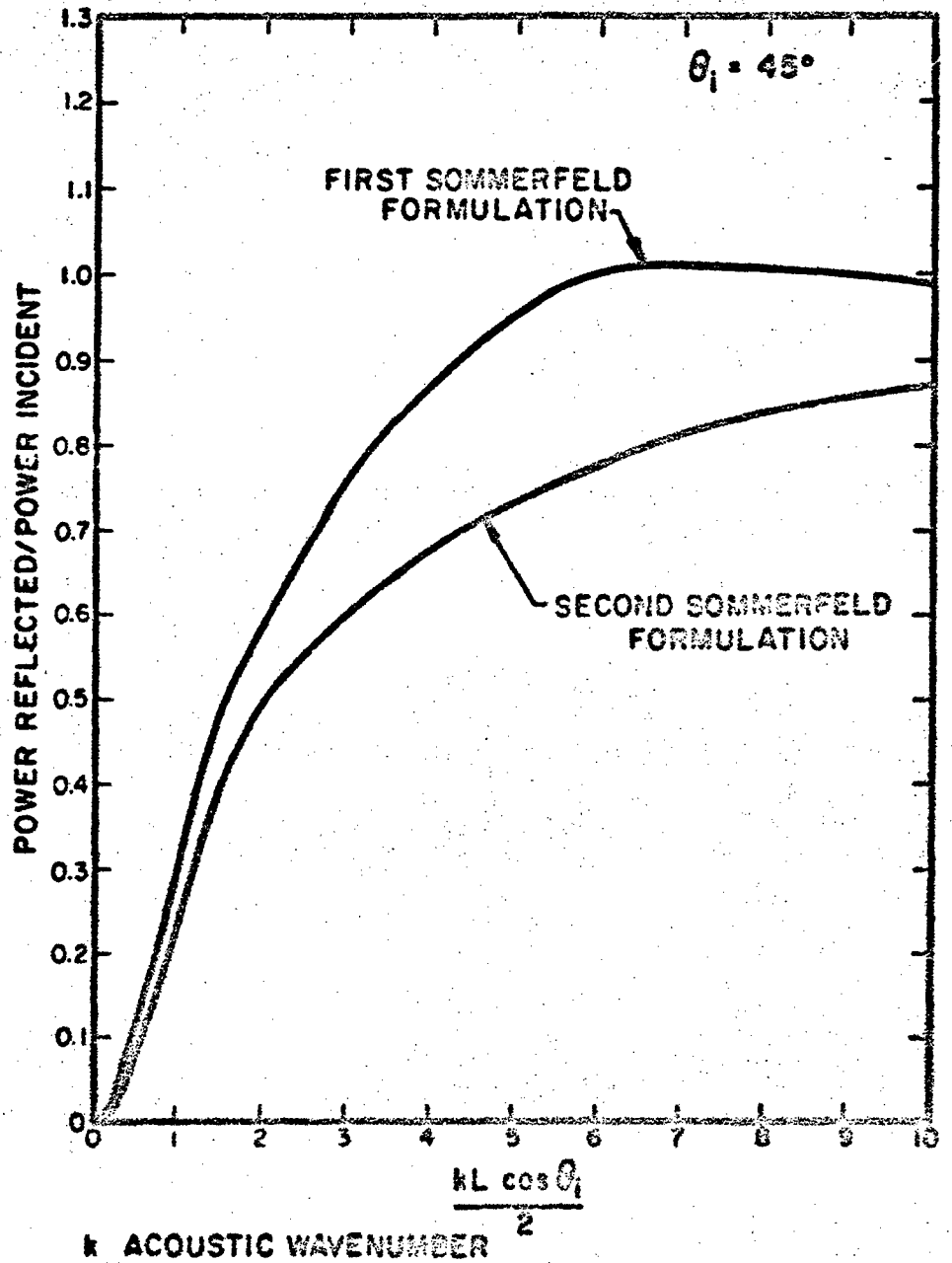

k ACOUSTIC WAVENUMBER

L LENGTH OF ONE SIDE OF THE REFLECTOR

θ_i ANGLE OF INCIDENCE FROM A NORMAL TO THE REFLECTOR

FIG. 20 REFLECTED ACOUSTIC POWER FOR AN INCIDENT PLANE WAVE.

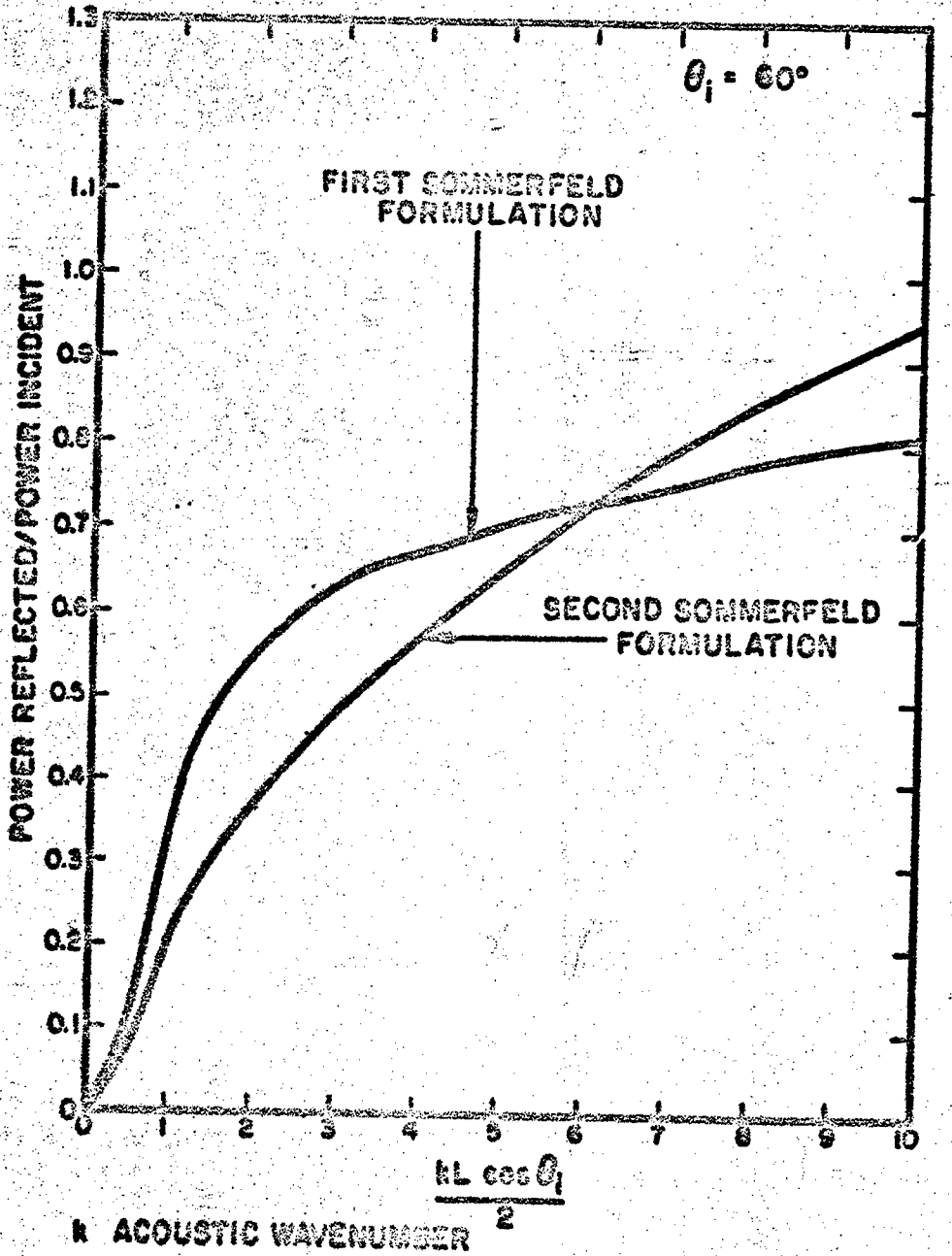

k ACOUSTIC WAVENUMBER

L LENGTH OF ONE SIDE OF THE REFLECTOR

θ_i ANGLE OF INCIDENCE FROM A NORMAL TO THE REFLECTOR

FIG. 21 REFLECTED ACOUSTIC POWER FOR AN INCIDENT PLANE WAVE.

several values of the angle of incidence of a plane wave. Two curves are presented in each figure corresponding to the FRS and SRS approximate formulations for the reflected field. The EK formulation will give results which are the average of these two curves. At high frequencies (k large) the ratio of reflected power to incident power approaches one as would be expected based on a geometrical optics point of view. At lower frequencies, however, the ratio of reflected to incident power varies between the different formulations. The FRS formulation gives ratios which fluctuate in frequency and which for certain values of $kL\cos\theta_i/2$ exceed one. The ratio of reflected to incident power can exceed one because of our definition of the incident power as the intensity of the incident wave when the reflector is removed times the projected area of the reflector on a plane normal to the direction of propagation of the wave.

The fluctuations of the FRS solution are largest for $\theta_i = 0^\circ$ and disappear for large angles of incidence. The ratio of reflected to incident power given by the FRS formulation for low values of $kL\cos\theta_i/2$ is strongly dependent on the angle of incidence. The ratio at $kL\cos\theta_i/2$ equal to one is as follows:

θ_i	Π_r/Π_i from FRS formulation with $\frac{kL\cos\theta_i}{2} = 1$
0°	0.5
30°	0.4
45°	0.3
60°	0.2

where Π_r is the reflected power and Π_i is the incident power.

The SRS approximate formulation gives predictions which are well below those given by the FRS formulation except for large angles of incidence. The SRS formulation approaches one as $kL\cos\theta_i/2$ increases but not as rapidly as the prediction given by the FRS formulation. The fluctuations exhibited by the FRS formulation do not occur for the SRS formulation. And, finally, the SRS formulation gives predictions for the ratio of reflected to incident power which are nearly independent of angle of incidence, as shown below.

θ_1	Π_r/Π_i from SRS formulation with $\frac{kL\cos\theta_1}{2} = 1$
0°	.25
30°	.22
45°	.22
60°	.20

The HK approximate formulation gives predictions which are the average of those given by the FRS and SRS formulations.

The causes of the differences between the three approximate formulations are the Kirchhoff approximations given by Eqs. 10 and 11. As discussed in Sec. 2.3 the far-field pressures at specular reflection predicted by the three approximate formulations are identical. Thus, the differences between the FRS and SRS predictions for total radiated power result from differences in the predicted amount of power radiated in directions nearly parallel to the plane of the reflector.

For the purpose of shaping an acoustic field the directivity of the reflected power is as important as the total reflected power. As a measure of the directivity of the radiated field we have numerically calculated the power reflected within a cone of angles defined by θ. This reflected power is given by

$$\Pi_r(\theta) = \int_0^{2\pi} d\phi_r \int_0^{\theta_r} d\theta_r \, R_r^2 \sin\theta_r \, I(R_r,\theta_r,\phi_r) \qquad (92)$$

where $\Pi_r(\theta)$ is the time-average power reflected in the cone of angles defined by θ, the angle θ is measured relative to a normal to the reflector, and I is the far-field intensity given by Eq. 88. Plots of the reflected power, $\Pi_r(\theta)$, for different values of $kL/2$ are shown in Figs. 22 through 24. All plots shown are for the case of normal incidence. These three plots show the behavior predicted above. The FRS and SRS approximate formulations give nearly the same prediction for the power radiated into a cone of angles for small values of θ. If we consider angles up to 30°, the prediction from the two formulations are within 20% for any value of $kL\cos\theta_1/2$. We conclude that the question of which formulation to use is not of great importance for our particular

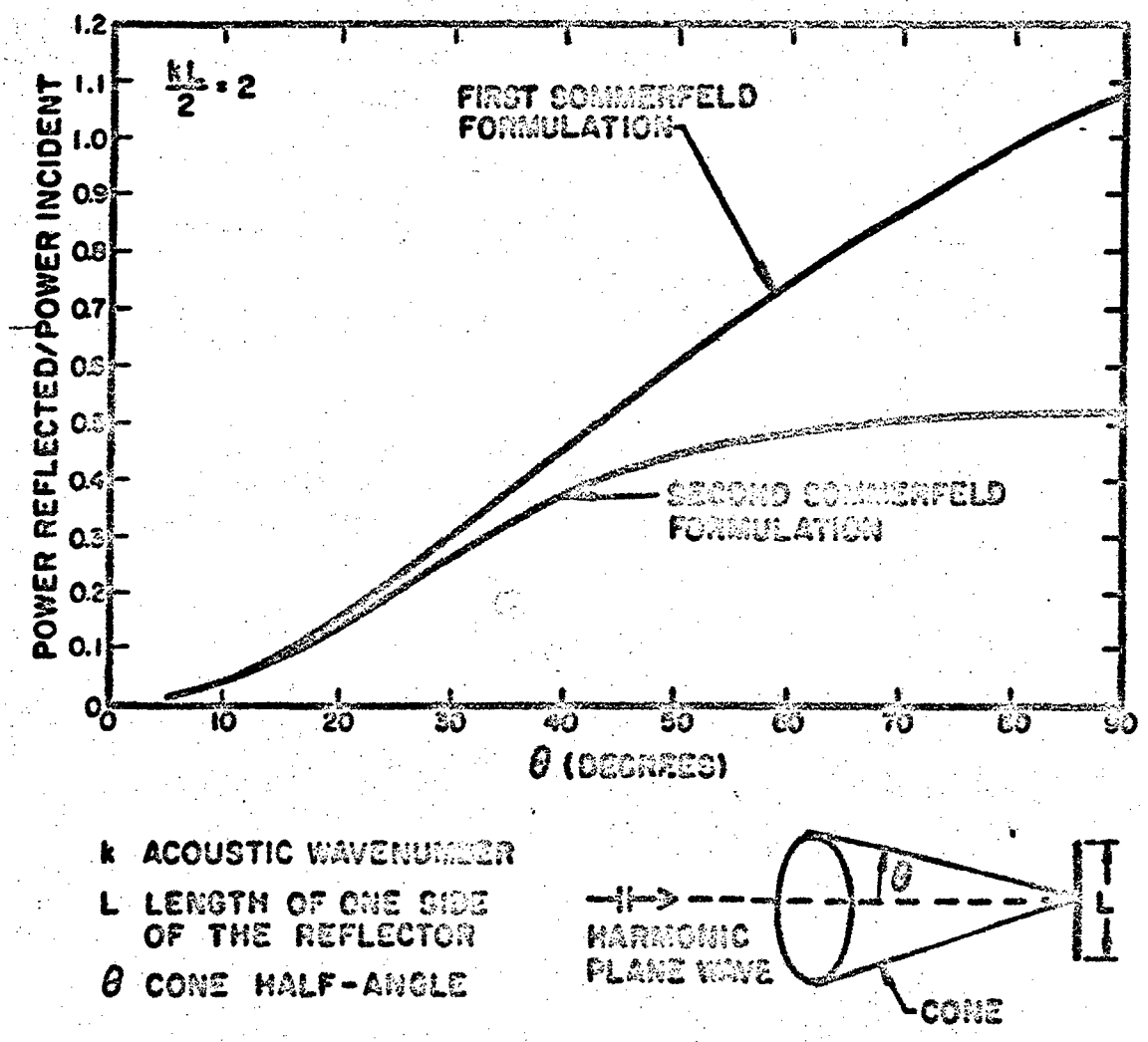

FIG. 22 DIRECTIVITY OF THE REFLECTED ACOUSTIC POWER.

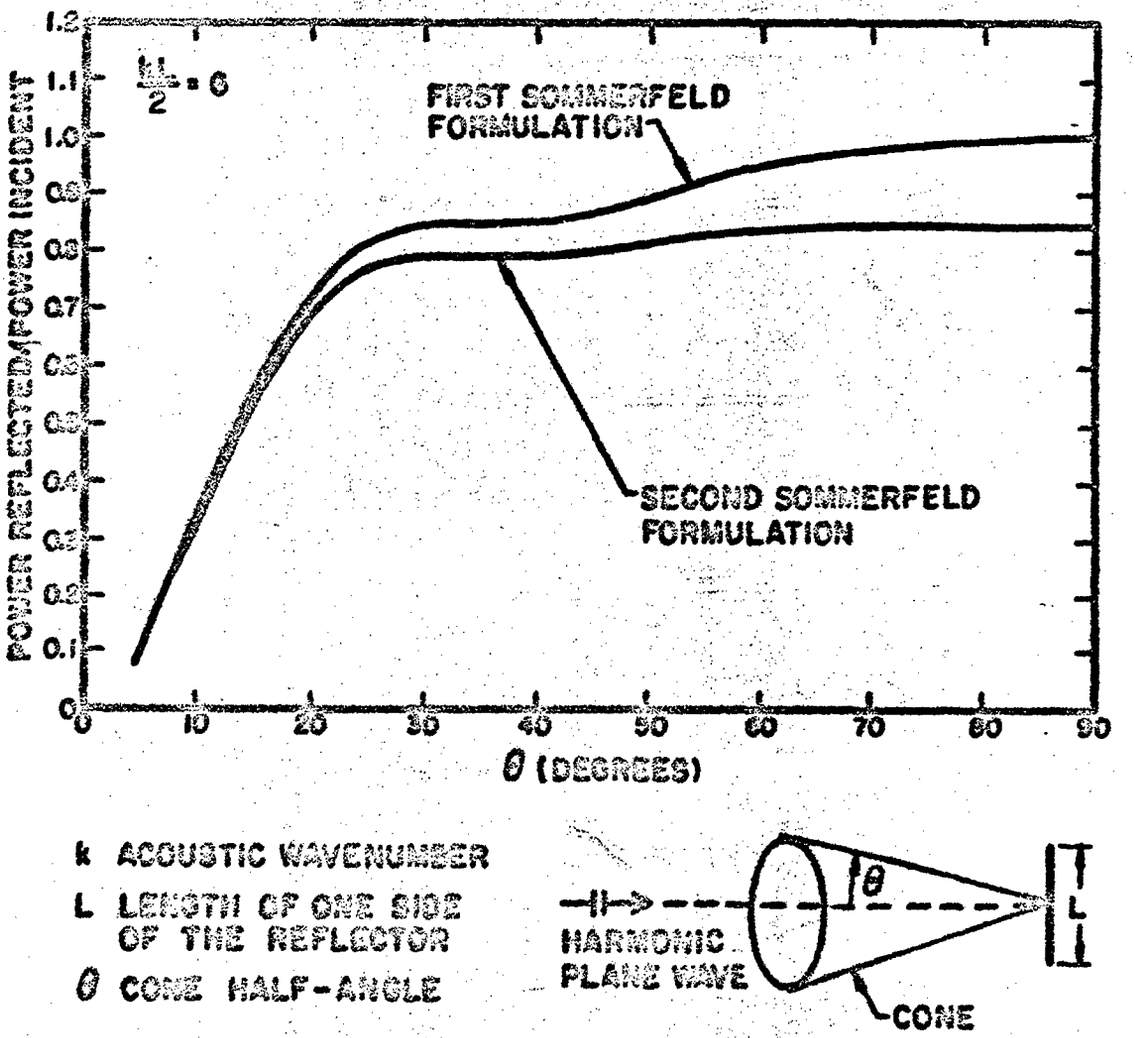

FIG 23 DIRECTIVITY OF THE REFLECTED ACOUSTIC POWER.

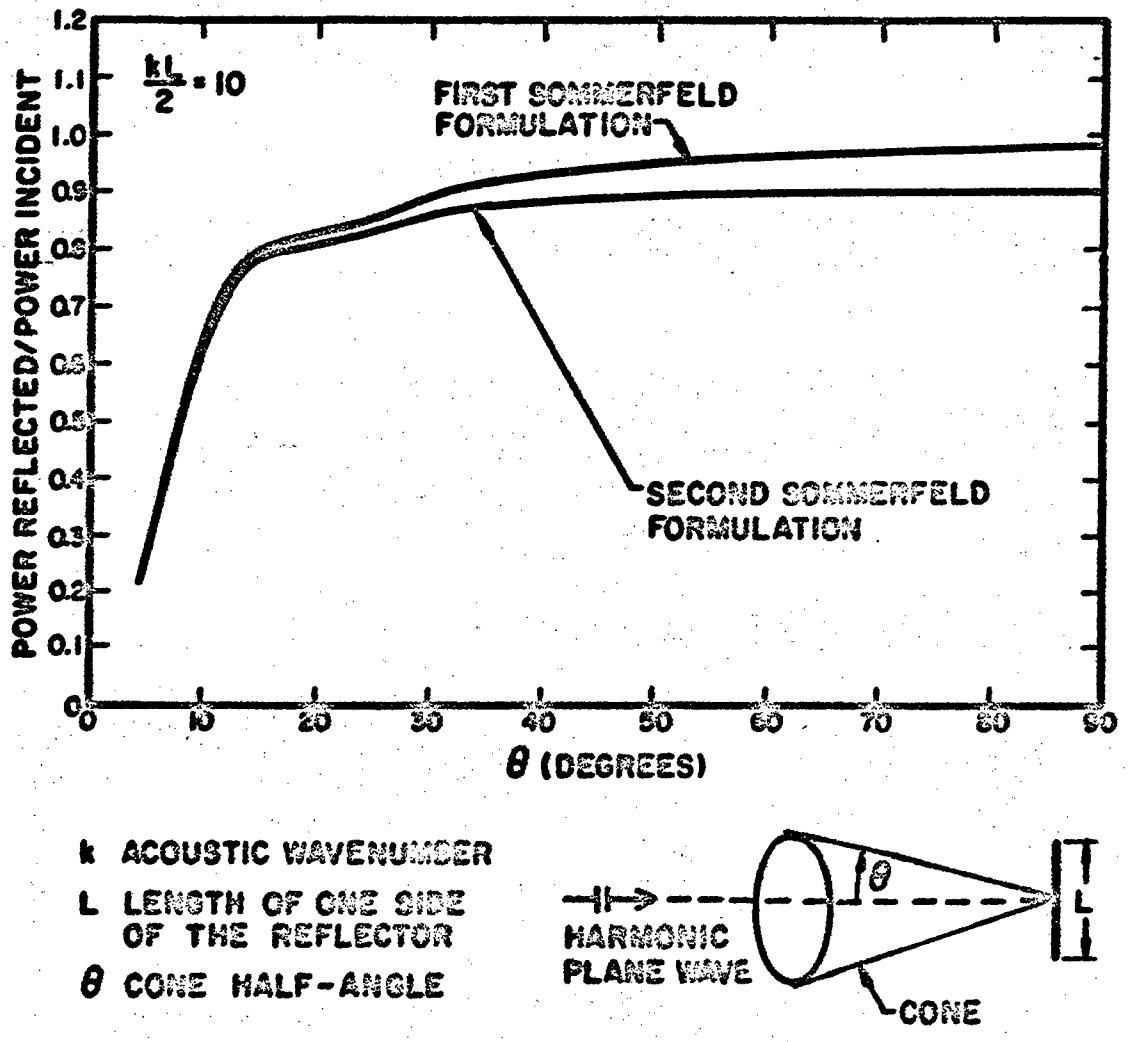

FIG. 24 DIRECTIVITY OF THE REFLECTED ACOUSTIC POWER.

problem, since we are mostly interested in the reflected pressure near the specular angles, $\theta_r = \theta_i$ and $\psi_r = \psi_i + 180°$.

In Part 4 of this report we will use calculations of reflected power as a basis for practical design charts. These calculations will be based on the SRS approximate formulation and, therefore, will be conservative estimates of reflector performance.

2.7 Reflection of a Band of Acoustic Noise

The predictions for the reflected field in previous sections have been obtained for a single frequency pure tone. To be practically useful these expressions must be averaged in frequency in order to predict the reflection of random noise.

The reflection of an acoustic field will be assumed to be linear even though the levels of the field are high enough to cause nonlinearities in the propagation of the wave. With this assumption linear input-output relations can be used. The spectrum of the pressure at point $\underline{x}_r$ is related to the spectrum of the point or plane wave source by a frequency dependent constant,

$$S_{p(\underline{x}_r)}(f) = S_i(f)|H(\underline{x}_r,f)|^2 \tag{93}$$

where $S_{p(\underline{x}_r)}$ is the spectrum of the pressure at point $\underline{x}_r$, f is the frequency, S_i is the spectrum of the source, and H is the complex frequency response. The function H is the complex pressure amplitude at point $\underline{x}_r$ resulting from a pure tone source with unity amplitude. The complex pressure amplitude for a pure tone has been calculated in previous sections and is given by

$$H(\underline{x}_r,f) = P_i(\underline{x}_r,f) + P_s(\underline{x}_r,f) \tag{94}$$

where P_i is the complex amplitude of the incident pure tone waves at point $\underline{x}_r$ and P_s is the amplitude of the scattered pressure field at point $\underline{x}_r$. The magnitude-squared of $H(\underline{x}_r,f)$ is

$$|H(\underline{x}_r,f)|^2 = |P_i(\underline{x}_r,f)|^2 + |P_s(\underline{x}_r,f)|^2 + P_i(\underline{x}_r,f)\, P_s^*(\underline{x}_r,f) + P_i^*(\underline{x}_r,f)\, P_s(\underline{x}_r,f) \; . \tag{95}$$

The last two terms of Eq. 95 result from the interaction of the incident field with the reflected field. We will show that the average of these interaction terms over a band of frequencies tends to zero and can be ignored. Then the magnitude-squared of the transfer function can be written as

$$\langle |H(\underline{x}_r,f)|^2 \rangle_{\Delta f} = \langle |P_i(\underline{x}_r,f)|^2 \rangle_{\Delta f} + \langle |P_s(\underline{x}_r,f)|^2 \rangle_{\Delta f} \qquad (96)$$

where Δf is a band of frequencies, and f is the band-center-frequency.

2.7.1 Interaction of the incident field with the reflected field

To show the interaction of the incident field with the reflected field we consider a point source generating random noise. The strength of the source will be somewhat arbitrarily set to be the spectrum of the pressure at s = 1. To find the complex frequency response we will calculate the complex pressure amplitude at $\underline{x}_r$ due to a pure tone source with unity amplitude, $A_{pt} = 1$. The incident pressure amplitude for this case can be found from Eq. 18,

$$P_i(\underline{x}_r,f) = \frac{e^{iks}}{s} \qquad (97)$$

where k is the acoustic wavenumber and s is the distance from the source to point $\underline{x}_r$. If we limit our consideration to points in the far field, the reflected pressure amplitude is given by Eq. 48 or 50 as

$$P_s(\underline{x}_r,f) = -\frac{2ik}{\pi} \frac{e^{ik(R_s+R_r)}}{R_s R_r} G(\underline{x}_r,\underline{x}_s) \begin{Bmatrix} \cos\theta_s \\ \cos\theta_r \end{Bmatrix} \qquad (98)$$

where P_s is the reflected pressure amplitude.

The $\cos\theta_s$ is used for the FRS approximate formulation, the $\cos\theta_r$ is used for the SRS formulation and one-half the sum of these factors is used for the HK formulation. Combining Eqs. 97 and 98 we calculate the interaction terms in Eq. 95 to be

$$P_i(\underline{x}_r,f)P_s^*(\underline{x}_r,f) + P_i^*(\underline{x}_r,f)P_s(\underline{x}_r,f) =$$

$$\frac{2k}{\pi}\frac{G(\underline{x}_r,\underline{x}_s)}{R_r R_s R_d}\sin k(R_r + R_s - R_d) \qquad (99)$$

where R_d is the distance from the source to point $\underline{x}_r$. All terms in Eq. 99 are positive and vary slowly in frequency except the sine term. Thus, the average of the interaction terms over a narrow band of frequencies becomes

$$\langle P_i P_s^* + P_i^* P_s \rangle_{\Delta f} = \frac{2k_c}{\pi}\frac{G_c(\underline{x}_r,\underline{x}_s)}{R_r R_s R_d}$$

$$\langle \sin k(R_r + R_s - R_d)\rangle_{\Delta f} \qquad (100)$$

where k_c is the wavenumber at the band center frequency, G_c is the function G evaluated at the band center frequency, and Δf is the bandwidth. If the bandwidth is sufficiently wide that the condition

$$\frac{\Delta f}{f_c} > \frac{\lambda_c}{(R_r+R_s-R_d)} \qquad (101)$$

where f_c is the band-center frequency and λ_c is the acoustic wavelength at f_c holds, the average of the sine term over Δf will be small and will tend to zero. In the far field the distances R_r and R_s must be much greater than λ_c, so that the condition expressed by Eq. 101 will be met at all points. We conclude that neglecting the interaction terms to calculate the reflection of a band of noise generated by a point source is a reasonable approximation in the far field.

2.7.2 Reflection of one-third octave and octave bands of noise

The mean-square sound pressure in a one-third octave or octave band is given by

$$\langle S_{p(\underline{x}_r)}(f)\rangle_{\Delta f} = \langle S_1(f)|H(\underline{x}_r,f)|^2\rangle_{\Delta f} \qquad (102)$$

where < > signifies a frequency average and Δf is the bandwidth. If we assume the source spectrum to be constant over the band, then

$$\langle S_{p(\underline{x}_r)}(f)\rangle_{\Delta f} = S_1(f)\langle|H(\underline{x}_r,f)|^2\rangle_{\Delta f} \qquad (103)$$

where $\langle|H(\underline{x}_r,f)|^2\rangle_{\Delta f}$ is given by Eq. 96. For a point source the frequency average of $|H|^2$ is given by

$$\langle|H(\underline{x}_r,f)|^2\rangle_{\Delta f} = \frac{1}{R_d^2} + \frac{4}{\pi^2}\frac{\langle k^2G^2\rangle_{\Delta f}}{R_s^2R_r^2}\begin{Bmatrix}\cos^2\theta_s\\ \cos^2\theta_r\end{Bmatrix} \qquad (104)$$

where $\underline{x}_r$ is assumed to be in the far field, R_d is the distance from the source to the receiver and the term $\cos^2\theta_s$ is used for the FRS formulation while the term $\cos^2\theta_r$ is used for the SRS formulation. The term $\langle k^2G^2\rangle_{\Delta f}$ is given by

$$\langle k^2G^2\rangle_{\Delta f} = \frac{\pi^2L_x^2L_y^2}{4c_s^2}\frac{1}{\Delta f}\int_{f_1}^{f_2} df\left(\frac{\sin\alpha f}{\alpha f}\frac{\sin\beta f}{\beta f}f\right)^2 \qquad (105)$$

where f_1 and f_2 are the lower and upper limits of the band and

$$\alpha = \frac{\pi L_x}{c_s}(\sin\theta_r\cos\psi_r + \sin\theta_s\cos\psi_s)$$

$$\beta = \frac{\pi L_y}{c_s}(\sin\theta_r\sin\psi_r + \sin\theta_s\sin\psi_s)\ . \qquad (106)$$

The integral in Eq. 105 cannot be evaluated analytically for the most general case. However, for specular reflection, $\theta_s = \theta_r$ and $\psi_s = \psi_r + 180^\circ$, and both α and β equal zero so that

$$\langle k^2G^2\rangle_{\Delta f} = \frac{\pi^2 L_x^2 L_y^2}{4c_s^2}\,\frac{1}{\Delta f}\int_{f_1}^{f_2} df\, f^2 \quad , \qquad \text{for } \alpha = \beta = 0 \; . \tag{107}$$

This integral can be easily evaluated to give

$$\langle k^2G^2\rangle_{\Delta f} = \frac{\pi^2 L_x^2 L_y^2}{12c_s^2}\,\frac{1}{\Delta f}\,(f_2^3 - f_1^3) \quad , \qquad \text{for } \alpha = \beta = 0 \; . \tag{108}$$

For one-third octave or octave bands Eq. 108 can be written

$$\langle k^2G^2\rangle_{\Delta f} = \frac{\pi^2 L_x^2 L_y^2}{12c_s^2}\left(\frac{2^{3n}-2^{-3n}}{2^n-2^{-n}}\right) f_c^2 \quad , \qquad \text{for } \alpha = \beta = 0 \tag{109}$$

where $n = 1/2$ for octave bands, $n = 1/6$ for one-third octave bands and f_c is the band center frequency. The spectrum of the sound pressure at angles corresponding to specular reflection is given by

$$\frac{\langle S_{p(\underline{x}_r)}(f)\rangle_{\Delta f}}{S_i(f)} = \frac{1}{R_d^2}\left(\begin{matrix}1.170\\1.025\end{matrix}\right)\frac{L_x^2 L_y^2}{R_s^2 R_r^2}\,\frac{f_c^2}{c_s^2}\cos^2\theta_s \tag{110}$$

where the factor 1.170 is used for octave bands and the factor 1.025 is used for one-third octave bands. Comparison of Eqs. 110 and 58 shows that except for the factors 1.170 and 1.025

$$\langle S_{p(\underline{x}_r)}(f)\rangle_{\Delta f} = S_{p(\underline{x}_r)}(f_c) \text{ for specular reflection} \; . \tag{111}$$

This result allows us to use the pure tone calculations for frequencies equal to the band-center frequencies in order to calculate the sound pressure spectrum at the specular angles of reflection.

The first term in Eq. 110 is the contribution to the pressure spectrum from the incident sound field. In a practical application the source will be directive so that the incident field

sound pressures will be small in comparison to the reflected field pressures at locations of interest. Then the first term in Eq. 110 will not be present. Results for the directive source will be presented in Sec. IV of this Report. The effect of one-third octave band pressure spectrum at nonspecular angles of reflection can also be evaluated using Eq. 107. The most general case with both α and β nonzero must be evaluated numerically. However, without losing much generality, we can take ψ_s and ψ_r equal to zero so that $\beta = 0$. Then

$$\langle k^2G^2\rangle_{\Delta f} = \frac{\pi^2 L_x^2 L_y^2}{4c_e^2}\,\frac{1}{\Delta f}\int_{f_1}^{f_2} df\left(\frac{\sin\alpha f}{\alpha}\right)^2 , \qquad \text{for } \beta = 0 . \quad (112)$$

This integral can be evaluated analytically to give

$$\langle k^2G^2\rangle_{\Delta f} = \frac{\pi^2 L_x^2 L_y^2}{4c_e^2}\left[\frac{1}{2\alpha^2}\left(1 - \frac{\sin\alpha\Delta f}{\alpha\Delta f}\right)\right.$$

$$\left. + \frac{\sin\alpha\Delta f}{\alpha\Delta f}\left(\frac{\sin\alpha f}{\alpha}\right)^2\right] , \qquad \text{for } \beta = 0 \quad (113)$$

where $f = (f_1 + f_2)/2$. The frequency averaged value of the magnitude-squared of the complex frequency response can be obtained by using Eq. 113 in Eq. 104.

The results of frequency averaging are shown in Figs. 25 and 26. The factor

$$10\log_{10}\left\{\frac{\langle k^2G^2\rangle_{\Delta f}}{k_c^2}\,\frac{1}{4}\left[\cos^2\theta_s + \cos^2\theta_r\right]\right\} \quad (114)$$

where k_c is the wavenumber at the band-center frequency is plotted in these figures for one-third octave and octave band averaging. The unaveraged value of the above factor is also plotted in these figures for comparison.

The effect of the frequency averaging is to smooth out the peaks and nulls in the reflected field directivity pattern. The

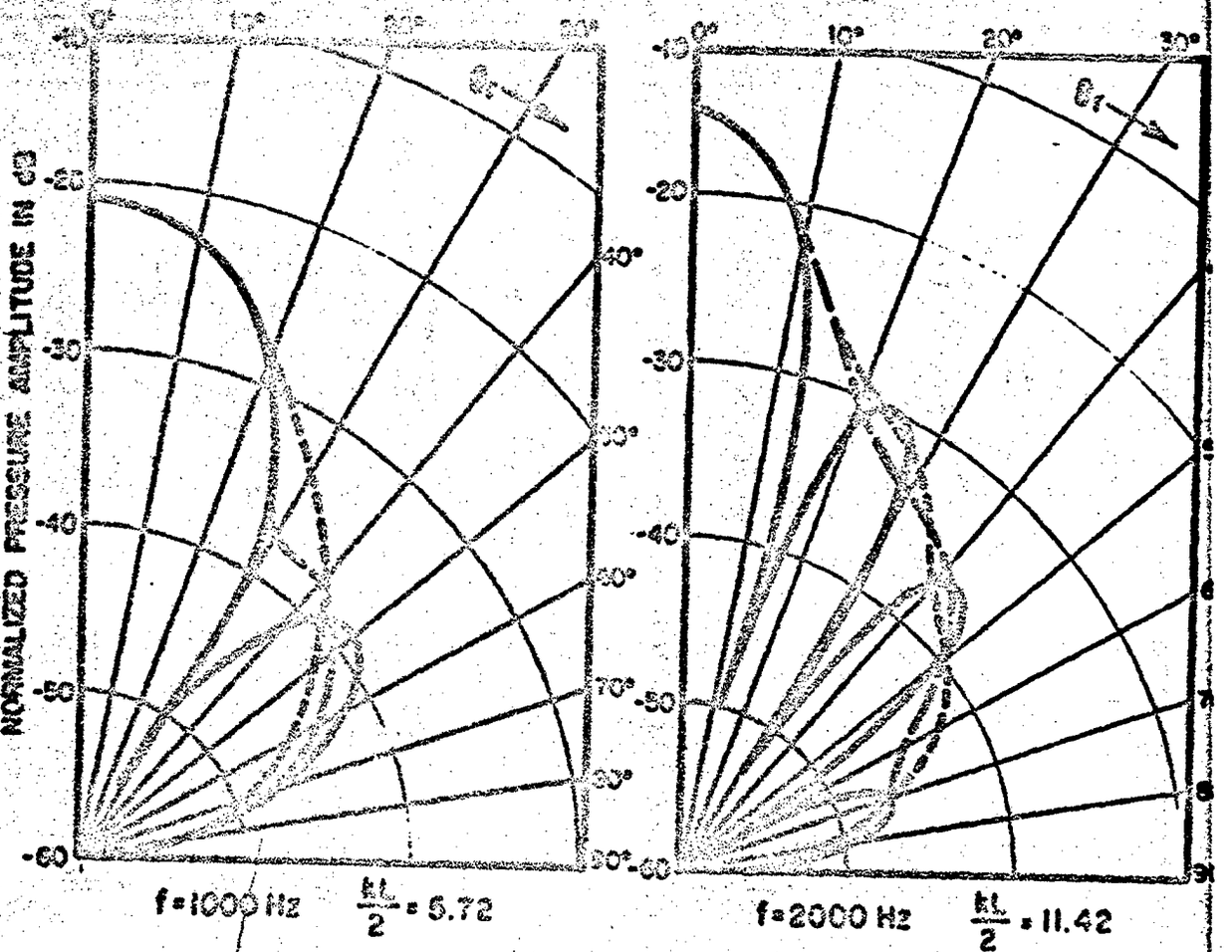

SECOND SOMMERFELD FORMULATION
——— NO FREQUENCY AVERAGING
– – – – AVERAGED OVER A ONE-THIRD OCTAVE BAND
— — — AVERAGED OVER AN OCTAVE BAND
NOTE: FREQUENCIES GIVEN ARE APPLICABLE TO A 4' x 4' REFLECTOR

$\theta_i = 0°$

FIG. 25 REFLECTED FIELD PRESSURE AMPLITUDES FOR BANDS OF NOISE.

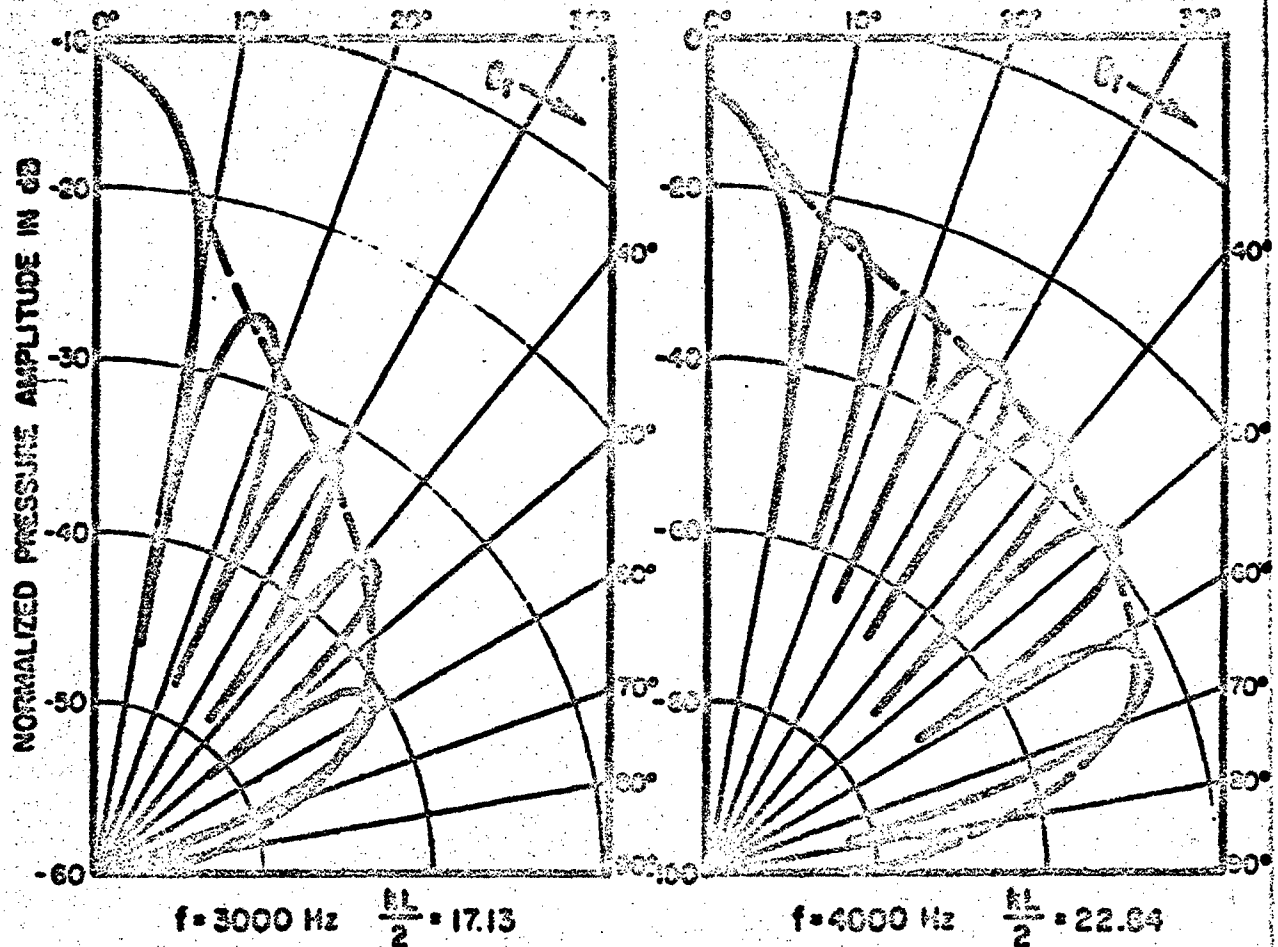

SECOND SOMMERFELD FORMULATION

——— NO FREQUENCY AVERAGING

—·— AVERAGED OVER A ONE-THIRD OCTAVE BAND

NOTE: FREQUENCIES GIVEN ARE APPLICABLE TO A 4' x 4' REFLECTOR

$\theta_i = 0°$

FIG. 26 REFLECTED FIELD PRESSURE AMPLITUDES FOR BANDS OF NOISE.

smoothing effect is more pronounced at higher frequencies where the bandwidths are larger and where the unaveraged reflected field has many lobes in its directivity pattern. The smoothing effect is also more pronounced where octave band averaging expressions must be used to calculate the reflected acoustic noise field at locations which do not correspond to specular reflection. However, at locations corresponding to specular reflection the pure tone result evaluated at the band center frequency can be used for the noise field. In the practical utilization of a reflector the greatest interest is in the reflected noise field at locations of specular reflection, since the reflected field has its greatest levels at these locations. Thus, the pure tone calculations will be of great practical use.

The effect of frequency averaging on the reflected power is not significant, since the reflected power is a fairly smooth function of frequency. A reasonably accurate estimate of the reflected power in a one-third octave or octave band can be obtained by using the pure tone prediction at the band center frequency. A more exact expression can be obtained by averaging the plots shown in Figs. 18 through 21.

2.8 Reflection of High Level Sound Waves

The sound pressure levels required to simulate many actual environments are so high that nonlinearities in the equations governing the propagation of the sound waves must be considered. These nonlinearities cause the wavefront of an initially harmonic sound wave to steepen as the wave travels until the limiting form of a sawtooth is reached. For practical test levels in the range from 150 to 180 dB the transition from a harmonic disturbance to a sawtooth disturbance takes place over a number of wavelengths of the disturbance. For this reason we will treat the actual reflection process as linear even though nonlinearities may have to be considered in the propagation of the reflected sound waves.

Our technique for studying the reflection of high level sound waves will be to express the incident waves at the reflection as a sum of harmonic waves and to calculate the reflected acoustic field for each of these harmonic components. As shown in previous sections the high-frequency harmonic components will be more effectively reflected. Thus, the waveform of the reflected sound waves will have relatively greater high-frequency content and will have a shape different than that of the incident wave. For the present program we are more interested in the intensity of the reflected field and will limit our consideration to calculation of this quantity.

We will assume that the incident waveform at the reflector is a sawtooth. Then, the incident pressure is given by the equation

$$p_i(\underline{x},t) = P_i g(k_e x \cos\theta_s \cos\psi_s + k_e y \cos\theta_s \sin\psi_s - \omega_e t) \qquad (115)$$

where P_i is a real amplitude, g is a sawtooth waveform, $\underline{x}$ is a point in the plane of the reflector, k_e is the wavenumber at frequency ω_e, ω_e is the fundamental frequency of the sawtooth and θ_s and ψ_s define the angle of incidence of the sound wave. The function g is periodic and is given by

$$g(x) = \frac{x}{\pi} - 1 \qquad 0 < x < 2\pi \; . \qquad (116)$$

The intensity of the incident wave is simply

$$I_i = \frac{\langle p_i^2 \rangle_t}{\rho_e c_e} = \frac{P_i^2}{3\rho_e c_e} \; . \qquad (117)$$

To calculate the reflection of this incident sawtooth wave we will express p_i as a sum of harmonic waves,

$$p_i(\underline{x},t) = \mathrm{Re}\, \frac{2iP_i}{\pi} \sum_{n=1}^{\infty} \frac{1}{n} e^{in(k_e x \cos\theta_s \cos\psi_s + k_e y \cos\theta_s \sin\psi_s - \omega_e t)} \qquad (118)$$

The scattered sound field for an incident harmonic plane wave is given by Eqs. 48 or 50 and 51. Because of the assumed linearity of the problem we can add the harmonic solutions for the components making up the incident sawtooth wave. The result is

$$p_s(\underline{x},t) = \mathrm{Re}\, \frac{4k_e}{\pi^2} P_i \begin{Bmatrix} \cos\theta_s \\ \cos\theta_r \end{Bmatrix} \frac{1}{R_r} \sum_{n=1}^{\infty} G_n e^{in(k_e R_r - \omega_e t)} \qquad (119)$$

where $\cos\theta_s$ is used for the FRS formulation, $\cos\theta_r$ is used for the SRS formulation, G_n is the value of G as given by Eq. 49 at $k = nk_e$. The normalized intensity is given by

$$\frac{I_s(R_r,\theta_r,\psi_r)}{I_1} = \frac{4}{\pi^2}\frac{k_e^2}{R_r^2}\frac{\cos^2\theta_s}{\cos^2\theta_r}\frac{6}{\pi^2}\sum_{n=1}^{\infty} G_n^2 \qquad (120)$$

with

$$G_n = \frac{L_x L_y}{4}\frac{\sin n\alpha f_e}{n\alpha f_e}\frac{\sin n\beta f_e}{n\beta f_e} \qquad (121)$$

where α and β are given by Eq. 106. Evaluation of the summation must be accomplished numerically. We have done this for the particular case of θ_s and $\psi_s = 0$ and $\psi_r = 0$. The SRS formulation for the normalized intensity is plotted in Fig. 27 for a value of $k_e L/2 = 1$. It can be compared with the result for the reflection of an incident harmonic wave of frequency f_e. The comparison shows a very interesting result. The intensity is infinite at angles corresponding to specular reflection, $\theta_r = 0$ for this case. The fact that the intensity goes to infinity at specular angles of reflection is not physically unrealizable since the total reflected power is finite.

The reflection of high level random sound waves can be handled quite simply. Since the reflection process is linear we treat the reflection of high level random sound waves the same way as low level random waves. The reflected power in a given band is found by multiplying the incident power in that band by the ratios shown in Figs. 18 through 24. The effect of nonlinearities must, of course, be considered in studying the propagation of the high level reflected sound waves.

2.9 Comparison of the Approximate Solutions with the Exact Solutions for a Disk

The exact solution for the scattered field from a rigid disk with a normally incident plane harmonic wave has been found by Bouwkamp [*14*] among others [*15,16*]. The disk is a particular shape for which an exact solution can be found because the boundary conditions expressed in an oblate spheroidal coordinate system

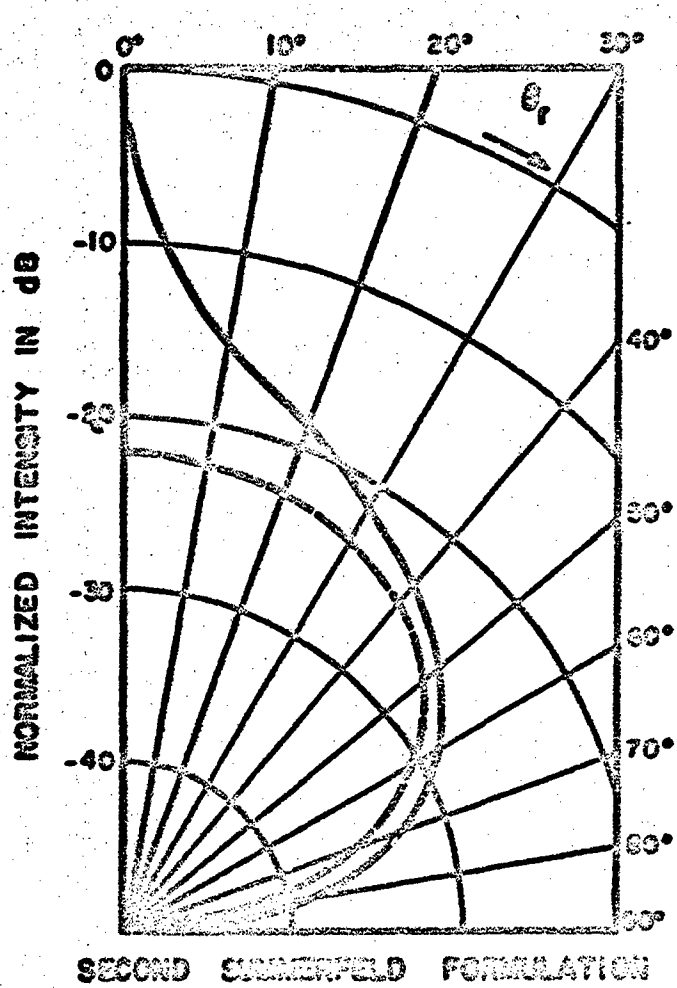

FIG. 27 REFLECTED FIELD ACOUSTIC INTENSITY FOR AN INCIDENT SAWTOOTH WAVE.

for the problem are not mixed. Theoretically, a solution for any angle of incidence could be found. In practice, however, only the solution for normal incidence is tabulated. A detailed comparison of the exact solution and the approximate solutions discussed in this report has been made by Leithner [15]. We summarize this comparison by presenting the exact and approximate solutions for the total reflected power in Fig. 28. The exact solution has been taken from Ref. 16. We see that the FRS approximate formulation is in much better agreement with the exact solution than the SRS approximate formulation. However, as discussed previously the difference between the FRS and SRS solutions for normal incidence is in the prediction of the amount of power radiated in directions corresponding to high values of θ_r. Unfortunately, Baars' [16] experimental results lead to the opposite conclusion. The question of which formulation to use for nonspecular angles of reflection is still open. But since we are mostly interested in specular reflection in this report, we can leave this question unanswered.

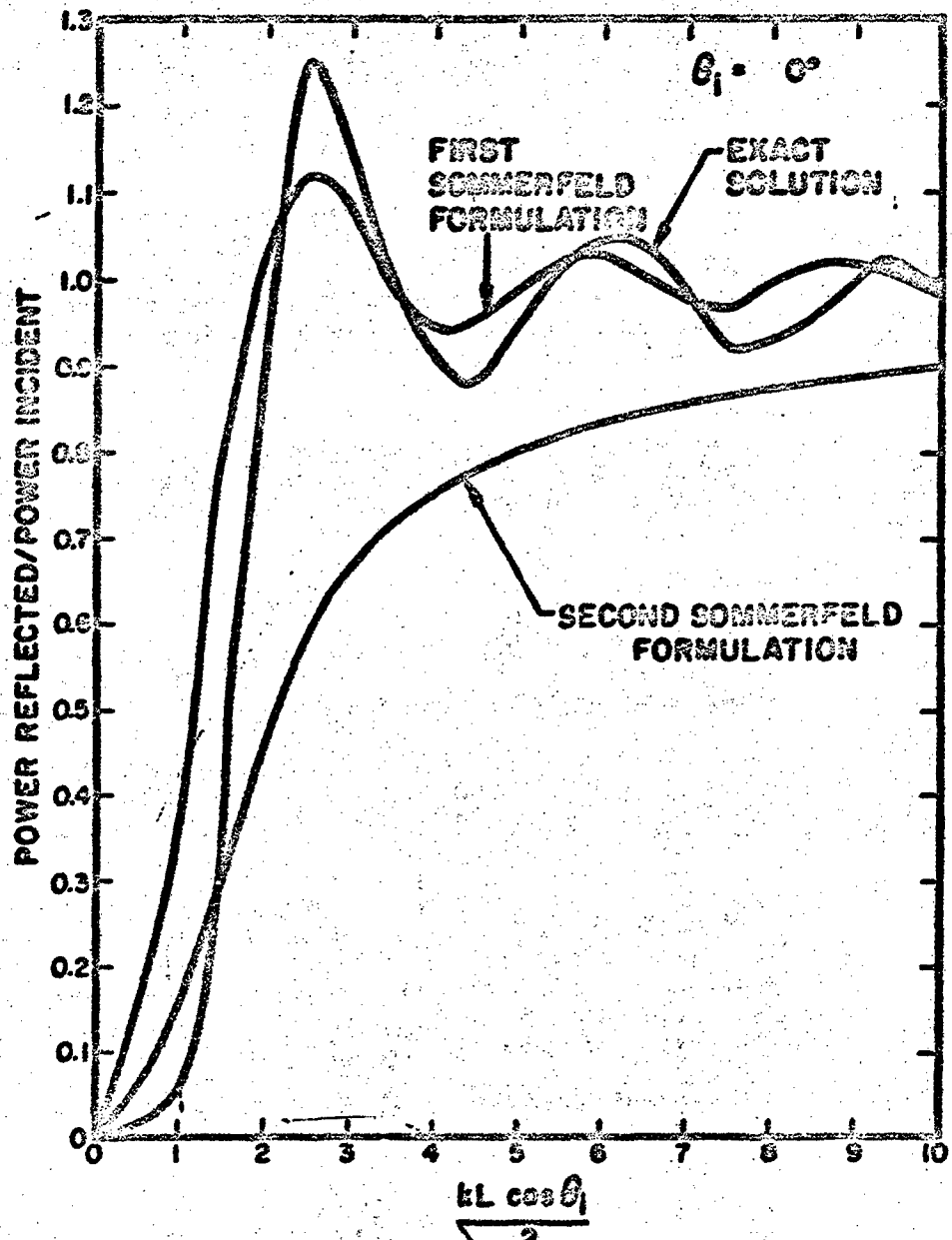

k ACOUSTIC WAVENUMBER

L LENGTH OF ONE SIDE OF THE REFLECTOR

θ_i ANGLE OF INCIDENCE FROM A NORMAL TO THE REFLECTOR

FIG. 28 COMPARISON OF THE APPROXIMATE SOLUTIONS WITH THE EXACT SOLUTION FOR A DISK.

SECTION III

EXPERIMENTS

Two sets of experiments were conducted to complement the theoretical work outlined in Sec. II. The first set of experiments was conducted to support the validity of the approximate formulations for the reflected field. These experiments are discussed in Secs. 3.2 to 3.4. Section 3.1 compares the approximate formulations with data obtained from Ref. 3. The second set of experiments was conducted to study the interaction of the acoustic field near a test object with that near a reflector. The use of a reflector to form a resonant cavity, see Fig. 3, and to reflect sound away from a test object, see Fig. 2, was investigated in this set of experiments. These experiments are discussed in Sec. 3.5.

3.1 Data From Experiments Conducted by Sakurai and Maekawa [3]

Sakurai and Maekawa [3] have studied the far-field reflection of an incident plane wave by a rigid square panel. They conducted both a theoretical and experimental study.

Although the authors of Ref. 3 carried out their program to understand the use of reflectors as "clouds" in a large auditorium, their results are equally relevant to the problem being discussed in this report.

Sakurai and Maekawa used a Fresnel evaluation of the HK approximate formulation - see discussion following Eq. 45. A comparison of their Fresnel evaluation with the far field evaluation of the FRS approximate formulation is shown in Figs. 29 and 30. These figures were obtained from Ref. 3. To make the comparison we added the curves giving the far-field evaluation.

The experimental values shown in Figs. 29 and 30 were obtained by Sakurai and Maekawa using a setup similar to that described in the next Section. The measured sound pressure levels are normalized by the sound pressure level that would exist a distance $R_s + R_r$ from the point source, where R_s is the distance from the source to the reflector and R_r is the distance from the receiver to the reflector. The source was an electrostatic loudspeaker located 3.5 meters from the center of the reflector. The receiving microphone was mounted on a rotating arm 1.5 meters from the center of the reflector. Note: the microphone was located at 1 meter from the reflector for the experiments with a 6 cm ($2a = 6$) reflector. The distances of the source and the

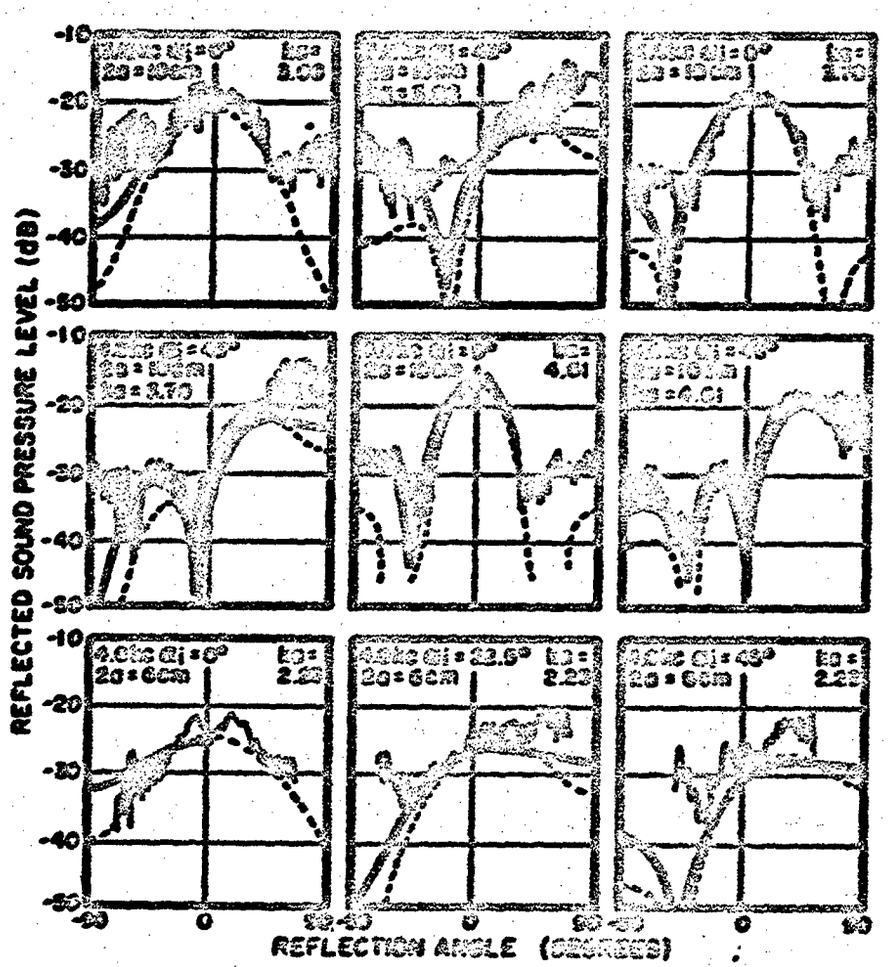

——— FAR FIELD EVALUATION OF FIRST SOMMERFELD FORMULATION

——— EXPERIMENTAL VALUES

------ FRESNEL EVALUATION OF HELMHOLTZ-KIRCHOFF FORMULATION

α_i -ANGLE OF INCIDENCE kc-KILOCYCLES PER SECOND

2a-LENGTH OF ONE SIDE OF THE REFLECTOR k-ACOUSTIC WAVENUMBER

FIG. 29 COMPARISON OF THE APPROXIMATE SOLUTIONS WITH DATA FROM REF. 3.

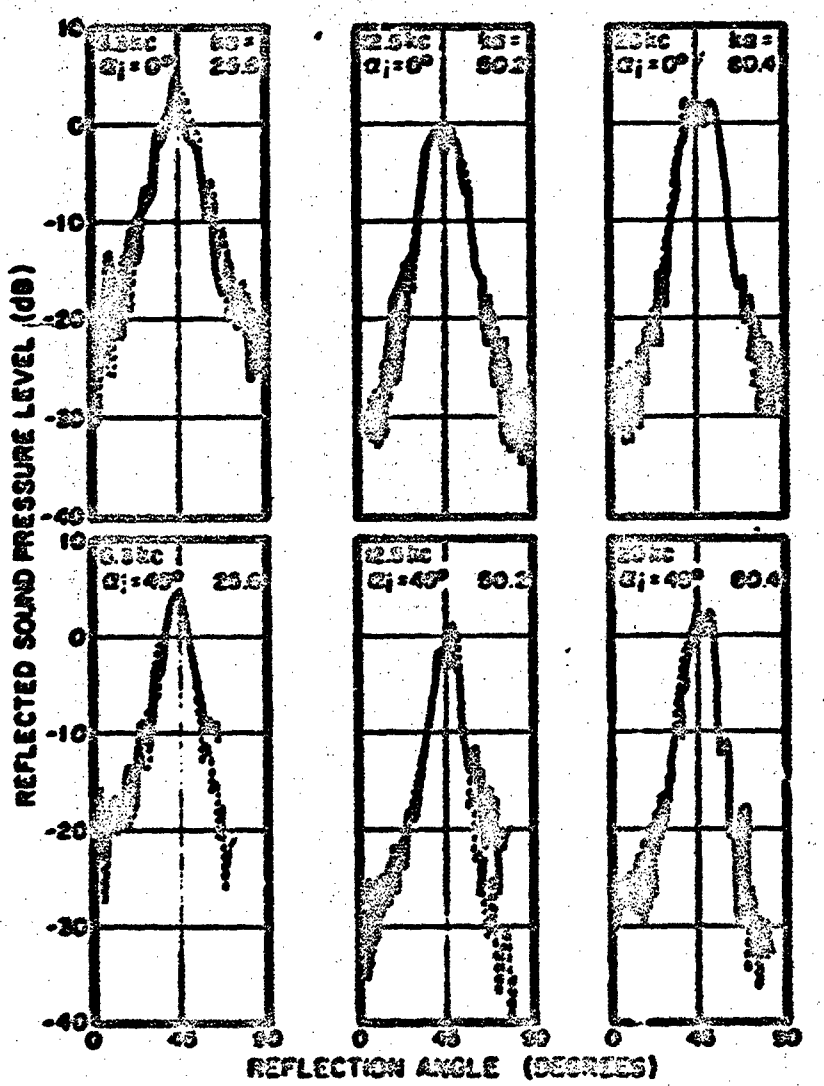

——— COMPUTER EVALUATION OF FIRST SOMMERFELD FORMULATION

——— EXPERIMENTAL VALUES

------ FRESNEL EVALUATION OF HELMHOLTZ-KIRCHOFF FORMULATION

α_i - ANGLE OF INCIDENCE kc - KILOCYCLES PER SECOND

2a - LENGTH OF ONE SIDE OF THE REFLECTOR= 43.5cm k - ACOUSTIC WAVENUMBER

FIG. 30 COMPARISON OF THE APPROXIMATE SOLUTIONS WITH DATA FROM REF. 3.

receiving microphone from the reflector are sufficiently large that the far-field solutions are applicable.

The comparison between the far-field solutions and the experimental values in Figs. 29 and 30 are satisfactory in most cases. The lack of agreement for low values of ka is believed to be more a result of errors in the measurements due to background noise than to errors in the theory. For these low values of ka the sound pressure level of the reflected field at the measurement point is 20 to 40 dB below the level of the incident field.

To gain further support for the theoretical results, we conducted additional experiments. These are described in the following Sections.

3.2 Experimental Setup to Study the Reflected Field

Experiments to measure the reflected pressure field were conducted in BBN's anechoic chamber. The working area of this chamber is 8 ft by 8 ft by 10 ft. It is anechoic above 400 Hz. A sketch of the test apparatus is shown in Fig. 31. A schematic of the test setup and the instrumentation is shown in Fig. 32. A pulsed tone technique was used to measure just the reflected pressure field and not the sum of the incident plus the reflected fields. A tone burst consisting of a number of sine wave cycles was used to excite the electrostatic speaker. By making the distance from the source directly to the receiver, R_d, significantly less than the sum of the distances from the source to the reflector and the reflector to the receiver, $R_s + R_r$, an interval of time will occur, after the burst has ended, in which only the reflected pressure field will be measured. The duration of this interval is given by

$$T = \frac{R_s + R_r - R_d}{c_0} \qquad (122)$$

where T is the duration of the interval and c_0 is the speed of sound. Measurements of the reflected field pressure levels were taken during this time interval. A 1-in. B&K microphone was used to measure the sound pressure. The microphone was pointed directly at the reflector for all measurements. The output of the microphone was amplified by a fixed gain preamplifier, attenuated by a variable attenuator, high pass filtered and displayed on an oscilloscope. Measurements were taken by adjusting the attenuator to give a predetermined level on the oscilloscope. The microphone signal was filtered to alleviate the low-frequency

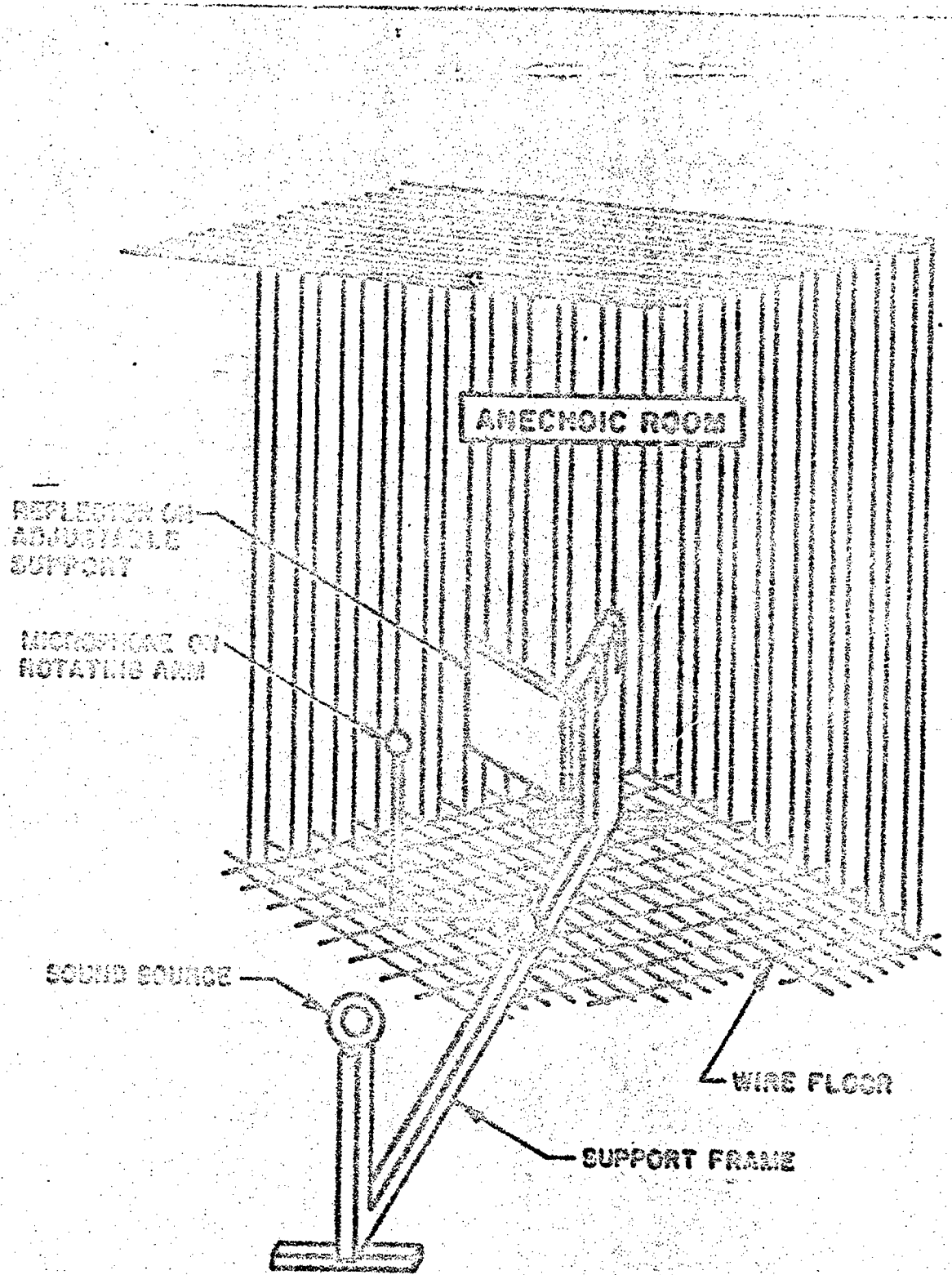

FIG. 31 THE EXPERIMENTAL SET-UP.

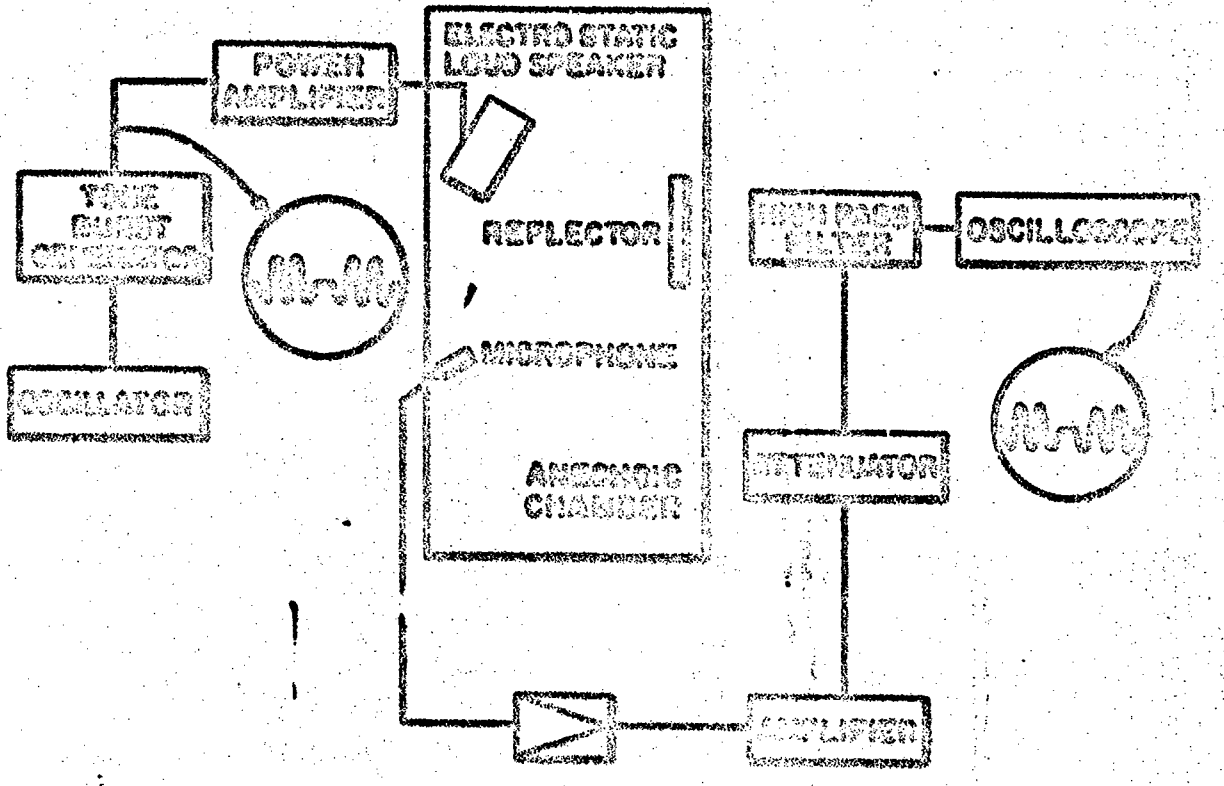

FIG. 32 SCHEMATIC OF THE INSTRUMENTATION.

reverberation in the chamber. The cutoff frequency of the filter was at least one octave below the test frequency. Overall accuracy of the measurement system was judged to be ±1 dB.

The amplitude of the incident tone burst was measured by the same system. The reflector was removed and the microphone put in its place. The microphone was pointed at the source and the incident sound pressure level was measured.

The different experiments that were conducted and the results of these experiments are presented in the following Sections.

3.3 Reflection of a Pure Tone

Because of the small size of the BBN anechoic chamber most experiments were conducted with a 1 ft by 1 ft reflector. This would represent a 1/4 in. scale model of a typical size for actual use in shaping a sound field. The frequencies for the experiments were 1000 to 8000 Hz. Results for the 1 ft by 1 ft reflector in this frequency range would be applicable for a 4 ft by 4 ft reflector in the frequency range 250 to 2000 Hz.

A summary of the experiments conducted is given in Table I. The range of values of the dimensionless parameter kL/2 is 2.78 to 22.24. The angles of incidence for the experiments were $\theta_s = 30°$ and $\phi_s = 0°$. For each set of experiments the receiving microphone was placed at various values of θ_r but with $\phi_r = 180°$.

The first series of experiments was conducted with the receiver 36 in. from the reflector. At this distance the receiver is in the intermediate region between the near and the far fields. Thus, we found it necessary to use the numerical evaluation from Sec. 2.4. Four frequencies were used, 1000, 2000, 4000, and 8000 Hz. The measured reflected sound pressure levels normalized by the level of the incident field at the center of the reflector are presented in Figs. 33 and 34. For comparison we have plotted the numerical evaluation of the FMB approximate formulation. The agreement between the theory and the measured values is excellent, thereby supporting the validity of the approximate FMB formulation.

The second series of experiments was conducted with the receiver 18 in. from the reflector. At this distance the receiver was in the near field. Thus, the numerical evaluations from Sec. 2.4 were again used to obtain a theoretical prediction. The theoretical predictions and the measured values of reflected sound pressure level are shown in Figs. 35 and 36. Again the agreement between the theoretical prediction and the measured values is excellent.

TABLE I

	Frequency (Hz)	kL/2	Reflector to Reflector Receiver Distance	Reflector to Reflector Thickness (in.)	Reflector Size
Series 1	1000	2.86	36	0.0625	12" × 12"
	2000	5.72	"	"	"
	4000	11.42	"	"	"
	8000	22.84	"	"	"
Series 2	1000	2.86	18	0.0625	12" × 12"
	2000	5.72	"	"	"
	4000	11.42	"	"	"
	8000	22.84	"	"	"
Series 3	500→8000	0.7→11.12	36	0.0625	6" × 6"
Series 4	1000	2.86	36	0.021	12" × 12"
	2000	5.72	"	"	"
	4000	11.42	"	"	"
	8000	22.84	"	"	"

Common Parameters

Reflector Material	Aluminum
Source to Reflector Distance	50 in.
Angle of Incidence	30°

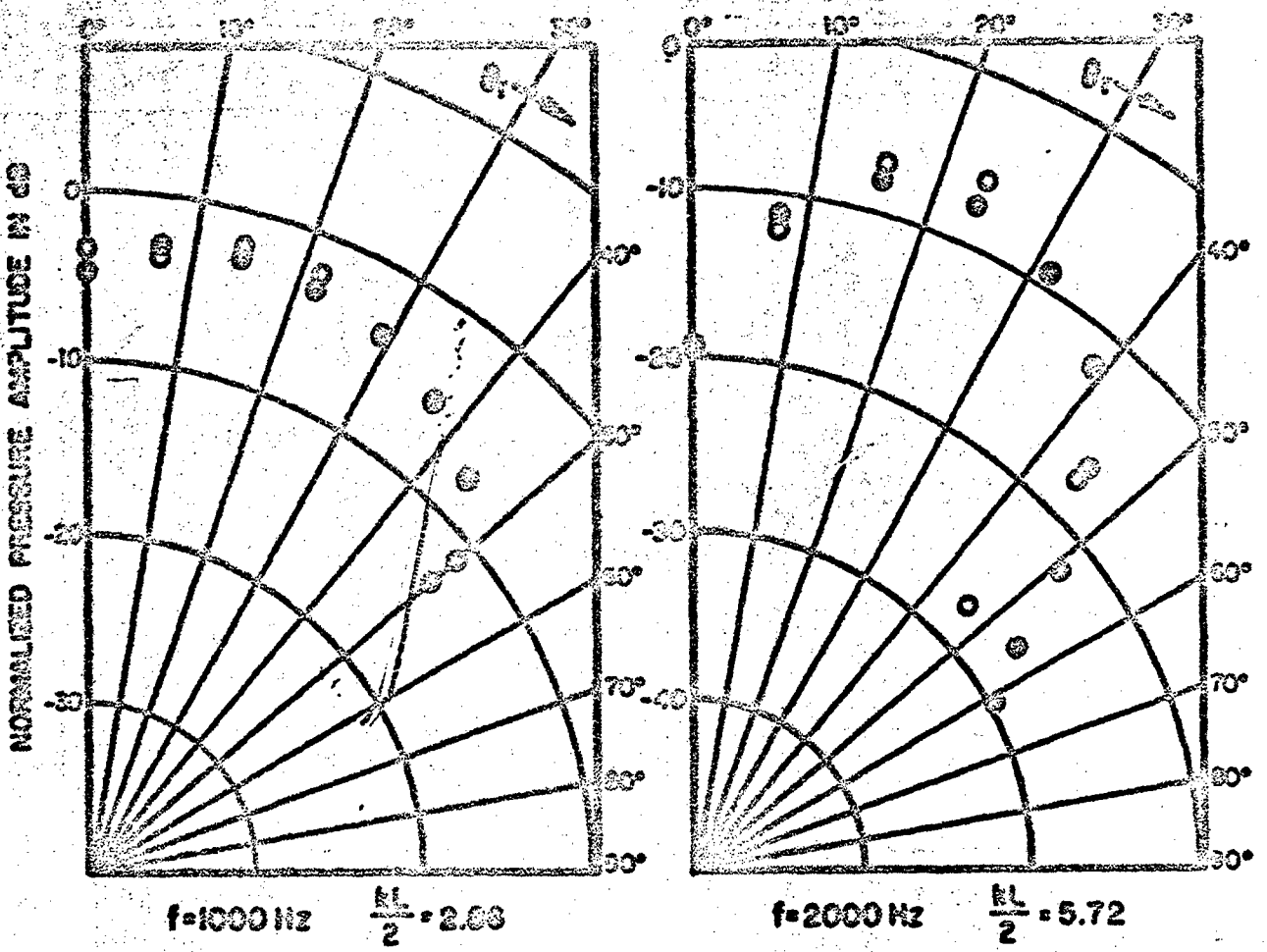

● COMPUTER EVALUATION OF FIRST SOMMERFELD

○ MEASURED VALUES

ANGLE OF INCIDENCE	30°
SOURCE TO REFLECTOR	90 in
REFLECTOR TO RECEIVER	36 in
REFLECTOR THICKNESS	1/16 in
REFLECTOR SIZE	12 x 12 in.

FIG. 33 COMPARISON OF THE APPROXIMATE SOLUTIONS WITH DATA — RECEIVER 36 in. FROM THE REFLECTOR.

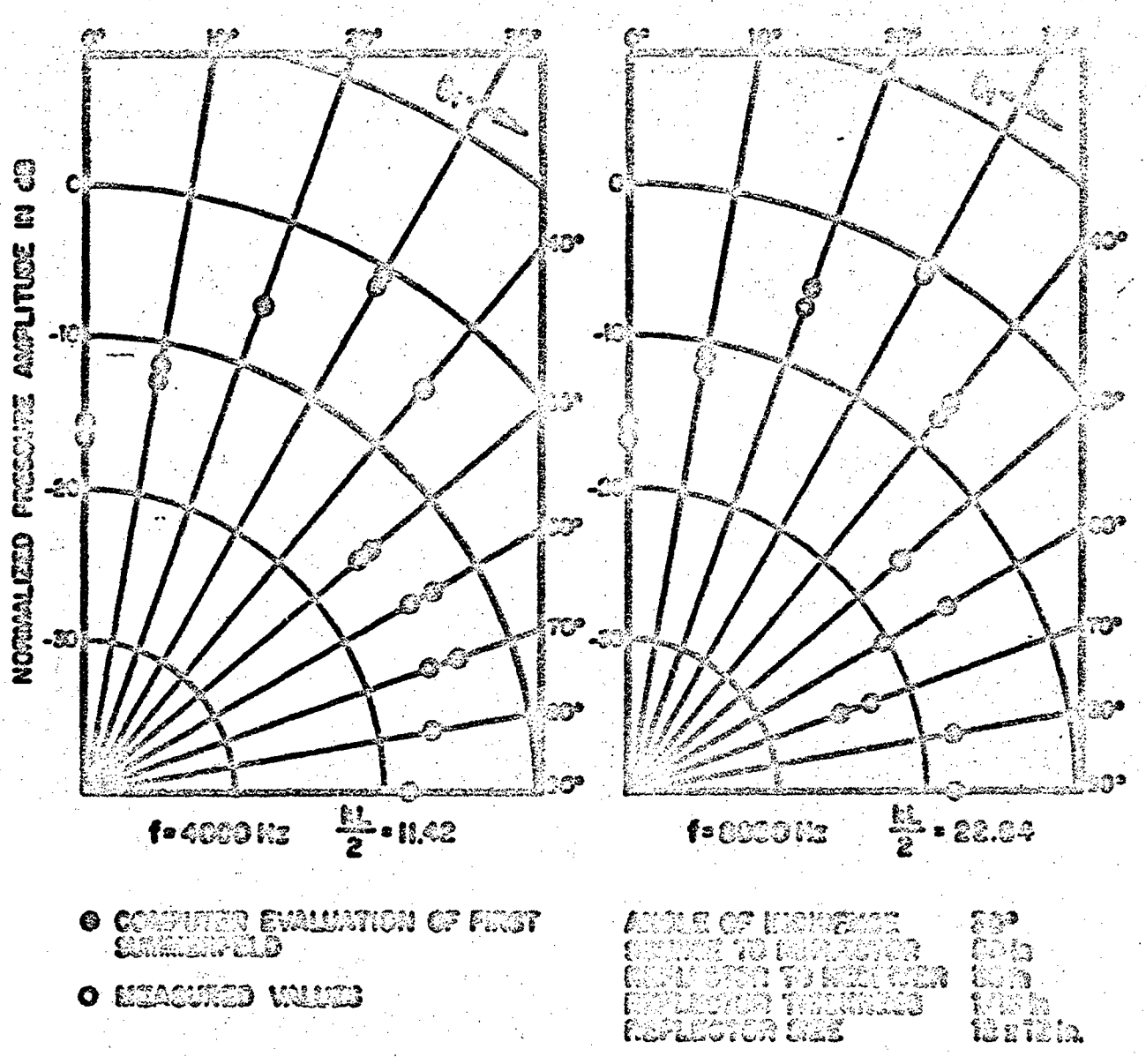

FIG. 34 COMPARISON OF THE APPROXIMATE SOLUTIONS WITH DATA — RECEIVER 36 in. FROM THE REFLECTOR.

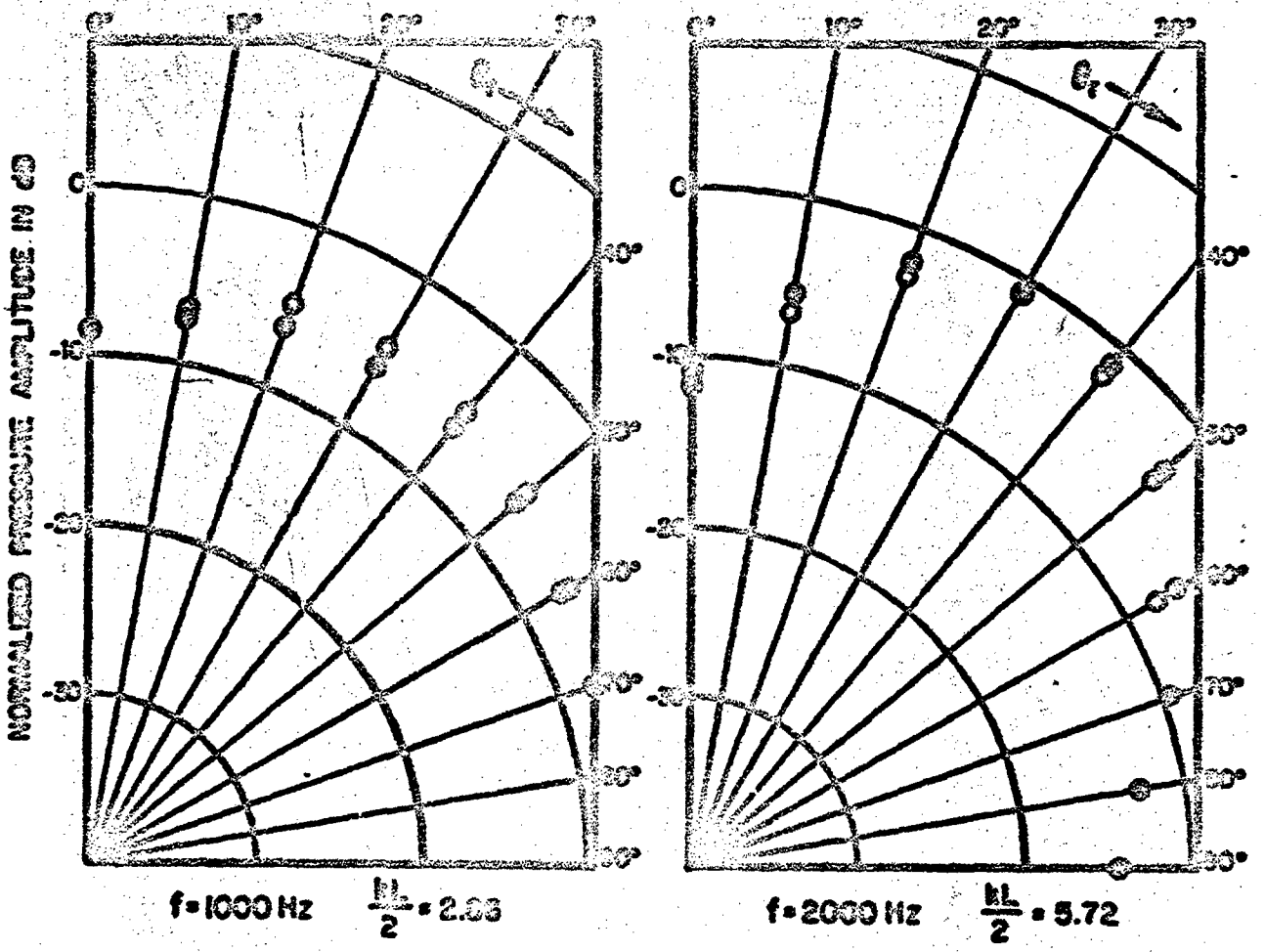

FIG. 35 COMPARISON OF THE APPROXIMATE SOLUTIONS WITH DATA — RECEIVER 18 in. FROM THE REFLECTOR.

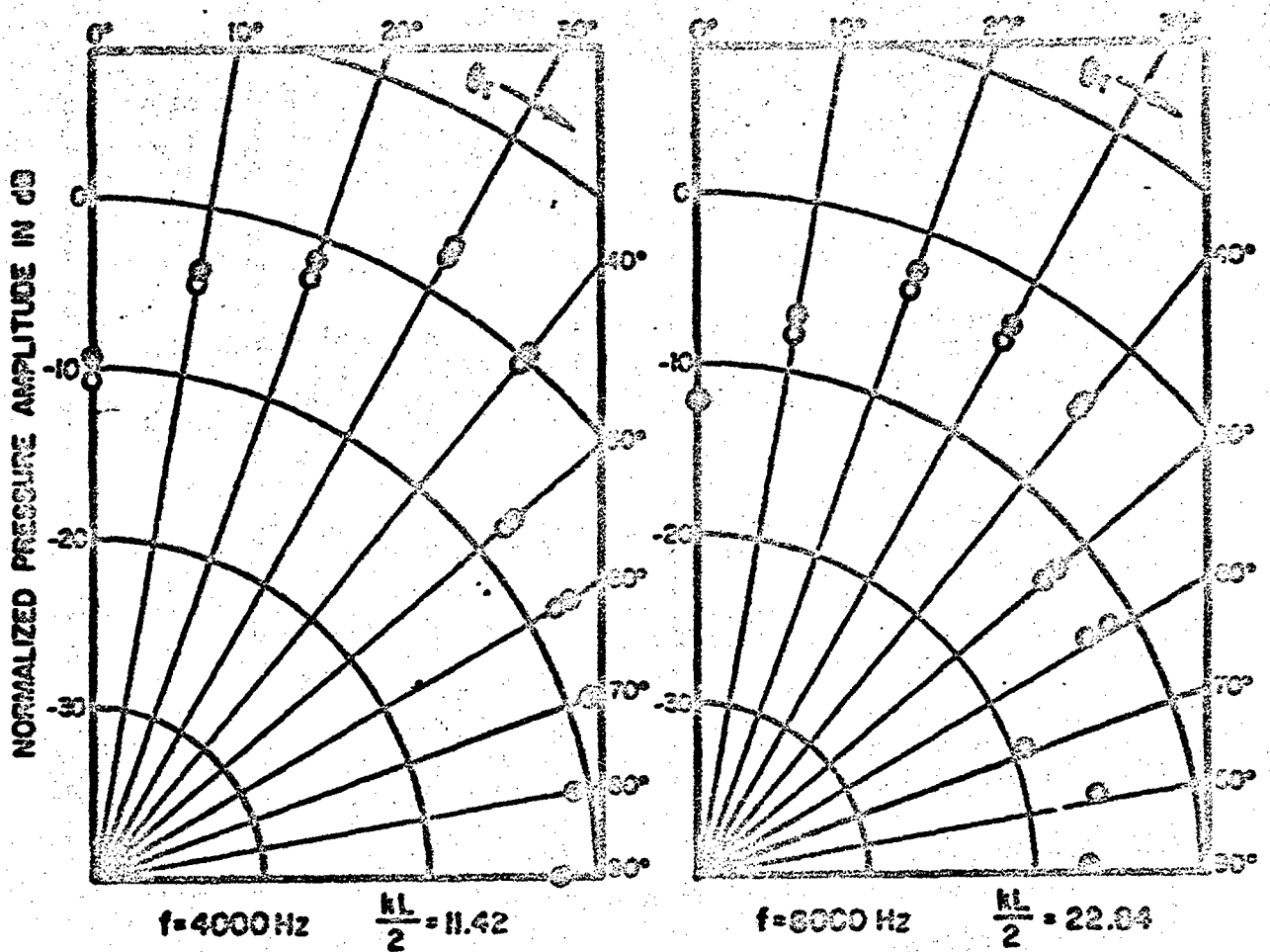

● COMPUTER EVALUATION OF FIRST SOMMERFELD

○ MEASURED VALUES

ANGLE OF INCIDENCE	30°
SOURCE TO REFLECTOR	30 ft
REFLECTOR TO RECEIVER	18 ft
REFLECTOR THICKNESS	1/16 in
REFLECTOR SIZE	12 x 12 ft

FIG. 36 COMPARISON OF THE APPROXIMATE SOLUTIONS WITH DATA — RECEIVER 18 ft. FROM THE REFLECTOR.

A third experiment was conducted in which the receiving microphone was located at one position corresponding to specular reflection – R_r = 36 in., $\theta_r = 30^\circ$ and $\phi_r = 180^\circ$ – for a number of different frequencies. The measurement technique for this experiment was like that used for the first two series of experiments. The measured sound pressure levels are shown in Fig. 37. For comparison the numerical evaluation of the FRS approximate formulation is also shown. The agreement between theory and experiment is again excellent.

The fourth series of experiments was conducted to investigate the effect of reflector response on the reflected sound field. The first three series of experiments were conducted with a 1/16-in. aluminum panel. Agreement between the results of these experiments and the theoretical predictions for a rigid panel indicated that the response of the 1/16-in. panel had no effect. To further support the predicted result that the response of a panel, which is not paper thin, has no effect on the reflected field, we conducted experiments using a 0.021-in. thick panel. The parameters for this series of experiments are given in Table I. The results are shown in Figs. 38 and 39. These results show that the response of the two panels used, 1/16-in. and 0.021-in. thick, had no observed effect on the reflected field.

We conclude from the above experiments that the approximate formulations for the reflected field serve as a valid base on which to predict the performance of a reflector in shaping an acoustic field in a test chamber.

Experiments using an incident random sound wave were not conducted in this phase of the program because of the difficulty in measuring the reflected field separately from the incident field. The pulsed tone technique could not be adapted to random sound waves since the measurement interval, T, was not long enough in our experiments to allow accurate measurement of the mean-square pressure of a random sound field.

3.4 Reflection of an Incident Sawtooth Sound Wave

The experiments described in this Section were conducted to investigate the reflection of an incident sawtooth sound wave, which represents an incident high level sound wave. However, the experimental difficulties precluded any definitive results. Because of the excellent agreement between theory and experiment for the case of an incident pure tone we feel that the analytical technique of expressing the sawtooth wave as a sum of pure tones to calculate the reflected field for an incident sawtooth wave is valid, even though we have no experimental verification of the resulting predictions.

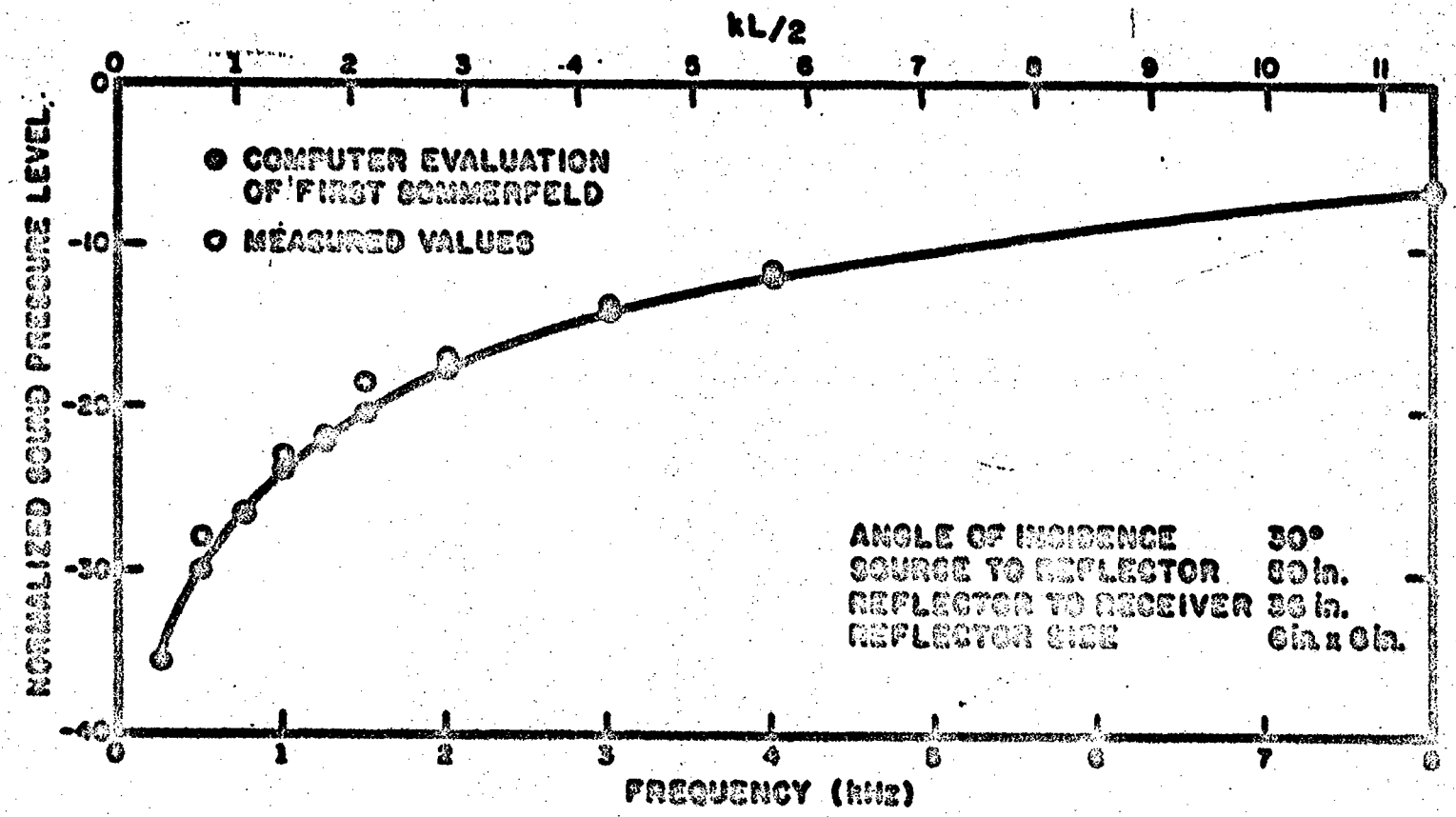

FIG. 37 COMPARISON OF THE APPROXIMATE SOLUTIONS WITH DATA AS A FUNCTION OF FREQUENCY OF THE INCIDENT WAVE.

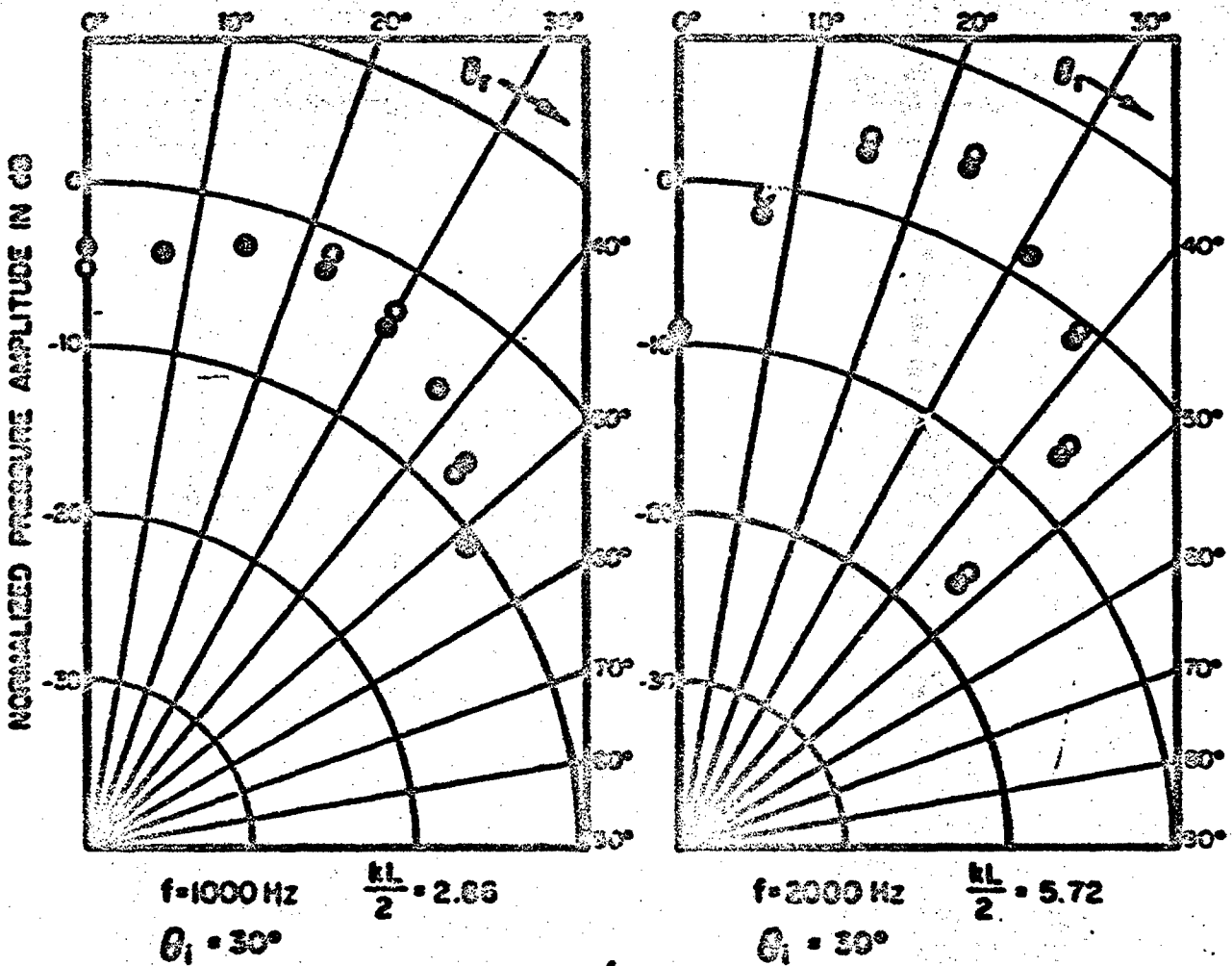

● MEASURED VALUES FOR 1/16 INCHES THICK REFLECTOR

○ MEASURED VALUES FOR 0.001 INCHES THICK REFLECTOR

ADDITIONAL TEST PARAMETERS ARE GIVEN IN TABLE I, PAGE 78

FIG. 38 COMPARISON OF DATA FOR REFLECTORS OF VARIOUS THICKNESS.

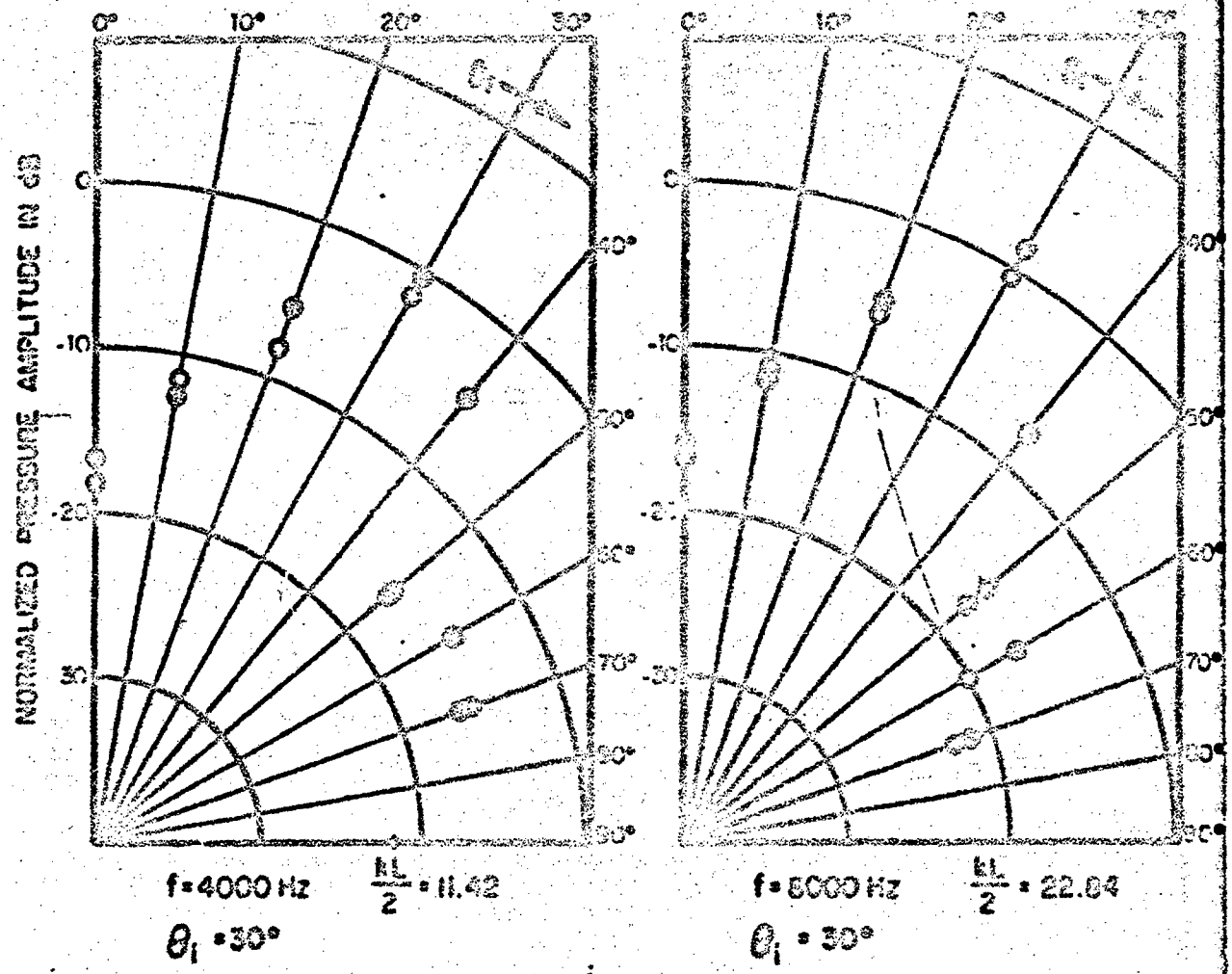

● MEASURED VALUES FOR 1/16 INCHES THICK REFLECTOR

○ MEASURED VALUES FOR 0.021 INCHES THICK REFLECTOR

ADDITIONAL TEST PARAMETERS ARE GIVEN IN TABLE I, PAGE 78

FIG. 30 COMPARISON OF DATA FOR REFLECTORS OF VARIOUS THICKNESS.

Briefly the experimental problems were as follows. First, we tried to create an acceptable sawtooth acoustic wave by feeding an electronic sawtooth signal directly into an electrostatic speaker. The amplitude response of the speaker was sufficiently wide to transmit the acoustic energy spectrum to the acoustic media. However, the phase distortion of the speaker was so great that the sawtooth waveform was destroyed. We next filtered the electronic sawtooth input signal by adjustable high and low pass filters. By adjusting the cutoff frequencies of the filters we found it possible to generate an acoustic wave which bore some resemblance to the desired sawtooth. Unfortunately, the resemblance was not sufficient to allow us to use the generated waveform to represent a sawtooth.

3.5 Reflector — Structure Interaction

When a reflector is placed in close proximity to a test structure the scattered fields created by the two objects interact and form a complex spatial distribution of sound pressure level. Two counteracting effects occur. First, the reflector and the test structure form a partially cavity in which a reverberant sound field can be established. The reverberant field has significantly higher levels than those in the surrounding acoustic field. Second, the reflector blocks the incident sound waves and keeps them from impinging on the test structure; thereby lowering the sound pressure levels on the structure. A theoretical study of these two counteracting effects is beyond the state of the art and was not attempted for this program. Instead, a complete experimental study was conducted.

For the experimental study we fabricated a simple test structure, shown in Fig. 40. This structure is a 4 ft by 4 ft aluminum panel 1/16-in. thick stiffened in each direction by two "L" section stringers. The "L" cross section measures 3/4 in. by 3/4 in. and is made from 1/8-in. aluminum sheet. The stringers are riveted to the aluminum panel with rivets every 1-1/2 in. The stringers are positioned on the structure so as to form nine (9) equal subsections. To facilitate the fabrication of the structure two stringers running in one direction were placed on one side of the panel while the two running in the other direction were placed on the other side of the panel. Location of the stringers in this way avoids the problem of intersecting stringers.

The test structure was suspended by nylon cord in a semi-reverberant, 3000 cu ft, test chamber. Reverberation times in the chamber are approximately 1 sec in the frequency range 400 to 4000 Hz.

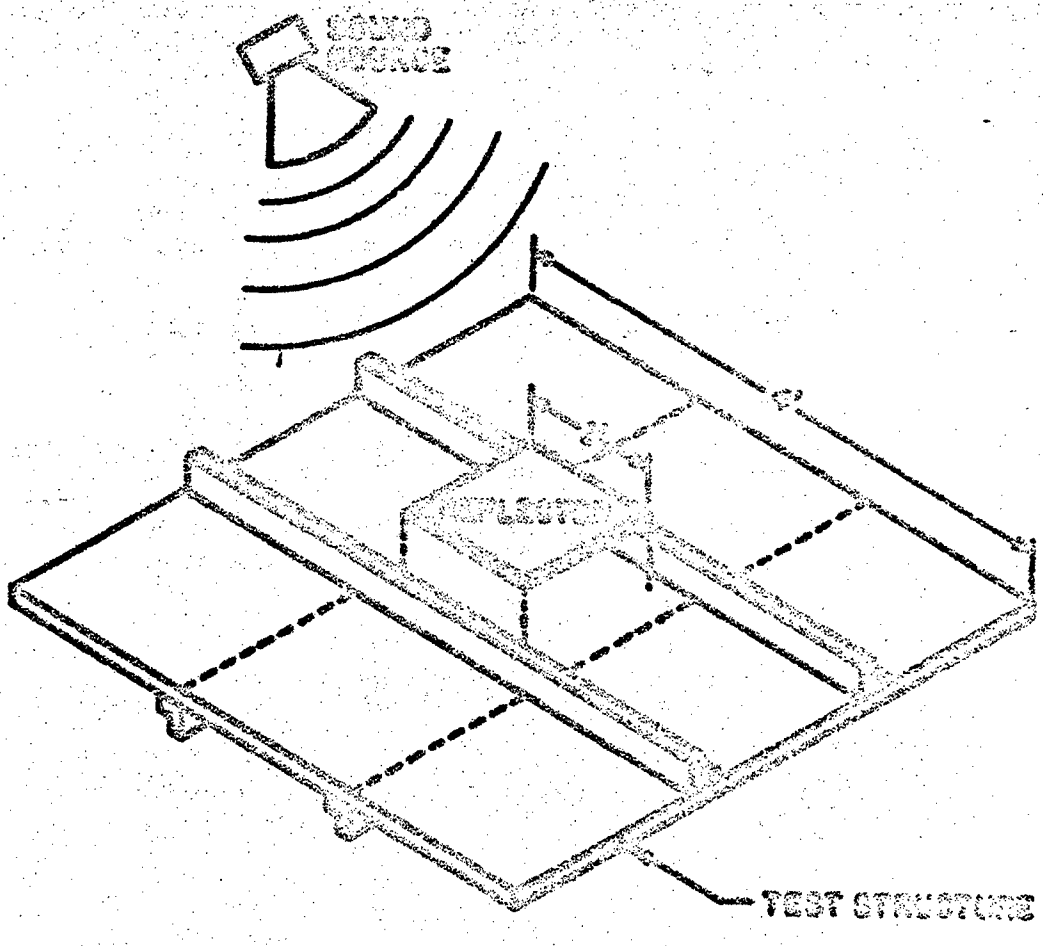

FIG. 40 TEST SETUP OF A REFLECTOR NEAR A SIMULATED TEST STRUCTURE.

A 1 ft by 1 ft aluminum panel 1/16-in. thick was selected as a reflector. This panel was positioned parallel to the surface of the test structure over the center subpanel using three rods extending at right angles from the structure. The distance from the reflector to the test structure was continuously adjustable from 0 to 6 in.

An incident acoustic noise field for the experiments was created by an electromagnetic driver and horn. This sound source was located 8 ft from the center of the test object and directed toward it. Three angles of incidence were used for the experiments — normal to the test structure surface, 45° from the normal, and grazing to the structures surface.

— Sound pressure levels on the surface of the test structure were measured by a 1/2-in. B&K microphone taped directly to the structure. The acceleration levels of the test structure were measured using a 2-gm B&K accelerometer. The microphone and accelerometer outputs were analyzed in one-third octave bandwidths using a General Radio spectrum analyzer.

The experiments were conducted by exciting the sound source with broadband random noise and measuring the sound pressure level and acceleration level in one-third octave bands as a function of the reflector location and the angle of incidence. Measurements of sound pressure level and acceleration level without the reflector in place were used as a reference level for the other experiments. For normal angles of incidence the sound pressure levels on the illuminated side of the panel are approximately 5 dB greater than on the shadow side, indicating that the test structure is in the near field of the source.

Measurements of the sound pressure level at the center of the subpanel under the reflector for six (6) reflector locations and three (3) angles of incidence are presented in Figs. 41 through 43. A significant altering of the sound pressure levels on the test structure is evident. A pronounced resonant behavior occurs for small reflector to structure spacing in the one-third octave bands centered on 800 and 1600 Hz. The resonances in these bands correspond to the 1st and 5th resonance frequencies of a two-dimensional acoustic space with pressure release boundary conditions. The 2nd, 3rd and 4th resonances of such a space occur at 1250, 1250 and 1540 Hz. However, since the mode shapes at these resonances are zero at the center of the space, our measurements did not detect the resonant behavior at these frequencies. At larger reflector to structure distances the resonant behavior is not as pronounced and the resonance frequencies decrease slightly.

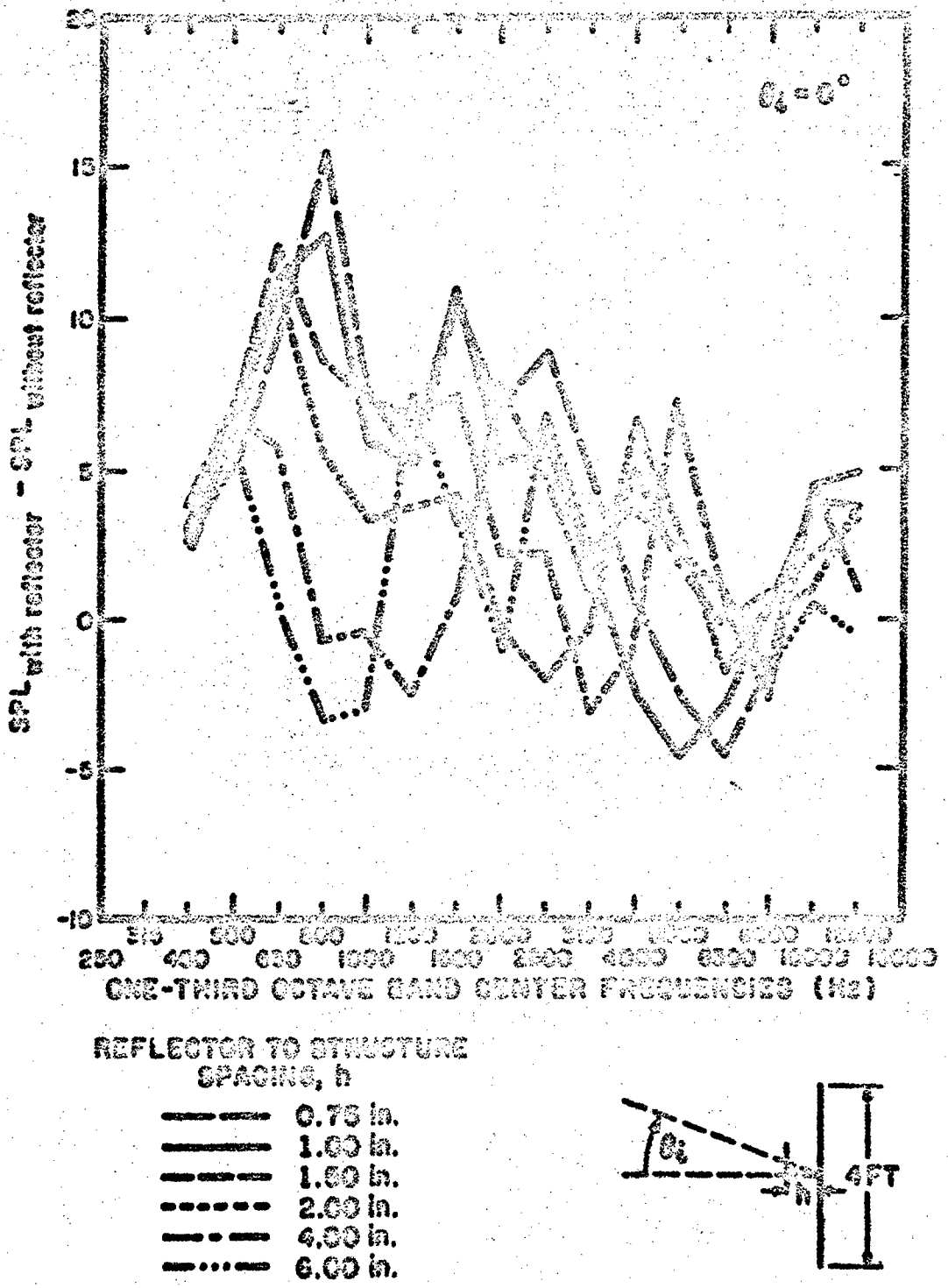

FIG. 41 SOUND PRESSURE LEVELS MEASURED IN A CAVITY FORMED BY A REFLECTOR FOR 0^0 ANGLE OF INCIDENCE.

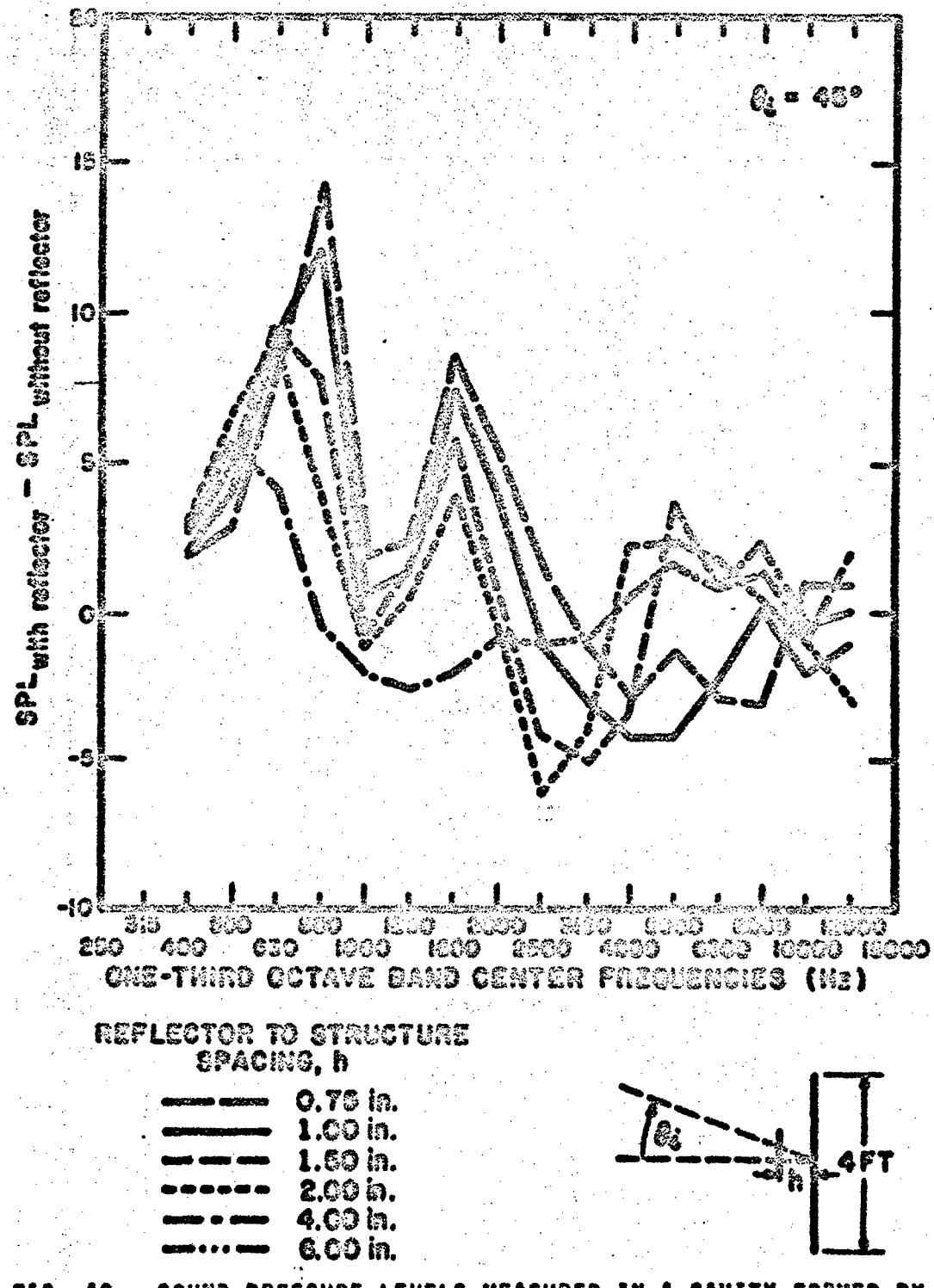

FIG. 42 SOUND PRESSURE LEVELS MEASURED IN A CAVITY FORMED BY A REFLECTOR FOR 45° ANGLE OF INCIDENCE.

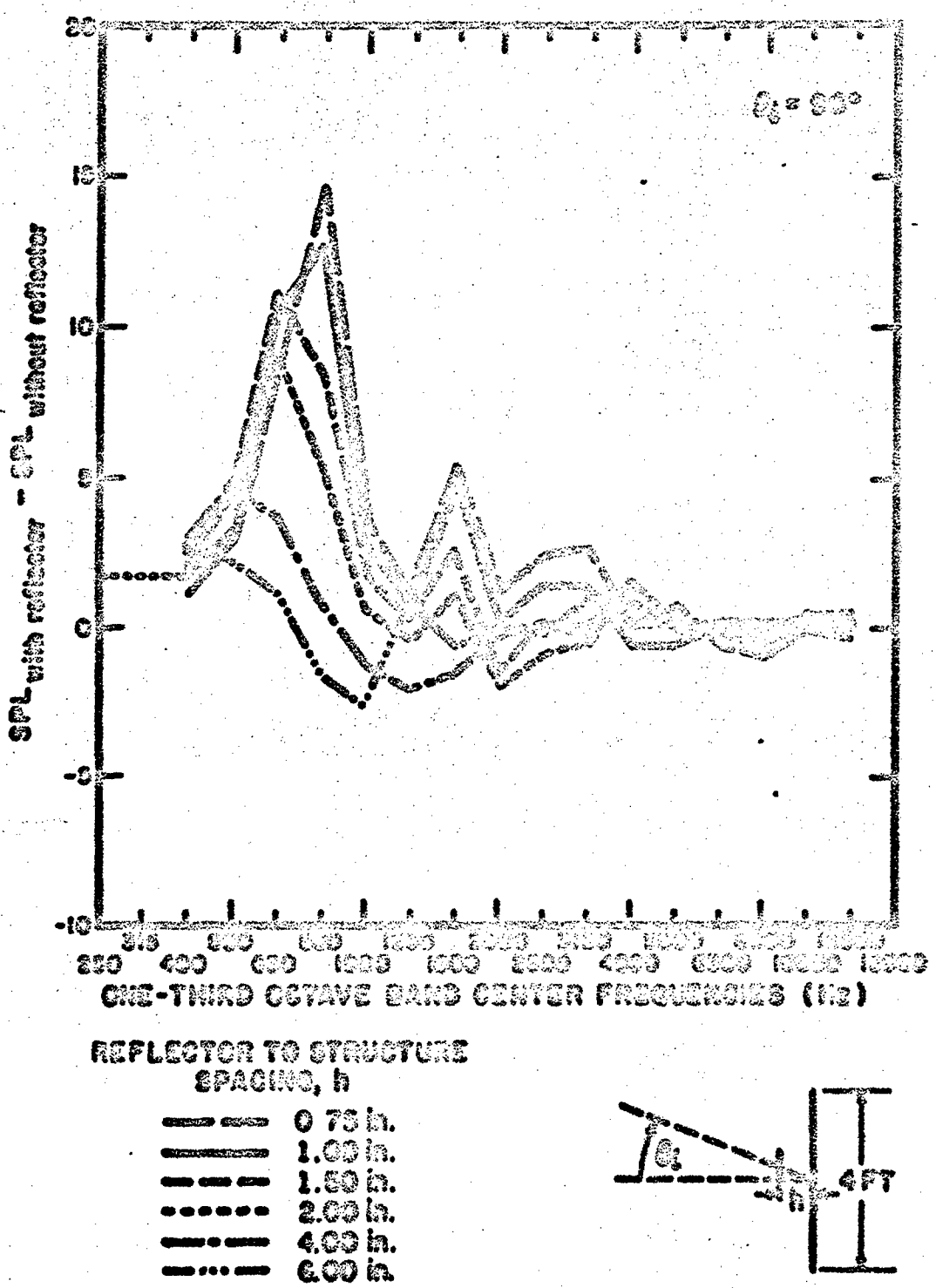

FIG. 43 SOUND PRESSURE LEVELS MEASURED IN A CAVITY FORMED BY A REFLECTOR FOR 90° ANGLE OF INCIDENCE.

At high frequencies for normal and 45° angles of incidence the reflector affects the sound pressure levels on the structure but not in a systematic way. For a grazing angle of incidence the high frequency results show that the reflector has no effect on the measured sound pressure level. This result is supported by a geometrical optics analysis.

Measurements of the test structure response were also made. The response acceleration spectrum at the center of each subpanel was measured for each set of parameter conditions described above. The effect of the altered sound pressure levels on the panel response measurements was negligible, less than ±2 dB. This result is somewhat surprising since the sound pressure levels were increased by as much as 15 dB in the one-third octave band centered on 800 Hz. We should note, however, that when the reflector is close to the test structure the radiation impedance changes significantly. It is possible that this change in impedance acts to keep the response constant.

We conclude as a result of the above experiments that the effects associated with the formation of a resonant cavity dominate those associated with the shielding of the structure from the incident sound waves. However, this result would not be valid if the back of the reflector were covered with an absorptive material which would damp the resonant behavior of the cavity. For this case some shielding would no doubt occur. Although the sound pressure levels can be increased significantly by forming a resonant cavity, this technique is not useful for shaping a sound field since the response of the structure does not increase.

SECTION IV

PRACTICAL UTILIZATION

Sections II and III of this report have presented a basic theoretical and experimental study of the reflection of incident acoustic waves by a flat rectangular panel. We now come to the most important part of the report dealing with the actual use of a reflector to shape a sound field in the test chamber.

As discussed in the Introduction, a reflector can be used in three ways: to reflect incident sound waves onto the test object as shown in Fig. 1, to reflect incident waves away from the structure as shown in Fig. 2, and to form a resonant cavity as shown in Fig. 3. The use of a reflector for the latter two purposes is discussed in Sec. 3.5. One conclusion of that Section is that the use of reflectors to form a resonant cavity is not a valid technique for shaping a sound field since the close proximity of the reflector inhibits the response of the test structure. A second conclusion is that use of a reflector to "shield" the test object from the incident sound waves also results in the formation of a resonant cavity. The reverberant buildup in the cavity exceeds the effects due to shielding so that the sound pressure levels on the test structure either stay the same or *increase*. A reduction in the sound pressure levels acting on the test structure was not observed for any value of reflector to structure spacing. For large spacing diffraction of the sound waves around the reflector eliminated any shielding effect. For small spacing the reverberant buildup eliminated any shielding effect. A possible technique for using a reflector as a shield would be to cover the back of the reflector with acoustically absorptive material. Then, the reverberant buildup would be well damped and a shielding effect possible. Use of reflectors in this way represents an area of great promise. The test technique would be to bring the reverberant field of the test chamber to the highest sound pressure level needed. Then by placing reflectors of an appropriate size over the test structure, the sound pressure level could be reduced in selected areas to achieve the correct distribution of sound pressure level. However, the effect of the reflector and its absorptive backing on the response characteristics of the structure must not be ignored. We have not pursued the use of reflectors as shields beyond the work presented in Sec. 3.5.

The use of a reflector to reflect sound waves onto a test structure in order to increase the sound pressure levels on the structure is of limited practical value. In a reverberant diffuse field sound waves are incident from all directions. Thus, a reflector diverts as much sound away from the structure as toward

it and no increase in the sound pressure level on the structure is possible. *Flat reflectors are of no use in a diffuse field.*

In the near field of the sound source or sources the sound pressure levels are higher than in the reverberant field and result predominantly from sound waves travelling away from the source.

Typically, the sound pressure levels are highest directly in front of the source. A typical contour of equal sound pressure level near a directive source is shown in Fig. 4. At low frequencies the pattern becomes more nondirective, while at high frequencies the opposite happens. By placing a reflector in the near field of a source, the sound waves coming directly from the source can be deflected onto the test structure to increase the sound pressure levels. However, an inherent limitation exists for a flat reflector. The sound pressure level in the reflected field cannot be larger than the level of the incident field a distance $R_s + R_r$ from the source, where R_s is the distance from the source to the center of the reflector and R_r is the distance from the receiving point to the center of the reflector. In other words, a flat reflector cannot extend the near field but only redirect the main lobe in the directivity pattern, as shown in Fig. 4. Thus, *the use of a reflector to redirect sound waves onto the test structure in order to increase the sound pressure level is limited to cases in which both the reflector and the test structure are within the maximum extent of the near field,* i.e., the extent of the near field directly in front of the source.

4.1 Extent of the Near Field

The extent of the near field in a sonic test chamber depends upon whether and how much anechoic treatment is used to cover the walls, ceiling and floor of the chamber. In a fully reverberant condition, the near field sound pressure levels will exceed the reverberant field pressure levels only in a very small region near the sources. This region will be so small that it can be generally stated that reflectors will not be useful in a fully reverberant acoustic test chamber.

When the absorption in the chamber is increased by the use of anechoic treatment, the region in which the near field sound pressure levels exceed the reverberant field sound pressure levels becomes larger. The sound pressure level measured in front of a sound source in a reverberant chamber is given by [17]

$$SPL = PWL + 10 \log_{10}\left[\frac{Q}{4\pi R_d^2} + \frac{4}{R_T}\right] \qquad (123)$$

where SPL is the sound pressure level in dB re 0.0002 μbar, PWL is the source power level in dB re 10^{-13} watts, Q is the directivity factor, R_d is the distance from the source to the receiving point, and R_T is the room constant in sq ft. The directivity factor, Q, is defined so that it equals one for a nondirective point source. The term $Q/4\pi R_d^2$ represents the contribution to the sound pressure level from sound waves coming directly from the source. The term $4/R_T$ represents the contribution from the reverberant sound waves. It follows that the direct sound pressure level is larger than the reverberant sound pressure level for distances which satisfy the condition

$$R_d < \left(\frac{QR_T}{16\pi}\right)^{1/2} \qquad (124)$$

where we have taken the receiver to be directly in front of the source.

As an example, the preceding discussion is applied to the large acoustic test chamber of the AFFDL Sonic Fatigue Facility. While the directivity function of the sound sources is not known accurately, it is estimated to rise smoothly from 2 at 250 Hz to 8 at 2000 Hz. This estimate should be checked by experimental measurement. The room constant, R_T, is given by

$$R_T = \bar{\alpha}S = \frac{V}{20T_{rev}} \qquad (125)$$

where $\bar{\alpha}$ is the average absorption coefficient, S is the surface area of the chamber walls, V is the chamber volume, and T_{rev} the reverberation time in seconds. The surface area of the test chamber walls is 17,416 ft^2. The volume is 155,000 ft^3. The reverberation time in the chamber with the anechoic curtains down can be approximated by a constant value of 1/2 sec in the frequency range 250 Hz to 2000 Hz. The room constant in this frequency range is calculated to be 15,500 ft^2. Using these values in Eq. 124 we find that the near field extends up to 20 ft from the sources at 250 Hz and up to 40 ft from the sources at 2000 Hz.

Both the reflector and the test structure must be within these distances from the source to obtain any practical benefit from the use of reflectors.

To obtain a 10-dB increase in the sound pressure level on the test structure the limitations on the locations of the reflector and the test structure are more limited. First, the sum of the distances from the source to the reflector and from the reflector to the test object must satisfy the condition

$$R_s + R_r < \left(\frac{QR_T}{160\pi}\right)^{1/2} . \qquad (126)$$

For the AFFDL Sonic Fatigue Facility with the curtains down this condition will be met if the sum of the distances is less than 6-1/2 ft at 250 Hz to 13 ft at 2000 Hz with a smooth transition for intermediate frequencies. A second condition is that the sound pressure level on the test structure before the reflector is put in place is at least 10 dB less than the sound pressure level a distance $R_s + R_d$ from the source. These two conditions cannot be met simultaneously unless the source directivity is high. We conclude that the potential use of reflectors in the AFFDL Sonic Fatigue Facility is very limited. However, the use of reflectors in a more anechoic space may be worth considering since the near field in such a space will extend much further from the sources.

4.2 Performance of a Flat Rectangular Reflector

To effectively use a reflector to direct sound waves toward a structure we need a practically useful estimate of the maximum sound pressure level in the reflected field and the area over which the sound pressure level in the reflected field is large. Estimates of these quantities can be obtained from the theoretical work presented in Sec. II of this report.

4.2.1 Far field

The maximum sound pressure level in the reflected far field occurs at locations of specular reflection, $\theta_r = \theta_s$ and $\phi_r = \phi_s + 180°$, where the angles θ and ϕ are angles in a spherical coordinate system with its origin at the center of the reflector. The reflected sound pressure level at specular angles of reflection is given by

$$SPL_r = SPL_i + 20 \log_{10}\left[\frac{fA\cos\theta}{R_r c_e}\right]$$

at specular reflection in the far field (127)

where SPL_r is the SPL of the reflected field at locations of specular reflection a distance R_r from the reflector, SPL_i is the SPL of the incident sound waves at the location of the reflector before it is put in place, f is the frequency of the incident wave (band-center frequency for incident noise), A is the area of the reflector, θ is the angle of incidence and c_e is the speed of sound. The requirement for the far field is that

$$\frac{fA}{R_r c_e} << 1 \qquad (128)$$

so that

$$SPL_r << SPL_i \text{ in the far field .} \qquad (129)$$

The area in the far field over which the reflected SPL is large can be obtained from the expressions for reflected power presented in Sec. 2.6.

We know that most of the reflected power is reflected in directions at or near the direction of specular reflection. This observation is particularly true for the total reflected power predicted by the SRS approximate formulation. We will approximate the intensity in the reflected field to be equal to the maximum intensity over an area centered on a point corresponding to specular reflection and zero otherwise. The size of the area is selected so that the total reflected power agrees with the total reflected power given by the SRS approximate formulation.

4.2.2 Near field

In many cases the effective use of a reflector will require that the test object be placed in the reflected near field. The sound pressure levels in the near field are much higher than in the far field and are comparable to the SPL of the incident sound waves. Unfortunately, it is impossible to present completely general results for the near field. We have selected two particular cases of practical importance: first, the case of an incident plane wave with an angle of incidence of 45°; second, the

case of a point source located a distance 2L along a line 45° from a line normal to the reflector, where L is the length of one side of a square reflector. The reflected field SPL's for these two cases have been obtained by computer evaluation of the SRS approximate formulation. The results of these calculations are presented in Figs. 44 through 48.

Figures 44 through 48 can be used as practical design charts. Each figure presents results for a different value of kL/2, where k is the acoustic wavenumber, $k = 2\pi f/c_0$. The correspondence between the parameter kL/2 and the frequency f for a 4-ft-square reflector is

kL/2	f
1.375	125 Hz
2.75	250
5.5	500
11	1000
22	2000

To determine the reflection of a band of random noise the band-center frequency should be used to calculate the value of kL/2. In each of the Figs. 44 through 48, the SPL's along five lines parallel to a line from the center of the reflector to the source are shown. The distance of each of the five lines from the line connecting the source and reflector center point is given by the y-coordinate. Values of y = 0.5L, 1.0L, 1.5L, 2.0L, and 2.5L have been selected for the presentation. The SPL's at intermediate values of y can be found by interpolation. Distance along each of the five lines is measured by the coordinate x. The SPL's for each of the selected values of y are plotted as a continuous function of x. For each value of y and x the SPL relative to the SPL of the incident field is given by the distance from the point prescribed by the values of x and y and the heavy solid or dashed curve. For example, the SPL at y = 1.5L, $x = x_0$ in Fig. 44 is -12 dB. The SPL at y = 0.5L and $x = x_0$ is -5 dB.

An important observation on the results presented in Figs. 44 through 48 is that the reflected SPL from an incident plane wave is approximately equal to the reflected SPL for a point source a distance 2L from the reflector. Thus, as a practical matter distances from the source to the reflector greater than 2L do not rule out the use of these figures as design charts. A second point which should be mentioned is that the SPL's plotted are only due to the reflected sound field. The total sound

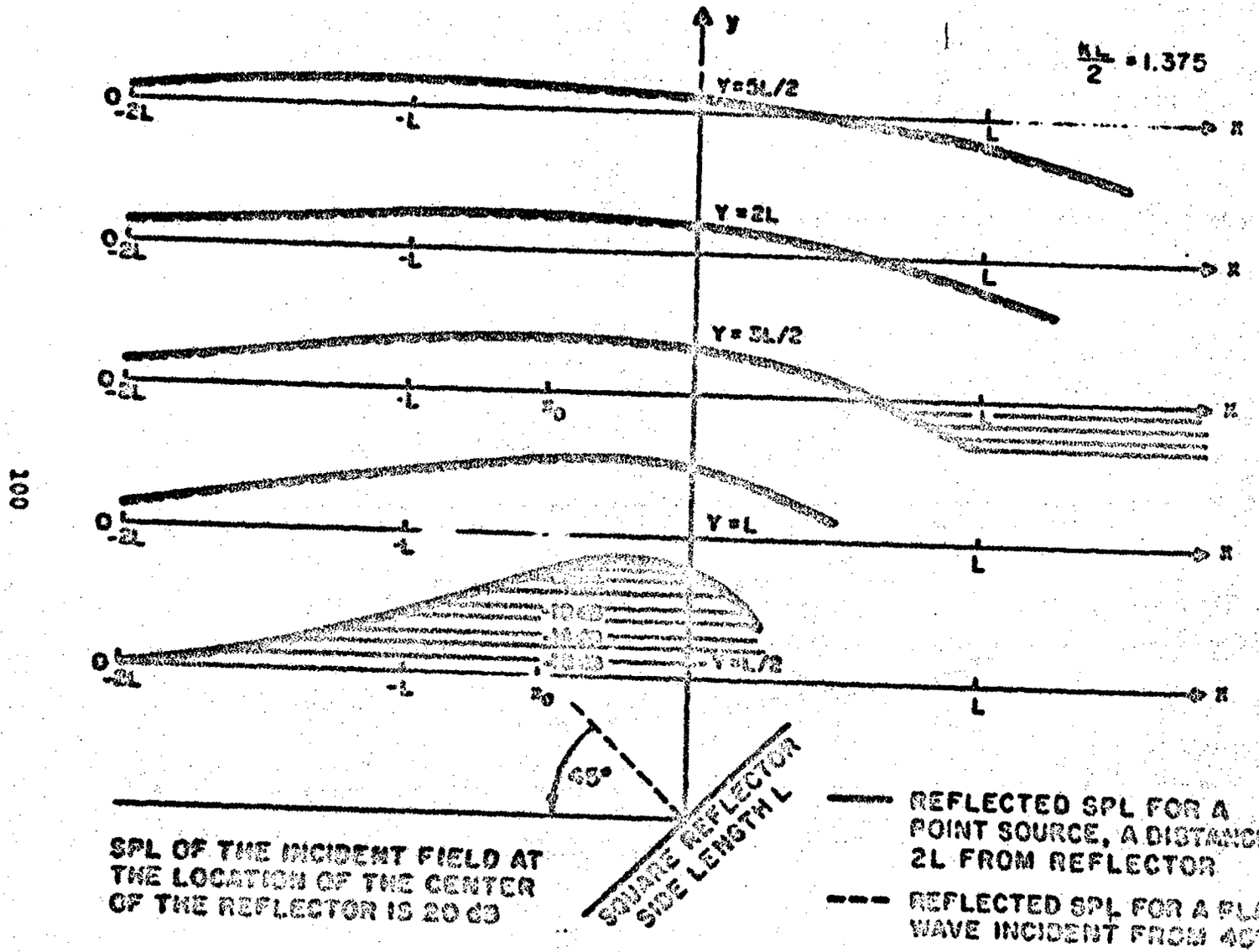

FIG. 44 REFLECTED SOUND PRESSURE LEVELS.

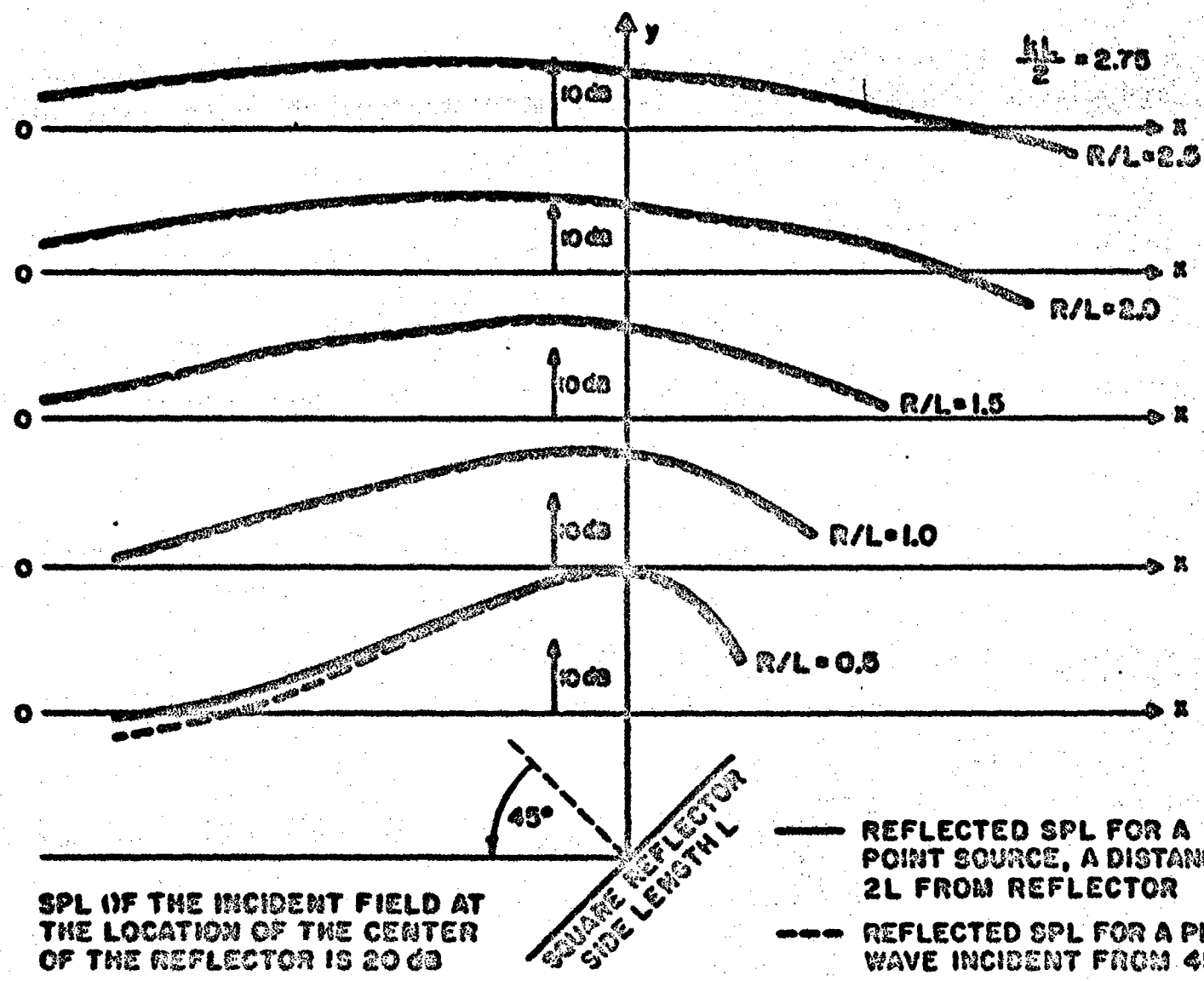

FIG. 45 DESIGN CHART GIVING THE SOUND PRESSURE LEVEL NEAR A SQUARE REFLECTOR -- $\frac{kL}{2}$=2.75

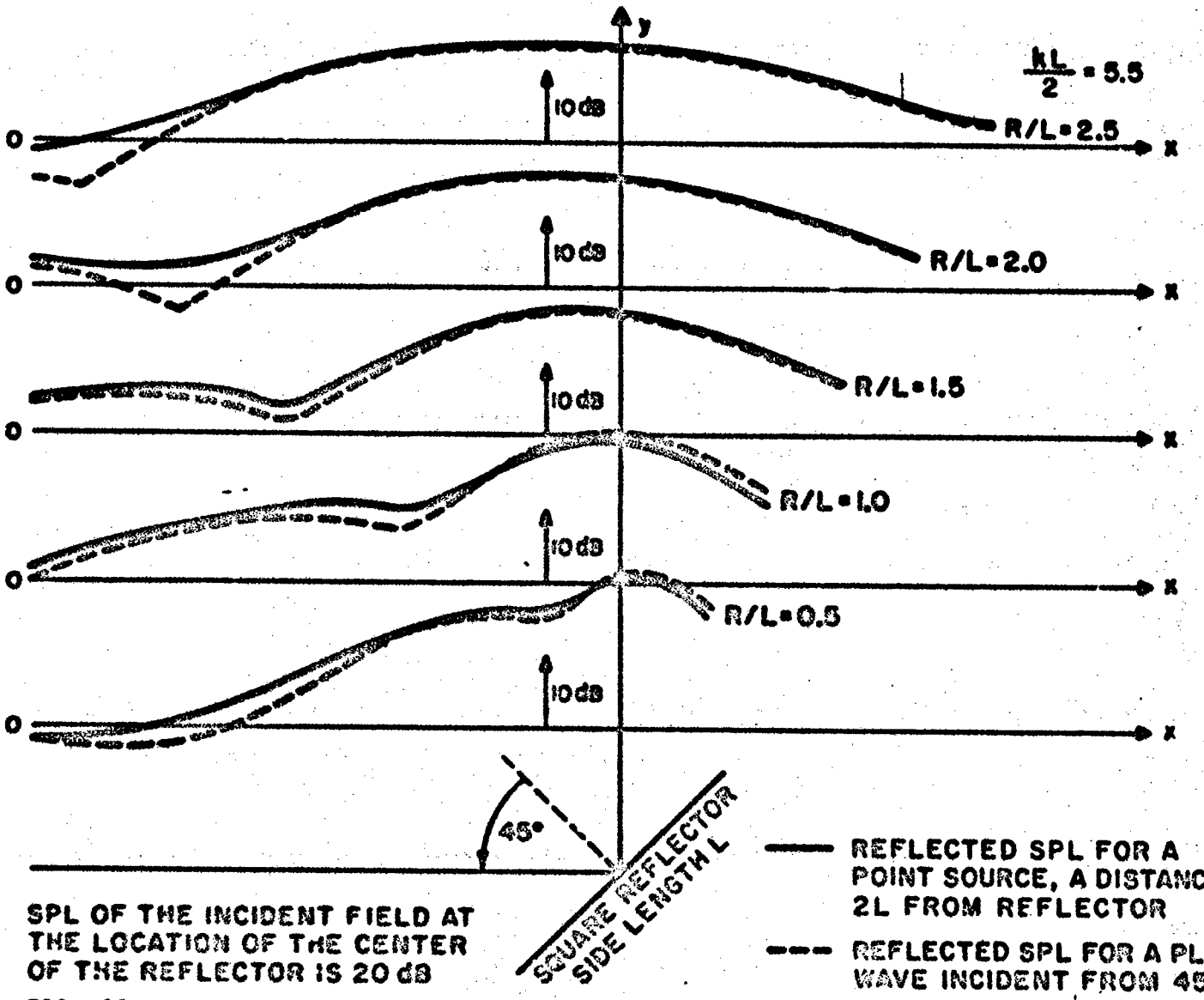

FIG. 46 DESIGN CHART GIVING THE SOUND PRESSURE LEVEL NEAR A SQUARE REFLECTOR -- $\frac{kL}{2} = 5.5$

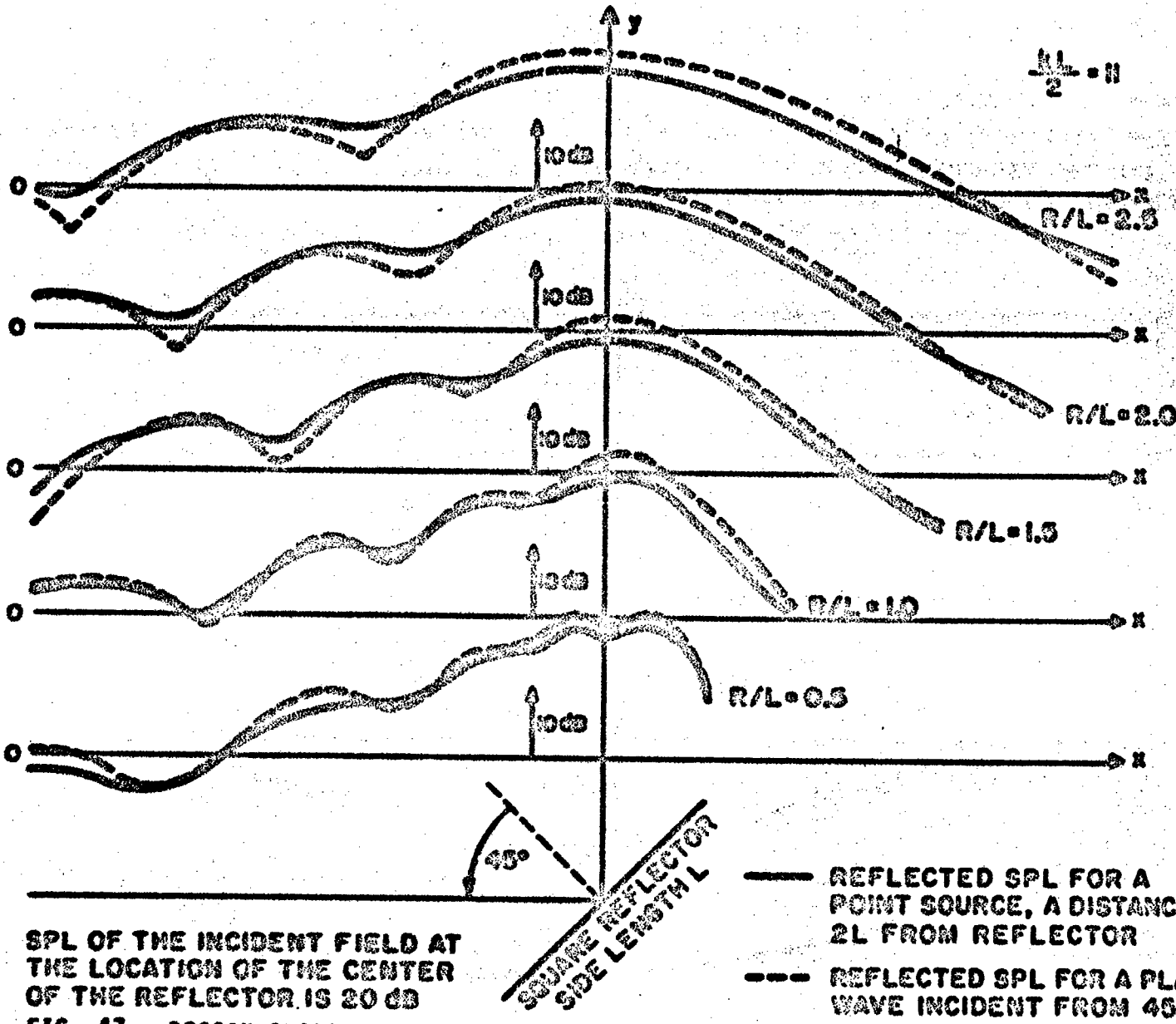

FIG. 47 DESIGN CHART GIVING THE SOUND PRESSURE LEVEL NEAR A SQUARE REFLECTOR -- kL/2 = 11

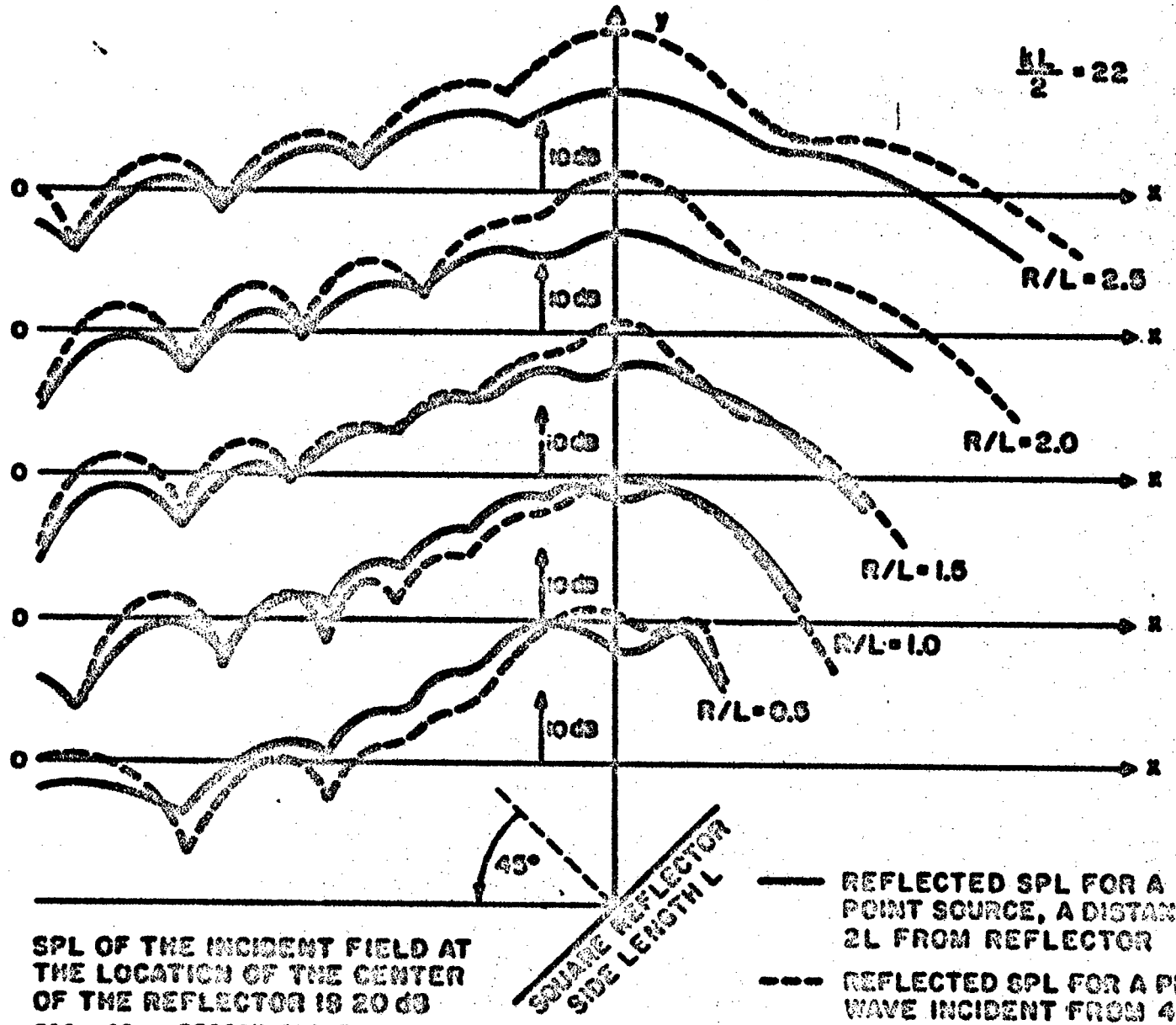

FIG. 48 DESIGN CHART GIVING THE SOUND PRESSURE LEVEL NEAR A SQUARE REFLECTOR -- kL/2 = 22

pressure at a point will be the sum of the incident and reflected sound pressures. Again, as a practical matter neglect of the incident field SPL does not limit the use of these figures, since we are only interested in the SPL's at locations where the incident sound pressures are quite low.

To complete our discussion we will illustrate the use of Figs. 44 through 48 as design charts. Assume that the SPL at a particular point on a test structure in the octave band centered on 1000 Hz is 135 dB. We wish to increase the SPL at this point to 145 dB. First, we must determine whether or not the point in question is in the direct or reverberant field of the test chamber. Only if the point is in the direct field will a reflector be of practical use. Assuming for the value of this example that the point is in the near field, we must next define the region in which the free-field SPL exceeds the desired level of 145 dB. Since a flat reflector cannot amplify the SPL, it must be placed within this region in order that the reflected field equal 145 dB on the test object. For this example let us assume that the SPL at a point 8 ft from the test object is 145 dB. By placing a 4-ft-square reflector at this point and orienting it so as to shine sound onto the test object we can increase the SPL. The exact amount of the increase depends on the angle of incidence of the sound waves emanating from the source on the reflector, the distance between the source and the reflector and the orientation of test object relative to the reflector. For design purposes we can use an approximate estimate of the SPL increase. This approximate estimate can be found from Fig. 47 even though the angle of incidence is not 45° and the distance from source to reflector is not equal to the two values for which results are presented. At a distance 8 ft from a 4-ft reflector ($y = 2L$, $x = 0$) for $kL/2 = 11$, the SPL is 1 dB below the level of the incident field. Thus, at the particular point on the test object which we are considering, the SPL due to the reflected field will equal 144 dB - a value sufficiently close to the desired objective.

The parameters selected for the above example were such that a reflector could be used to accomplish the desired objective. The reader should be warned that this may not always be the case.

REFERENCES

1. V. Griffing and F.E. Fox, "Theory of Ultrasonic Intensity Gain Due to Concave Reflectors", *J. Accust. Soc. Amer.*, 21, No. 4, 1949.

2. J.W. Goodman, *Introduction to Fourier Optics*. McGraw-Hill Book Co., New York, 1968, Chap. 3.

3. Y. Sakurai and Z. Maekawa, "Sound Reflection From Panels and a Panel Array", Memoirs of the Faculty of Engineering, Kobe University, No. 14 (1968), p. 107.

4. H. Lamb, *Hydrodynamics*. Dover Publications, New York, 1932, Art. 290.

5. S.N. Rscherekin, *A Course of Lectures on the Theory of Sound* (translated from the Russian by O.H. Blunn, translation edited by P.E. Doak). Pergamon Press, New York, 1963, p. 419.

6. P.M. Morse and H. Feshbach, *Methods of Theoretical Physics*. McGraw-Hill Book Co., New York, 1953, Vol. 2.

7. J.W. Goodman, *Introduction to Fourier Optics*. McGraw-Hill Book Co., New York, 1968, Chap. 3.4.

8. W.M. Baars, "Diffraction of Sound Waves by a Circular Disk", *Acoustica*, 14, p. 289, 1964.

9. H.A. Schenck, "Improved Integral Formulation for Acoustic Radiation Problems", *J. Accust. Soc. Amer.*, 44, pp. 41-58, 1968.

10. G. Chertock, "Sound Radiation From Vibrating Surfaces", *J. Accust. Soc. Amer.*, 36, pp. 1305-1313, 1964.

11. B.B. Baker and E.T. Copson, *The Mathematical Theory of Huygen's Principle*. Oxford Press, 1939, pp. 68-72 and 98-101.

12. P.W. Smith and R.H. Lyon, "Sound and Structural Vibration", NASA CR-160, 1965.

13. *Noise Reduction*, edited by L.L. Beranek, Chap. 13. McGraw-Hill Book Co., New York, 1960.

14. C.J. Bouwkamp, Thesis, University of Groningen, Wolters, Groningen, 1941.

15. A. Leither, "Diffraction of Sound by a Circular Disk", *J. Accust. Soc. Amer.*, 21, No. 4, p. 331, 1949.

16. W.M. Baars, "Diffraction of Sound Waves by a Circular Disk", *Acoustica*, 14, p. 289, 1964.

17. *Noise Reduction*, edited by L.L. Beranek, Chap. 14.